UNIVERSITÀ DEGLI STUDI DI PADOVA

DIPARTIMENTO DI BIOLOGIA

Corso di Laurea in Biologia Molecolare

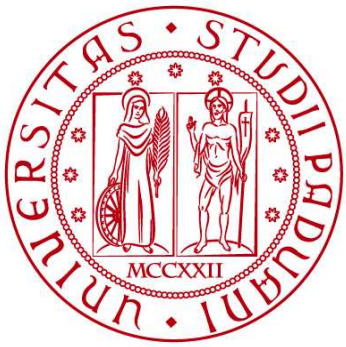

ELABORATO DI LAUREA

Un programma di invecchiamento/autoimmunità definisce la trasformazione precoce dei linfomi extranodali

Tutor: Prof. Alessandro Carrer
Dipartimento di Biologia

Co-tutor: Dott.ssa Beatrice Calciolari
Dipartimento di Biologia

Laureando: Giancarlo Angi

ANNO ACCADEMICO 2023/2024

Index

Abstract

Diffuse large B-cell lymphoma (DLBCL) is the most common and most aggressive type of non-Hodgkin lymphoma (NHL) and originates from an aberrant germinal center (GC) reaction. A third of diffuse DLBCL patients present with extranodal lymphoma dissemination, which is associated with dismal clinical outcomes and mainly affects patients bearing $MYD88^{L265P}$ mutation (MCD DLBCL subtype). The paper analyzed in the present thesis unveils how $MYD88^{L265P}$ favors extranodal dissemination of DLBCL. Venturutti *et al.* demonstrate that B cells expressing $MYD88^{L265P}$ activate, proliferate, and differentiate with minimal T-cell co-stimulation, seeding spontaneous GCs. Strikingly, they identify $CD11c^{+}T\text{-}BET^{+}$ aged/autoimmune memory B cells (AiBCs), which arise from GCs and accumulate with age in $Myd88^{L252P}$ ($MYD88^{L265P}$ murine equivalent) mice, as DLBCL precursors. These findings suggest that GC B cells may gradually progress to overt lymphoma, encompassing a defined aged/autoimmune step that could be exploited for DLBCL early detection.
Functional GCs are supported by epigenetic rewiring of B lymphocytes. During my internship, I explored the degeneration of GC B cell epigenome in physiological aging. Interestingly, I found that histone acetylation of GC B cells decreases with age in both mice and humans.

Thesis resume

Questa tesi riassume e discute i risultati del *paper* "An Aged/Autoimmune B-cell Program Defines the Early Transformation of Extranodal Lymphomas" (Venturutti *et al.,* Canc Discov, 2023), che fornisce un contributo cruciale alla comprensione del ruolo della mutazione $MYD88^{L265P}$ nella trasformazione precoce dei linfomi extranodali (sottotipo MCD del linfoma diffuso a grandi cellule B). Il Linfoma Diffuso a Grandi Cellule B (*Diffuse Large B Cell Lymphoma*, DLBCL) è la forma più comune e aggressiva di linfoma non Hodgkin e il sottotipo MCD, contraddistinto dalla presenza della mutazione $MYD88^{L265P}$, è caratterizzato da una spiccata propensione alla disseminazione extranodale, un fattore che contribuisce all'alto tasso di mortalità nei pazienti affetti da questo tipo di tumore.

Prima della pubblicazione di questo *paper*, il ruolo della mutazione $MYD88^{L265P}$ nei linfomi non era ancora stato caratterizzato. Sebbene ne fosse stata identificata la presenza nei pazienti affetti da MCD DLBCL, non erano stati pienamente chiariti i meccanismi attraverso i quali questa mutazione contribuisse alla tumorigenesi. Questo studio colma tale lacuna, dimostrando per la prima volta come la mutazione $MYD88^{L265P}$ inneschi specifici processi molecolari che conducono alla trasformazione maligna delle cellule B del centro germinativo.

Il lavoro evidenzia come la mutazione $MYD88^{L265P}$ conferisca alle cellule B del centro germinativo un vantaggio proliferativo, consentendo loro di sopravvivere e proliferare indipendentemente dalla co-stimolazione da parte delle cellule T helper follicolari, che è invece indispensabile in condizioni fisiologiche. Il programma trascrizionale attivato dalla mutazione $MYD88^{L265P}$ indirizza il differenziamento delle cellule B verso un fenotipo specifico, quello delle cellule B della memoria associate all'invecchiamento/autoimmuni (*Aged/autoimmune B cells,* AiBCs). Le cellule AiBCs sono caratterizzate da una marcata espressione di T-BET e da una forte attivazione della via di segnale dell'interferone-gamma (IFNγ); si accumulano con l'età e rappresentano la popolazione precursore dei linfomi del sottotipo MCD.

L'aspetto innovativo e di grande rilievo del *paper* è la dimostrazione che la mutazione $MYD88^{L265P}$ non solo promuove la trasformazione delle cellule B in linfomi, ma attiva anche un programma autoimmune e associato all'invecchiamento. Questo suggerisce una stretta interconnessione tra linfomi, invecchiamento e malattie autoimmuni, che potrebbero condividere radici genetiche comuni e percorsi di sviluppo simili. Lo studio dimostra inoltre, per la prima volta, che una popolazione cellulare associata all'invecchiamento è il precursore diretto di cellule tumorali, sorpassando il paradigma secondo cui l'invecchiamento predispone alla trasformazione tumorale attraverso il mero accumulo di mutazioni nel tempo.

Il *paper* rappresenta un avanzamento significativo nella comprensione della biologia del DLBCL, in particolare del sottotipo MCD. L'identificazione del programma associato all'invecchiamento/autoimmune come meccanismo centrale

nella trasformazione maligna delle cellule B offre una prospettiva innovativa per la diagnosi precoce dei linfomi MCD, ponendo le basi per l'utilizzo delle AiBCs come biomarcatori pre-tumorali di questa patologia, solitamente identificata in stadi avanzati.

Durante il mio tirocinio presso il laboratorio Carrer all'Istituto Veneto di Medicina Molecolare (VIMM) di Padova, ho studiato il rimodellamento epigenetico delle cellule B del centro germinativo durante l'invecchiamento. Ho osservato, tramite analisi immunoistochimica di organi linfoidi secondari, una riduzione dell'acetilazione istonica dei linfociti B che si associa all'invecchiamento sia nell'uomo che nel topo. Mentre lo studio di Venturutti e i suoi collaboratori caratterizza il programma trascrizionale di una popolazione di linfociti B associata all'invecchiamento a valle della mutazione $MYD88^{L265P}$, il mio esperimento dimostra che l'invecchiamento si associa, in condizioni fisiologiche, a rimodellamento epigenetico delle cellule B.

State of the Art

The Germinal Center (GC) reaction

The germinal center (GC) reaction is the core of T-dependent humoral immunity against foreign antigens and, indeed, a critical component of the adaptive immune system. The GC reaction allows affinity maturation of B Cell Receptor (BCRs) and immunoglobulin isotype switching, culminating in the generation of antibody-secreting long-lived plasma cells, each of which is specific for a cognate antigen type, and memory B cells, which trigger a faster and more efficient immune response upon antigen rechallenge.

GCs are transient microanatomical structures that form in the central follicular zones of secondary lymphoid organs as a result of the interaction between proliferating antigen-activated B cells, T follicular helper (Tfh) cells, and specialized antigen-presenting stromal cells called follicular dendritic cells (FDCs). Typically, GCs consist of two distinct regions: the dark zone (DZ), in which rapidly proliferating B cells are densely packed, giving strong hematoxylin signals, and the light zone (LZ), weakly stained by the same dye, where B cells are screened for their BCR affinity [1,2]. The cellular composition of the aforementioned regions is different. While the DZ exclusively contains B cells, the LZ is the site where they make contact with (FDCs) and Tfh cells. FDCs present antigens to GC B cells, which will be later selected by Tfh cells based on the antigen affinity of their BCRs. Remarkably, GC zones are not fixed because B cells recirculate between DZ and LZ.

The germinal center reaction begins with the migration of Tfh cells into the follicle, followed by antigen-stimulated B cells, which repeatedly proliferate and seed the DZ. During proliferation within the DZ, B cells mutate their immunoglobulin (Ig) V genes as part of a process called somatic hypermutation (SHM), which is catalyzed by the enzyme activation-induced cytidine deaminase (AID). Cytosine deamination into uracil converts C-G pairs into A-T pairs within DNA molecules; notably, this process carries significant risks, including the generation of unintended oncogenic mutations (B cell lymphoma) and potentially harmful autoantibodies [1]. After multiple divisions, DZ B cells (called centroblasts) stop dividing, and such heavily mutated nondividing B cells (termed centrocytes) migrate to the adjacent LZ. Here, B cells that have undergone SHM are tested for their ability to recognize antigens. Centrocytes endowed with high-affinity BCRs are more likely to capture their antigen, display it to Tfh cells, and receive CD40- and cytokine-mediated signals from T cells [2]. As a result, high-affinity B cells are selected to survive and differentiate. On the contrary, B cells bearing low-affinity or autoreactive BCR are cleared by apoptotic death in the light zone. Indeed, a failure of Tfh control over BCR affinity can result in the positive selection of autoreactive and low-proficient B cells [1]. Remarkably, most B cells carry intermediate affinity BCR and return from the DZ to the LZ. After multiple selection rounds, positively selected B cells exit the GC as plasmablasts that will home in the bone marrow and differentiate into long-

lived plasma cells. Instead, B cells that underwent limited somatic hypermutation become memory B cells and can recirculate between secondary lymphoid organs [2].

GC B cells exhibit numerous characteristics typical of cancer cells. These include sustained proliferation and clonal expansion, downregulation of tumor-suppressor genes to enable cell cycle progression, genomic instability, resistance to DNA damage, metabolic and epigenetic rewiring, and immune evasion [1]. Not surprisingly, most B-cell neoplasms originate from the GC reaction, distinctively displaying an abundance of point mutations, structural genomic aberrations, and clonal diversity from genetic and epigenetic perspectives. The predominant biological theme of GC-derived lymphomas is the mutation of genes involved in epigenetic regulation (KMT2D, CREBBP, EP300, EZH2, ARID1A, and ARID1B) and immune receptor signaling (BCR signaling, NF-κB signaling, PI3K, Toll-like receptor, and NOTCH signaling), which play pivotal roles at critical transitional stages of the germinal center reaction [1].

Molecular hallmarks of GC B cells are hijacked by Non-Hodgkin Lymphomas (NHLs), which primarily originate from B cells that have passed through the GC reaction [2]. GC-derived lymphomas are diffuse large B-cell lymphoma (DLBCL), follicular lymphoma (FL), and Burkitt lymphoma (BL) [2]. DLBCL is the most aggressive and common NHL, with 30-40% of patients failing to respond to standard treatment. It is a heterogeneous disease that can arise from B cells at various developmental stages within the GC: GCB DLBCL subtype originates from LZ B cells, while ABC-DLBCL arises from GC-derived plasmablasts. FL arises from the light zone of the GC; it is an indolent tumor of older individuals, with around 3% transforming to a more aggressive form. BL is a rare but highly aggressive GC-derived lymphoma that mainly affects children. It derives from dark zone GCBs and is characterized by t(8;14) chromosomal translocation, which relocates MYC gene under the control of the immunoglobulin heavy or light chain *loci*, resulting in its overexpression.

Diffuse Large B Cell Lymphoma (DLBCL)

Diffuse large B-cell lymphoma is the most common group of non-Hodgkin's lymphoid neoplasms and predominantly affects adults or elderly individuals. Overall, non-Hodgkin’s lymphomas are the seventh most common type of cancer in the US, with a rate of 5.5 new cases per 100,000 people per year [3]. At the molecular level, DLBCL tumorigenesis is indeed a by-product of SHM during the GC reaction. DLBCL driver mutations mainly affect cell cycle, chromatin modifiers, GC regulators, and immune recognition programs [1].

Diffuse large B-cell lymphomas exhibit substantial clinical and biological heterogeneity [4], which is also responsible for the elevated resistance and relapse rates to R-CHOP (rituximab in combination with cyclophosphamide, hydroxydaunorubicin, vincristine, and prednisone), the standard-of-care for this type of cancer. Many approaches, ranging from genetic to transcriptomic and metabolic profiling, have been established to elucidate this heterogeneity. Indeed, this would help identify class-specific vulnerabilities and promote subtype-guided

therapy. Gene expression profiling has categorized DLBCL into two broad subgroups that mirror distinct normal mature B-cell developmental states (cell-of-origin classification, COO) and bear prognostic relevance: GCB-DLBCL, which derives from LZ B cells, and ABC-DLBCL, which originates from B cells at later differentiation within GCs, namely plasmablasts [1]. These molecular phenotypes have predictive value, with ABC-DLBCL exhibiting a more aggressive clinical course and less favorable outcome than GCB-DLBCL. A recent study has leveraged next-generation sequencing of DLBCL to develop a probabilistic algorithm, LymphGen, that enables the subclassification of DLBCL into seven molecularly discrete cohorts: MCD, BN2, MYC^{+}, MYC^{-} ST2, A53, and N1, with corresponding prognostic associations [5]. Remarkably, LymphGen-based genetic subtypes also share gene expression profiles, immune microenvironments, and outcomes following immunochemotherapy. This classification also reveals genetic similarities between DLBCL subtypes and various indolent and extranodal lymphoma types, suggesting a shared pathogenesis. In particular, it identified a highly aggressive subtype known as "C5" or "MCD" with the highest frequency of extranodal dissemination.

Indeed, although DLBCL is characterized by the initial involvement of a single lymph node followed by the rapid expansion of the tumor mass, approximately a third of patients have tumors in non-lymphoid organs, such as immune-privileged sites. The latter scenario is associated with a detrimental prognosis and high relapse rates, posing significant clinical challenges. Standard treatments, including chemotherapy, anti-B-cell antibodies, and radiotherapy, are largely ineffective for most of these patients and come with substantial side effects. Additionally, no reliable means exist to detect these tumors early, when they might be more responsive to targeted therapies.

The role of MYD88 in DLBCL and autoimmunity

MCD and primary extranodal tumors in immune-privileged sites share founder mutations targeting MYD88, CD79B, and TBL1XR1. Approximately 70% of these tumors carry $MYD88^{L265P}$ gain-of-function missense mutation.

Myeloid differentiation primary response 88 (MYD88) is a protein encoded by the MYD88 gene involved in signal transduction, primarily within immune cells. It acts as an adapter of signaling receptors known as Toll-Like Receptors (TLRs). Receptors of the Toll-like family are located either on the cellular surface (TLR1, TLR2, TLR4, TLR5, TLR6) or within endosomes (TLR3, TLR7, TLR8, TLR9) and can sense extracellular or phagocytosed pathogens, respectively. Different subsets of immune and non-immune cell types, such as monocytes, macrophages, dendritic cells, neutrophils, B cells, T cells, fibroblasts, endothelial cells, and epithelial cells, express various combinations of TLRs. Upon ligand binding, all TLRs, apart from TLR3, interact with MYD88, which in turn interacts with transcription factors of the NF-kB and interferon-regulatory factor family and promotes inflammation.

$MYD88^{L265P}$ gain-of-function missense mutation facilitates proliferation and survival by activating NF-κB signaling and mitogen-activated protein kinases. This mutation has been identified in various human B cell tumors, including ABC-DLBCL, Waldenström's macroglobulinemia, and chronic lymphocytic leukemia, highlighting its widespread biological relevance [6]. However, L265P mutation does not induce oncogenic transformation *per se,* and additional genetic rearrangements (e.g., BCL2 overexpression) cooperate with $MYD88^{L265P}$ in GC-derived lymphomas [2]. Mice expressing $Myd88^{L252P}$ ($MYD88^{L265P}$ murine equivalent) in the B cell lineage develop lymphadenopathy and occasional lymphomas with old age. A similar mechanism may occur in humans, where diffuse large B-cell lymphoma incidence increases with age [3]. In line with that, combining $Myd88^{L252P}$ with Bcl2 overexpression in mice results in a higher incidence of lymphomas that closely resemble their human counterparts [7].

Besides cancer, activation of the MYD88 signaling pathway is central to the pathogenesis of autoimmune diseases, including systemic lupus erythematosus and multiple sclerosis [6].

Aged/autoimmune memory B cells (AiBCs)

Aged/autoimmune memory B cells (AiBCs) are a recently discovered B cell subset that is raising great scientific interest nowadays. The term indicates a naturally occurring population of antigen-experienced B cells that continuously expands with age in healthy individuals [8]. Yet, AiBCs can prematurely accumulate in people with autoimmune diseases and/or infectious diseases. In mice, B cells closely resembling AiBCs also arise during anti-viral immune responses.

AiBCs are $T\text{-}BET^{+}$ atypical memory B cells that are also $CD11b^{+}$ and/or $CD11c^{+}$ [8]. They depend on the expression of the transcription factor T-BET, which induces a transcriptional program that makes them substantially different from other B cell types in terms of activation requisites, functional capacities, and survival requirements. In contrast to naïve follicular (FO) or marginal zone (MZ) B cells, AiBCs survive but respond poorly to BCR engagement [8]. However, they vigorously proliferate in response to stimulation with TLR9 or TLR7 agonists, alone or in combination with BCR ligation [8].

Experimental approach

Transgenic mice

Transgenic mice are model organisms that have been genetically modified by introducing exogenous DNA into their genome. This approach allows researchers to study gene function and regulation in both physiological and pathological contexts. The generation of transgenic mice often exploits the Cre-loxP system. Cre recombinase is an endonuclease that mediates gene recombination at specific DNA sequences known as loxP sites. When a gene of interest is flanked by loxP sites, Cre recombinase can delete, invert, or translocate the gene. Indeed, the expression of Cre recombinase under tissue or developmental stage-specific promoters allows for controlled manipulation of gene function.

Rosa transgenic mice are widely used in conjunction with the Cre-lox system. Rosa26 locus is a widely used safe harbor site in the mouse genome that allows for consistent and widespread transgene expression. In Rosa26 transgenic mice, this locus contains a loxP-flanked stop cassette upstream of a reporter gene or a transgene of interest. By crossing Cre-expressing mice with Rosa26 transgenic mice, the stop cassette is excised in Cre-expressing cells, inducing the expression of the gene of interest.

To mimick MCD-DLBCL in mice, *Venturutti et al.* restricted the expression of $Myd88^{L252P}$ mutation to specific B cell subsets by exploiting transgenic mouse models. This approach also avoids artifactual effects due to the impact of $Myd88^{L252P}$ in other cell types. In Cre-expressing strains, the Cre recombinase gene was expressed under the control of either the (pre)-GC specific promoter *Cγ1* or *Cd19* promoter, which is expressed at the early stages of B-lymphocyte development. Cre-expressing strains were crossed with mice containing one Cre-inducible $Myd88^{L252P}$ allele. In turn, $Myd88^{L252P}$ allele had been generated by *in vivo* Cre-mediated deletion of wild-type exons. In this model, hGHpA is included within the $Myd88^{L252P}$ gene construct as a transcriptional stop signal to terminate transcription in cells that do not express Cre recombinase The hGHpA sequence is derived from the human growth hormone gene. It contains a polyadenylation signal critical for the proper processing and stabilization of mRNA, inducing the addition of a poly(A) tail to the 3' end of mRNA molecules, which terminates transcription.. This prevents the expression of downstream genes, namely mutant Myd88. Conversely, upon Cre recombinase expression, hGHpA signal is excised allowing $Myd88^{L252P}$ to be expressed. This strategy ensures that only cells expressing Cre recombinase will express the $Myd88^{L252P}$.

To analyze whether GC-derived MBCs co-expressed the canonical AiBC markers CD11b/CD11c in $Myd88^{L252P}$ and WT mice, *Venturutti et al.* used Rosa26YFP mice (fig. 4.B).
In these mice, Rosa26 locus contains a loxP-flanked stop signal followed by the Enhanced Yellow Fluorescent Protein gene (EYFP). In

Rosa26YFP;*Cγ1Cre*;*Myd88*$^{L252P/WT}$ animals, EYFP is expressed in GC B cells. This is a powerful tool for lineage tracing of Myd88^{L252P} GC B cells.

Chimeric mice

Chimeric mice are animals that contain cells from two or more different genetic lineages. This approach is valuable for investigating immune functions by tracking developmental fate decisions or assessing the impact of genetic modifications on the immune response. Chimeric mice are often created by injecting genetically modified embryonic stem cells into a developing embryo. They can also be generated by transplanting immune cells into adult mice. In this case, recipient mice are irradiated before bone marrow transplantation to deplete them from their own immune cells. This ensures that the immune cell population of interest solely derives from transplanted cells and avoids confounding effects due to the persistence of host cells.

To generate B cell chimeric mice, recipient mice are housed under sterile conditions and subjected to whole-body irradiation to deplete their bone marrow and immune cells. The irradiation dose typically ranges from 8 to 12 Gy. Meanwhile, B cells from donor mice are isolated using magnetic-activated cell sorting (MACS) or flow cytometry and checked for high viability. Next, appropriate numbers of GC B cells are tail-vein injected into the irradiated mice, which enables graft B cells to circulate and home to the bone marrow. After transplantation, mice are monitored for complications and given antibiotics to prevent infections. Chimerism is confirmed by analyzing blood or tissue samples by flow cytometry or molecular techniques.

In bone marrow transplantation experiments, CD45.1 and CD45.2 are often used as markers to distinguish between donor and recipient cells. This is crucial for monitoring the fate and function of different cell populations, especially in studies related to hematopoiesis, immunology, and transplantation. Generally, cells are not artificially engineered to express CD45.1 or CD45.2. In fact, since CD45.1 and CD45.2 alleles are naturally occurring genetic variants, chimeric mice can be generated by using donor and recipient mice that naturally express different isoforms.

Venturutti et al. generated B cell chimeric mice by transplanting an equal amount of bone marrow cells extracted from CD45.2 Myd88$^{L252P/WT}$ and CD45.1/2 WT mice. They used these mice as an *in vivo* model to assess whether and how Myd88^{L252P} mutation enhanced the competitive fitness of GCB (fig. 1.D, 2, 3).

Flow cytometry

Flow cytometry is a technique used to analyze the morphology and fluorescence of cells suspended in a fluid. Cells pass through a laser beam in a single file, and the instrument measures light scattering and fluorescence. This informs on cell size (forward scattered light), granularity (side scattered light), and biochemical properties of each cell. Indeed, antibodies tagged with fluorescent dyes stain cell

surface or intracellular proteins, allowing for precise identification and quantification of different cell types in the same sample, as well as for comparison of signal intensity across different conditions. Multiple lasers are used to analyze multiple markers simultaneously. Hence, critical applications of flow cytometry include immunophenotyping of blood samples, cell death assays, cell cycle analysis, and cell sorting (FACS). The latter is a specialized technique to isolate specific cell types based on their fluorescence properties. Flow cytometry is fast and versatile but requires expertise in analysis setting and fluorescence compensation. Most importantly, it can be applied only to single-cell suspensions.

Venturutti et al. used flow cytometry in multiple experiments (fig 1.D, 2, 3.B, 5.A, 5.B) to identify different B cell subpopulations (GC B; AiBCs, MBC, YFP-positive B cells) in splenocytes suspensions from transgenic mice. They used this technique also to quantify EdU incorporation by mutant and WT GC B (fig. 2)

Induction and inhibition of the GC reaction *in vivo*

Mice immunization stimulates immune responses *in vivo* by injecting a solution containing a specific antigen. This process is employed to study immune functions, to test vaccine efficacy, or to generate specific antibodies for research purposes. The injected antigen is recognized by the host immune system as non-self; hence, it induces a specific immune response that also envisions the production of antibodies tailored to the antigen. By immunizing mice, researchers can analyze how the immune system responds to infections and vaccinations and investigate whether and how different cell types are involved in this. Therefore, immunization studies represent a valuable approach to gain insights into immune mechanisms, but also to identify and test potential therapeutic strategies.

Immunization cocktails typically contain adjuvants and NP-conjugated antigens.
Adjuvants enhance the immune response to an antigen by stimulating the innate immune system, which in turn supports the development of a more vigorous and prolonged adaptive immune response. Adjuvants of widespread use are alum and CpG oligodeoxynucleotides, which activate antigen-presenting immune cells, such as dendritic cells.
NP-conjugation consists of chemically linking antigen molecules to the small hapten nitrophenyl (NP). NP is not immunogenic *per se,* yet it becomes highly immunogenic when attached to a larger carrier protein. NP-conjugated antigens allow researchers to study T-dependent immune responses. Through this approach, researchers can identify NP-specific B cells and measure the titer of anti-NP antibodies by enzyme-linked immunosorbent assay (ELISA).

To analyze GC B cells in their experiments, *Venturutti et al.* induced GC formation by immunizing mice with the T-cell-dependent antigen sheep red blood cells (SRBCs) (fig. 1, 2, 3, 4). GC B cells were profiled at the peak of the GC reaction (8-10 days after intraperitoneal injection of SRBCs). Chimeric mice were SRBC-immunized 45 days after bone marrow cell transplantation (1.D, 2, 3).

To assess whether Myd88^{L252P} lowers the requirement for T-cell-derived co-stimulatory signals, immunized mice were treated with 100 ug of anti-CD40L antibody on the 2nd, 4th and 6th day after SRBCs immunization. CD40L, also known as CD154, is a protein expressed on the surface of activated T cells and interacts with CD40 receptors expressed by antigen-presenting cells (APCs), such as B cells. The blockade of CD40-CD40L crosstalk upon induction of the GC reaction prevents B cell proliferation, full activation, and differentiation within GCs. As a control, anti-IgG antibody was used. IgG control is essential because it distinguishes the specific effect of anti-CD40L antibody on B cell activation and the immune response from any side-effects of antibody administration, such as changes in cell signaling or immune activation merely caused by antibody presence or binding to Fc receptors.

During my internship, mice were immunized according to a double SRBC immunization protocol [9]. On day 0, 10^9 SRBCs were injected intraperitoneally. On day 5, a booster dose (200 000 SRBCs) was given. PBS was injected as a control. This protocol takes advantage of the fact that the secondary immune response is much stronger than the primary response, leading to a more robust activation of B cells.

Immunohistochemistry (IHC) staining

Immunohistochemistry (IHC) is an immunostaining technique for detecting a specific antigen in tissue sections, allowing for its detailed visualization and analysis. 4-5 µm sections are obtained by sectioning formalin-fixed paraffin-embedded (FFPE) tissues using a microtome. First of all, sections are dewaxed and rehydrated. To expose the target antigens, antigen retrieval is performed heating samples into an appropriate buffer to break cross-links formed during fixation. Endogenous peroxidase activity is blocked when the detection enzyme is based on horseradish peroxidase (HRP). Next, sections are blocked with FBS- or BSA-containing buffers. A primary antibody specific to the antigen of interest is then applied to tissue sections. After that, the weakly bound primary antibody is washed away, and sections are incubated with a secondary antibody that allows signal detection. While primary antibodies specifically bind to antigens at the level of their variable region (Fab region), secondary antibodies recognize the constant region (Fc region) of the primary antibody, which is the same for all antibodies produced in a particular species. To detect the signal, HRP is often conjugated to the secondary antibody. Tissue sections are incubated with diaminobenzidine (DAB), which undergoes peroxidation by HRP in the presence of hydrogen peroxide, producing a brown precipitate at antigen sites. Then, nuclei are counterstained by hematoxylin, a basic dye that binds to the acidic components of the cell, primarily DNA in the nucleus. This binding stains the nucleus a blue to purple color. Next, tissue sections are dehydrated by washing with ethanol solutions at increasing concentrations and cleared with xylene to make them transparent. Lastly, sections are covered with a glass slide using a resin-based solution and imaged with a light microscope.

Venturutti et al. stained B cells (B220) and GCB (peanut agglutinin, PNA) by immunohistochemistry to compare GC numbers and size in Myd88$^{L252P/WT}$ and

WT mice (fig. 1A–C). During my internship at Alessandro Carrer's laboratory, I used immunohistochemistry to compare the levels of histone acetylation in GC B cells of old and young individuals (7.A) and mice (7.B). Spleens were fixed in formalin for 48 hours, paraffinized, and sectioned to 4 μm. Before IHC staining, sections were dewaxed and rehydrated. Antigen was retrieved in citrate buffer pH=6 with 0,05% Tween-20 for 30 minutes. IHC staining was performed by Mouse to Mouse HRP (DAB) Staining System (Histoline, #MTM002) according to the manufacturer's instructions. Following antibodies were incubated at 4°C, overnight: a-H3K27ac (GenTex, #GTX60887, 1:5000); a-tetra-ac-H4 (Sigma, # 05-1355, 1:5000); a-tri-ac-H4 (Invitrogen, #PA5-40083, 1:5000).

EdU-labelling

EdU (5-ethynyl-2'-deoxyuridine) labeling is a cell proliferation assay based on the incorporation of a thymidine analog, EdU, into newly synthesized DNA molecules during the S-phase of the cell cycle. EdU is detected by "click chemistry," a copper-catalyzed azide-alkyne cycloaddition reaction. In this reaction, the alkyne group in EdU reacts with a fluorescent azide probe to form a stable covalent bond, tagging DNA with a fluorescent marker. Remarkably, fluorescence intensity is proportional to the amount of newly synthesized DNA, allowing for a quantitative analysis of cell proliferation. This reaction is highly specific, fast, and minimizes cell damage. EdU fluorescence can be detected by microscopy, flow cytometry, or other fluorescence-based methods.

Venturutti et al. used this technique to quantify and compare the proliferative capacity of mutant and WT GCB (fig. 2).

RNA-Seq and pathway analysis

RNA sequencing (RNA-Seq) is a powerful technique that profiles the transcriptome of a cell, tissue, or organism, providing insights into gene expression patterns. The process begins with RNA isolation from a sample, which is typically enriched for messenger RNA (mRNA) by selecting polyadenylated RNA or depleting ribosomal RNA. mRNA is fragmented and converted into complementary DNA (cDNA) by reverse transcription. Then, sequencing adapters are added to both ends of the fragments. cDNA libraries are amplified by PCR and sequenced using high-throughput technologies, typically Illumina, generating millions of short reads. By computational approaches, reads undergo quality control and are aligned to a reference transcriptome to infer gene expression levels. Further analysis identifies differentially expressed genes and splice variants.

Combining RNA-Seq with pathway analysis allows researchers to link changes in gene expression to biological pathways and processes, providing a deeper understanding of the mechanisms driving cellular responses or disease states. By ascribing differentially expressed genes to annotated pathways, scientists can identify critical regulatory networks and potential therapeutic targets. This integrative approach offers a comprehensive view of gene regulation and function

and helps elucidate the functional implications of gene expression fluctuations in the context of broader biological systems.

Venturutti et al. used the combination of RNA-Seq and pathway analysis to gain mechanistic insight into the GCB phenotype of $Myd88^{L252P}$ cells (fig. 4.A). Moreover, they used published RNA-seq data to compare TBX21 expression in different types of DLBCL (fig. 6.A, 6.B).

Results

Myd88^{L252P} impacts the GC reaction

Most MCD-DLBCLs and primary extranodal tumors in immune-privileged sites carry the MYD88^{L265P} gain-of-function missense mutation. Venturutti *et al.* investigated the impact of this mutation on germinal center B cells (GCB) to dissect how MCD-DLBCL founder mutations shape pathogenic trajectories.

Notably, DLBCL arises from an aberrant GC reaction. Hence, Venturutti *et al.* characterized the GC reaction in a Myd88-mutant background. With this purpose, they crossed an existing Cre-inducible Myd88^{L252P} mouse model to the Cγ1Cre strain, restricting MYD88-mutant expression to (pre)germinal center B cells (GCB) and GC-derived cells. They immunized young Cγ1Cre;Myd88$^{L252P/WT}$ or Cγ1Cre;Myd88$^{WT/WT}$ (WT) mice with the T-cell-dependent antigen sheep red blood cells (SRBCs) and analyzed spleens at the peak of the GC reaction (10 days after immunization). Immunohistochemistry (IHC) staining for B cells (B220) and GCB (peanut agglutinin, PNA) revealed intact follicles harboring an increase in GC numbers and size in Myd88$^{L252P/WT}$ mice (fig. 1A–C). After this observation, they conducted mixed chimera experiments to assess whether Myd88^{L252P} mutation enhanced the competitive fitness of GCB. Upon immunization of chimeric mice, they observed that while mutant and WT B cell levels were almost the same, mutant GC B cells were approximately twice the number of their WT counterpart (fig. 1.D). These findings suggest that GCB harboring Myd88^{L252P} mutation possess a significant competitive advantage.
To gain insight into the competitive fitness of mutant GCB, Venturutti *et al.* analyzed the proliferative capacity of mutant and WT GCB. Mutant GCB exhibited higher incorporation of 5-ethynyl-2-deoxyuridine (EdU) than their WT counterparts (fig. 2), indicating increased DNA synthesis and proliferation downstream of Myd mutation. In addition, they tested whether GCB-Tfh crosstalk was essential for MYD88-mutant B-cell survival as it is during physiological GC reactions. To do so, CD40L-blocking or control antibodies were administered to SRBC-immunized chimeric mice (fig. 3.A). Myd88^{L252P}/WT GC B cell ratio was greater than 1 in both IgG and anti-CD40L-treated mice, confirming that in both cases mutant GC B cells show a competitive advantage over WT GCB (fig. 3.B). However, this ratio significantly increases upon anti-CD40L treatment (fig. 3.B), indicating that Myd88^{L252P} enables GC B cells to proliferate and survive independently of cognate T-cell help.

Together, these findings indicate that Myd88^{L252P} mutations provide a competitive advantage to GC B cells.

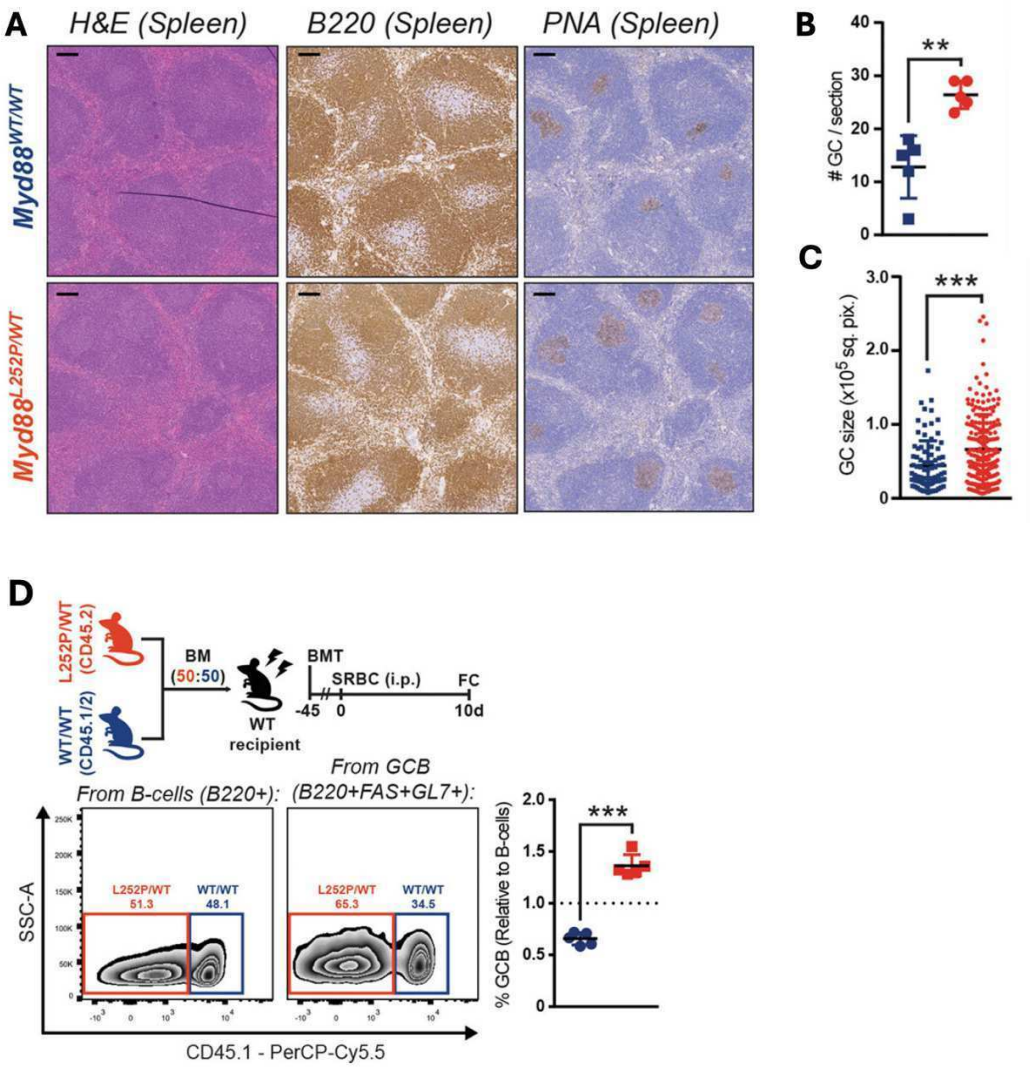

Figure 1. Myd88^{L252P} increases the competitive fitness of GCB. (Venturutti *et al.*)

A, H&E, B220 IHC staining, and PNA staining on consecutive splenic sections from mice immunized with SRBCs. Spleens were analyzed nine days after immunization. Scale = 100µm.

B-C, GC (B) numbers, or (C) individual area, based on PNA staining. Dots represent individual (B) animals or (C) GCs. Results for five animals per genotype.

D, Flow Cytometry (FC) analysis of Myd88$^{L252P/WT}$ and Myd88$^{WT/WT}$ relative contribution to B cells and GCB, based on CD45 allele frequencies.

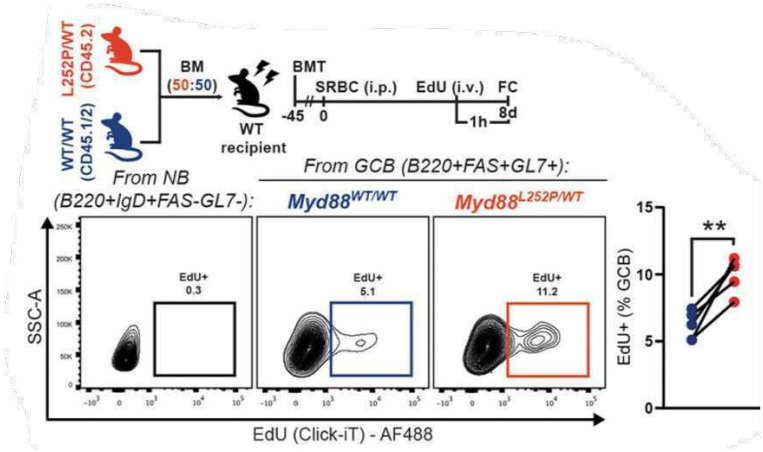

Figure 2. Myd88^{L252P} confers a proliferative advantage to GCB. (Venturutti *et al.*)
FC analysis of EdU incorporation by GCB. NB indicates non-proliferating cells.

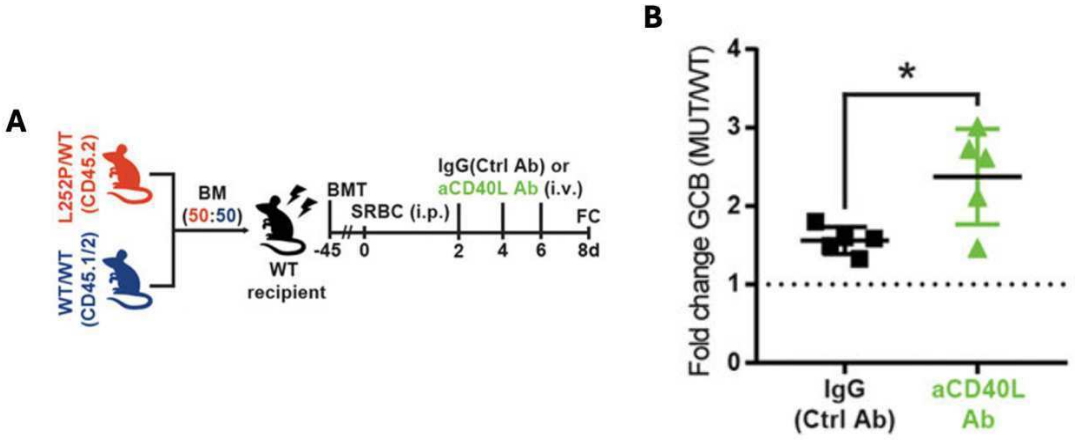

Figure 3. Myd88^{L252P} lowers the requirement for T-cell-derived co-stimulatory signals. (Venturutti *et al.*)
A, Experimental scheme for B.
B, FC analysis of the ratio of mutant and WT GCB.

Myd88^{L252P} triggers an aged/autoimmune-like program in GCB

To gain mechanistic insight into the observed GCB phenotype, an RNA-Seq analysis of Myd88^{L252P} LZ GCB was conducted (fig. 4.A). Pathway analysis revealed enrichment for advanced-stage DLBCL and WM signatures, underlying the reliability of this mouse model to recapitulate MYD88^{L265P} effects in human lymphomas (fig. 4.A). Mutant GCB showed increased expression of genes involved in proliferation and apoptosis (fig. 4.A), which is in line with the proliferative advantage observed in the experiments mentioned above (fig. 2). Moreover, as expected from the experiments shown in fig. 3, the transcriptional profile of mutant GCB is depleted of Tfh signatures, which further confirms a

lower reliance on T-cell help. Cell migration and chemotaxis signatures were enriched (fig. 4.A), which could relate to the highly prevalent extranodal presentation of MYD88^{L265P} tumors.

Most interestingly, the analysis revealed that Myd88^{L252P} mutation in germinal center B cells induced a gene expression program resembling that of aged/autoimmune B cells. In fact, Myd88^{L252P} GCB exhibited enhanced interferon-gamma (IFNγ) signaling (fig. 4.A), which induces the expression of the transcription factor T-BET in B cells, and drives the formation of "aged/autoimmune" B cells (AiBCs). In line with this, Myd88^{L252P} showed enrichment for signatures linked to autoimmune diseases like Systemic Lupus Erythematosus (fig.. 4.A).

These findings indicate that Myd88^{L252P} mutation can drive a transcriptional rewiring of GCB towards the AiBC-like phenotype. Venturutti *et al.* explored whether this actually resulted in the generation of AiBC-like Memory B Cells (MBC), discovering that a significantly higher fraction of GC-derived MBC co-expressed the canonical AiBC markers CD11b/CD11c in Myd88^{L252P} mice compared to WT (fig. 4.B). This shows that Myd88^{L252P} mutation causes a cumulative expansion of AiBC-like MBCs.

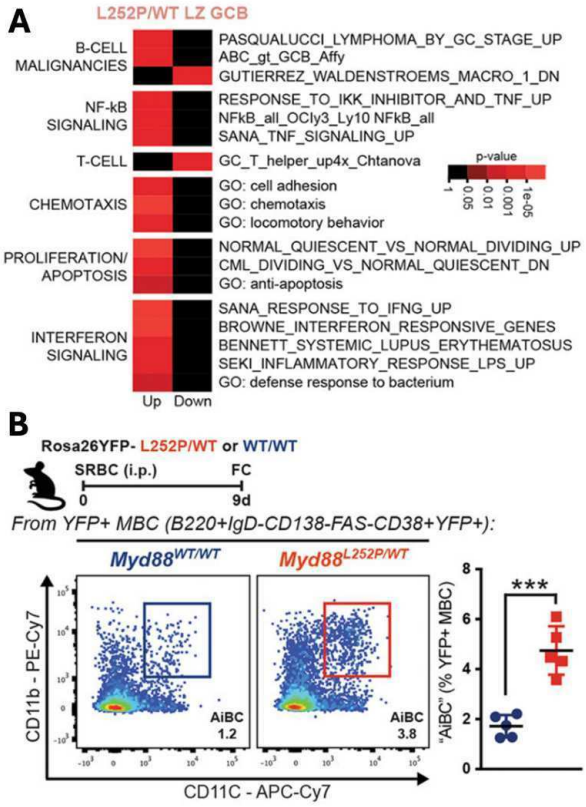

Figure 4. Myd88^{L252P} mutation triggers an aged/autoimmune-like program in GCBs. (Venturutti *et al.*)
A, Pathway analysis for differentially expressed genes in Myd88$^{L252P/WT}$ LZ GCB from mice immunized with SRBCs.
B, FC analysis of CD11b^{+}CD11c^{+}.

Accumulation of AiBC-like memory B cells leads to lymphoma development

Considering that Myd88^{L252P} mutation is associated with DLBCL and extranodal lymphoma dissemination, Venturutti *et al*. explored whether there was a correlation between the accumulation of AiBC-like memory B cells and lymphoma development. To investigate this, they used CD19Cre;Myd88^{L252P} mice, which express the mutation in all B cells. These mice develop lymphadenopathy and occasional lymphomas with old age (median survival ~70 weeks [7]). Strikingly, by cytofluorimetric analysis of splenic and extranodal tumor B cells, Venturutti *et al.* reported that, while a fraction of all splenic activated (IgD-) B cells expressed CD11b and/or T-BET, more than 90% of tumor cells expressed one or both of these markers (fig. 5). This observation supports the idea that MCD tumors arise from AiBC-like MBC that accumulate in the GC of Myd^{L252P} mutant mice.

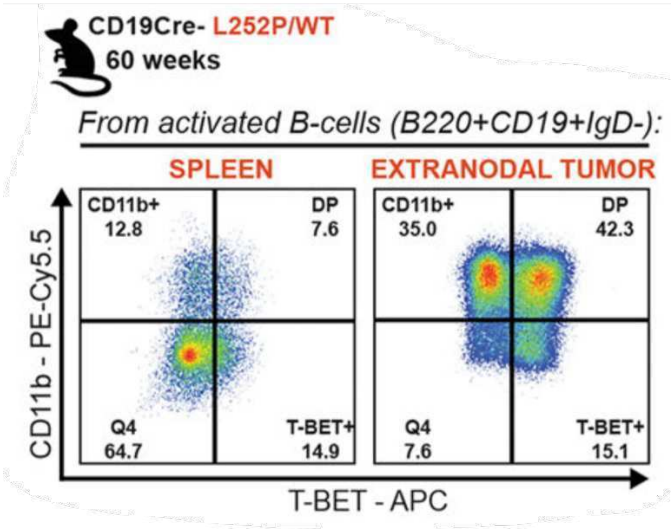

Figure 5. Myd88^{L252P} mutation causes a cumulative expansion of AiBC-like MBCs. (Venturutti *et al.*)
FC analysis of T-BET and CD11b expression in activated B cells from the spleen or extranodal tumor of non-immunized mice.

Human ABC-DLBCL tumors exhibit AiBC-like features

To check if the pathogenetic mechanism observed in mice could also occur in human lymphomas, Venturutti *et al*. analyzed the transcriptional profiles of primary tumors from the NCI and BCCA cohorts. ABC-DLBCL patients from both cohorts showed significantly higher TBX21 (T-BET) expression than GCB-DLBCLs (fig. 6.A). This confirms that even human ABC-DLBCL, which includes MYD-mutant tumors, exhibit AiBC-like features. Moreover, MCD, the DLBCL subtype with the highest frequency of extranodal dissemination, showed the highest levels of TBX21 among ABC-DLBCLs only after N1 tumors (another subtype thought to originate from MBC) (fig. 6.B). These analyses, supported by experiments on mice, suggest that an AiBC program defines the transformation of DLBCL and leads to their extranodal dissemination.

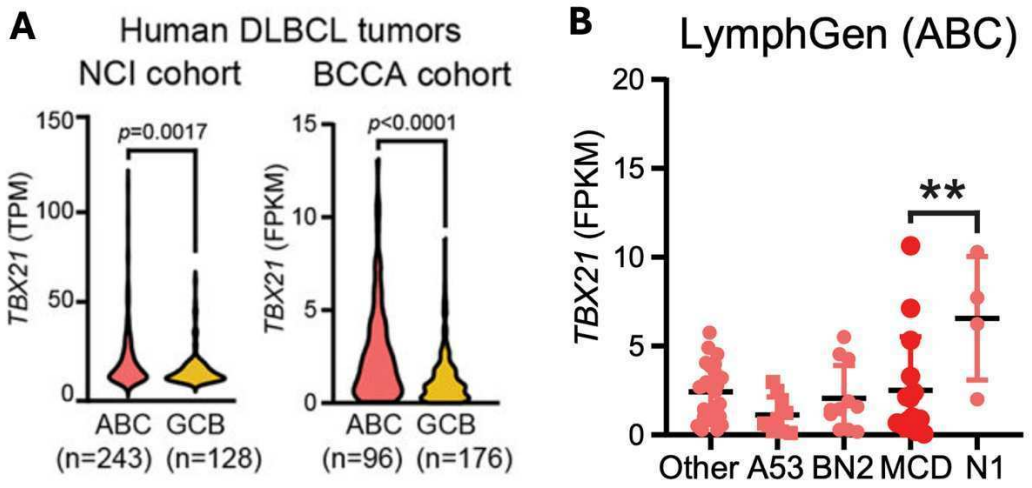

Figure 6. ABC-DLBCL tumors exhibit higher TBX21 expression, an AiBC-like feature, than GCB-DLBCLs. (Venturutti *et al.*)
A, Analysis of the transcriptional profiles of primary tumors from the NCI and BCCA cohorts.
B, RNA-Seq-based expression levels of TBX21 based on the LymphGen subclassification of ABC-DLBCL tumors from the BCCA cohort.

Discussion

The paper by Venturutti *et al.* delves into the molecular underpinnings of MCD-DLBCL, the type of DLBCL with the highest frequency of extranodal dissemination. Their work mainly focuses on a novel aged/autoimmune B cell population induced by $MYD88^{L265P}$ mutation, which is carried by most MCD-DLBCL patients presenting with extranodal dissemination. Venturutti *et al.* showed that $MYD88^{L265P}$ mutation confers a significant survival and proliferative advantage to GC B cells and directs them toward a memory B-cell fate. Memory B cells carrying this mutation can progress to MCD-DLBCL, contrasting with the previous belief that MCD-DLBCL originates from plasmablasts.

The MCD founder mutation MYD^{L265P} initiates a transcriptional program characterized by T-BET expression in murine GCBs, resembling that of aged/autoimmune B cells (AiBCs). MYD^{L265P}-driven transcriptional rewiring promotes self-reactivity and dysregulated immune responses, which can account for autoimmunity but also lymphomagenesis. Thus, this paper suggests that lymphoma and autoimmunity may exist simultaneously, challenging their traditional consideration as separate phenotypes.

Most importantly, by discovering that AiBCs represent the premalignant precursor population of MCD-DLBCL, Venturutti *et al*. point to this phenotype as a marker for the early detection of extranodal lymphomas. However, further research is needed to understand how T-BET and other activated B-cell features contribute to extranodal lymphomagenesis and their potential as predictive biomarkers for disease progression and treatment outcomes.

Internship

During my internship at Alessandro Carrer's laboratory at the Veneto Institute of Molecular Medicine (VIMM) in Padua, I explored the age-associated impairment of the GC reaction from an epigenetic point of view. I contributed to a broader project that studies the relationship between metabolism and epigenetic modifications during B cell development. Preliminary work from the Carrer laboratory identified an acetyl-CoA-dependent metabolic-epigenetic axis that sustains B cell activation in response to GC stimuli. This axis is centered on ATP-Citrate Lyase (ACLY), the main source of nucleo-cytosolic acetyl-CoA serving histone acetylation. Significantly, my colleagues proved that ACLY-dependent acetylation of nuclear histones promotes B-cell differentiation and the GC reaction *(unpublished data)*.

Older individuals fail to mount efficient humoral immunity in response to infection or vaccination. This can be mainly explained by the inability of naïve B cells to engage reactive GCs. Building on the evidence that epigenetic modifications support functional GC reaction [1], I tested whether an age-associated decline of immune functions could be attributed to epigenetic dysregulation of GC B cells. Particularly, I focused on the metabolic-epigenetic axis that my research team had previously identified and assessed histone acetylation levels at GCs of young and old mice and humans. First, I performed an immunohistochemistry analysis of formalin-fixed paraffin-embedded lymph nodes from healthy donors. I observed that histone acetylation at GCs decreases in aged individuals (> 70 years old) compared to younger donors (< 40 years old) (fig. 7.A). Second, I observed the same trend on the spleens of young (3-months old) and old (18-months old) SRBCs-immunized mice (fig. 7.B).

Based on the evidence I gathered during my internship, the project now aims to understand if epigenetic dysregulation of GC B cells during aging is linked to a rewiring of acetyl-CoA metabolism. In line with the preliminary finding that ACLY activity supports histone acetylation in activated B cells, ACLY-dependent histone acetylation may also sustain the GC reaction. In this view, the reduction in GC B cells histone acetylation which I reported might result from reduced acetyl-CoA production by ACLY.
The long-term goal of this project is to find metabolic targets that sustain the humoral response through epigenetic rearrangements of GC B cells in order to counteract humoral immune aging.

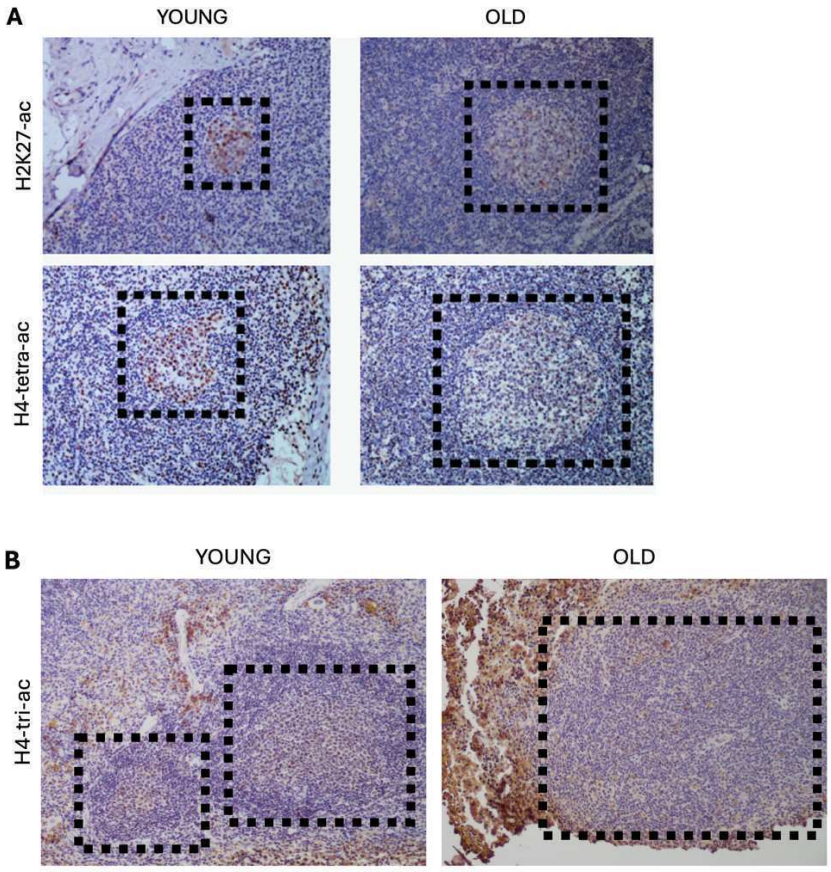

Fig 7: histone acetylation at GCs decreases with age in humans and mice. Boxes indicate B cell follicles—20x objective.
A, IHC analysis of FFPE human lymph nodes.
B, IHC analysis of FFPE murine spleens. Mice were immunized by intraperitoneal injection of SRBCs.

Bibliography

[1] Mlynarczyk C, Fontán L, Melnick A. Germinal center-derived lymphomas: The darkest side of humoral immunity. *Immunol Rev.* 2019;288:214-239. doi: 10.1111/imr.12755.

[2] Basso K, Dalla-Favera R. Germinal centers and B cell lymphomagenesis. *Nat Rev Immunol.* 2015 Mar;15(3):172-184. doi: 10.1038/nri3814.

[3] National Cancer Institute. SEER Cancer Stat Facts: Diffuse Large B-Cell Lymphoma (DLBCL). https://seer.cancer.gov/statfacts/html/dlbcl.html.

[4] Bakhshi TJ, Georgel PT. Genetic and epigenetic determinants of diffuse large B-cell lymphoma. *Blood Cancer J.* 2020;10(12):123. Published 2020 Dec 4. doi:10.1038/s41408-020-00389-w.

[5] Wright GW, Huang DW, Phelan JD, et al. A Probabilistic Classification Tool for Genetic Subtypes of Diffuse Large B Cell Lymphoma with Therapeutic Implications. *Cancer Cell.* 2020 Apr 13;37(4):551-568.e14. doi: 10.1016/j.ccell.2020.03.015.

[6] Kiripolsky J, Kasperek EM, Zhu C, et al. Immune-Intrinsic Myd88 Directs the Production of Antibodies With Specificity for Extracellular Matrix Components in Primary Sjögren's Syndrome. *Front Immunol.* 2021 Jul 26;12:692216. doi: 10.3389/fimmu.

[7] Knittel G, Liedgens P, Korovkina D, et al. B-cell-specific conditional expression of Myd88p.L252P leads to the development of diffuse large B-cell lymphoma in mice. *Blood.* 2016 Jun 2;127(22):2732-2741. doi: 10.1182/blood-2015-11-684183.

[8] Rubtsova K, Rubtsov AV, Cancro MP, Marrack P. Age-Associated B Cells: A T-BET-Dependent Effector with Roles in Protective and Pathogenic Immunity. *J Immunol.* 2015 Sep 1;195(5):1933-1937. doi: 10.4049/jimmunol.1501209.

[9] Meyer SN, Scuoppo C, Vlasevska S, et al. Unique and Shared Epigenetic Programs of the CREBBP and EP300 Acetyltransferases in Germinal Center B Cells Reveal Targetable Dependencies in Lymphoma. *Immunity.* 2019;51(3):535-547.e9. doi:10.1016/j.immuni.2019.08.006.

Thesis Writing and Artificial Intelligence

In preparing this thesis, two AI tools, namely Grammarly and ChatGPT, were utilized, each serving distinct purposes across different sections of the work. The use of these AI tools in this thesis fully aligns with the University of Padua's regulations, ensuring that all academic standards are upheld.

Grammarly was employed throughout the entire thesis for language refinement, ensuring grammatical accuracy, clarity, and precision in word choice. Its role was strictly confined to enhancing the linguistic quality of the text without influencing the content.

ChatGPT, on the other hand, was specifically used in the methods section to improve the quality of general descriptions. The AI-generated content often contained inaccuracies or needed to be completed. Consequently, every description generated by ChatGPT was rigorously checked against academic literature before being accepted. Furthermore, the descriptions provided by ChatGPT were never perfect or complete as generated; substantial modifications and instructions were applied to ensure their accuracy and adequacy, which took a significant amount of time. However, AI assistance has contributed to improving the quality of the general descriptions of the methods.

The detailed explanation of how the methods were applied in the research papers analyzed in this thesis and during the internship was entirely the product of independent intellectual effort. The integration of AI in this context should be regarded as a skillful application of emerging technology rather than a shortcut that reduces effort. As AI becomes an increasingly integral part of academic work, it is crucial to embrace these tools for their potential benefits while maintaining a solid commitment to intellectual rigor. This thesis demonstrates how AI can effectively support the research process without compromising scholarly integrity, exemplifying a balanced approach to leveraging technology in academic writing.

Appendix

RESEARCH ARTICLE

An Aged/Autoimmune B-cell Program Defines the Early Transformation of Extranodal Lymphomas

Leandro Venturutti[1,2,3], Martin A. Rivas[4], Benedikt W. Pelzer[4,5], Ruth Flümann[6,7], Julia Hansen[6,7], Ioannis Karagiannidis[4], Min Xia[4], Dylan R. McNally[4], Yusuke Isshiki[4], Andrew Lytle[1], Matt Teater[4], Christopher R. Chin[4,8,9], Cem Meydan[8,9], Gero Knittel[10], Edd Ricker[11], Christopher E. Mason[8,9], Xiaofei Ye[12], Qiang Pan-Hammarström[12], Christian Steidl[1,3], David W. Scott[1,3,13], Hans Christian Reinhardt[10], Alessandra B. Pernis[11], Wendy Béguelin[4], and Ari M. Melnick[4]

ABSTRACT

A third of patients with diffuse large B-cell lymphoma (DLBCL) present with extranodal dissemination, which is associated with inferior clinical outcomes. *MYD88*^{L265P} is a hallmark extranodal DLBCL mutation that supports lymphoma proliferation. Yet extranodal lymphomagenesis and the role of *MYD88*^{L265P} in transformation remain mostly unknown. Here, we show that B cells expressing *Myd88*^{L252P} (*MYD88*^{L265P} murine equivalent) activate, proliferate, and differentiate with minimal T-cell costimulation. Additionally, *Myd88*^{L252P} skewed B cells toward memory fate. Unexpectedly, the transcriptional and phenotypic profiles of B cells expressing *Myd88*^{L252P}, or other extranodal lymphoma founder mutations, resembled those of CD11c^{+}T-BET^{+} aged/autoimmune memory B cells (AiBC). AiBC-like cells progressively accumulated in animals prone to develop lymphomas, and ablation of T-BET, the AiBC master regulator, stripped mouse and human mutant B cells of their competitive fitness. By identifying a phenotypically defined prospective lymphoma precursor population and its dependencies, our findings pave the way for the early detection of premalignant states and targeted prophylactic interventions in high-risk patients.

SIGNIFICANCE: Extranodal lymphomas feature a very poor prognosis. The identification of phenotypically distinguishable prospective precursor cells represents a milestone in the pursuit of earlier diagnosis, patient stratification, and prophylactic interventions. Conceptually, we found that extranodal lymphomas and autoimmune disorders harness overlapping pathogenic trajectories, suggesting these B-cell disorders develop and evolve within a spectrum.

See related commentary by Leveille et al. (Blood Cancer Discov 2023;4:8–11).

[1]Centre for Lymphoid Cancer, BC Cancer, Vancouver, British Columbia, Canada. [2]Terry Fox Laboratory, BC Cancer, Vancouver, British Columbia, Canada. [3]Department of Pathology and Laboratory Medicine, University of British Columbia, Vancouver, British Columbia, Canada. [4]Division of Hematology/Oncology, Department of Medicine, Weill Cornell Medicine, New York, New York. [5]Mildred Scheel School of Oncology Aachen Bonn Cologne Düsseldorf (MSSO ABCD), Faculty of Medicine and University Hospital of Cologne, Cologne, Germany. [6]Department I of Internal Medicine, University Hospital Cologne, Cologne, Germany. [7]Max Planck Institute for Biology of Ageing, Cologne, Germany. [8]Department of Physiology and Biophysics, Weill Cornell Medicine, New York, New York. [9]The HRH Prince Alwaleed Bin Talal Bin Abdulaziz Alsaud Institute for Computational Biomedicine and the WorldQuant Initiative for Quantitative Prediction, Weill Cornell Medicine, New York, New York. [10]Department of Hematology and Stem Cell Transplantation, West German Cancer Center, University Hospital of Essen, University of Duisburg-Essen, Essen, Germany. [11]Autoimmunity and Inflammation Program, Hospital for Special Surgery, New York, New York. [12]Department of Biosciences and Nutrition, Karolinska Institutet, Huddinge, Stockholm, Sweden. [13]Department of Medicine, University of British Columbia, Vancouver, British Columbia, Canada.

Corresponding Authors: Leandro Venturutti, Centre for Lymphoid Cancer and Terry Fox Laboratory, BC Cancer Research Institute, 675 West 10th Avenue, Vancouver, BC V5Z 1L3, Canada. Phone: 604-675-8000; Fax: 604-877-0712; E-mail: lventurutti@bccrc.ca; and Ari M. Melnick, Division of Hematology/Oncology, Department of Medicine, Weill Cornell Medicine, 413 East 69th Street, New York, NY 10021. Phone: 646-962-6725; Fax: 646-962-0576; E-mail: amm2014@med.cornell.edu

Cancer Discov 2023;13:216–43

doi: 10.1158/2159-8290.CD-22-0561

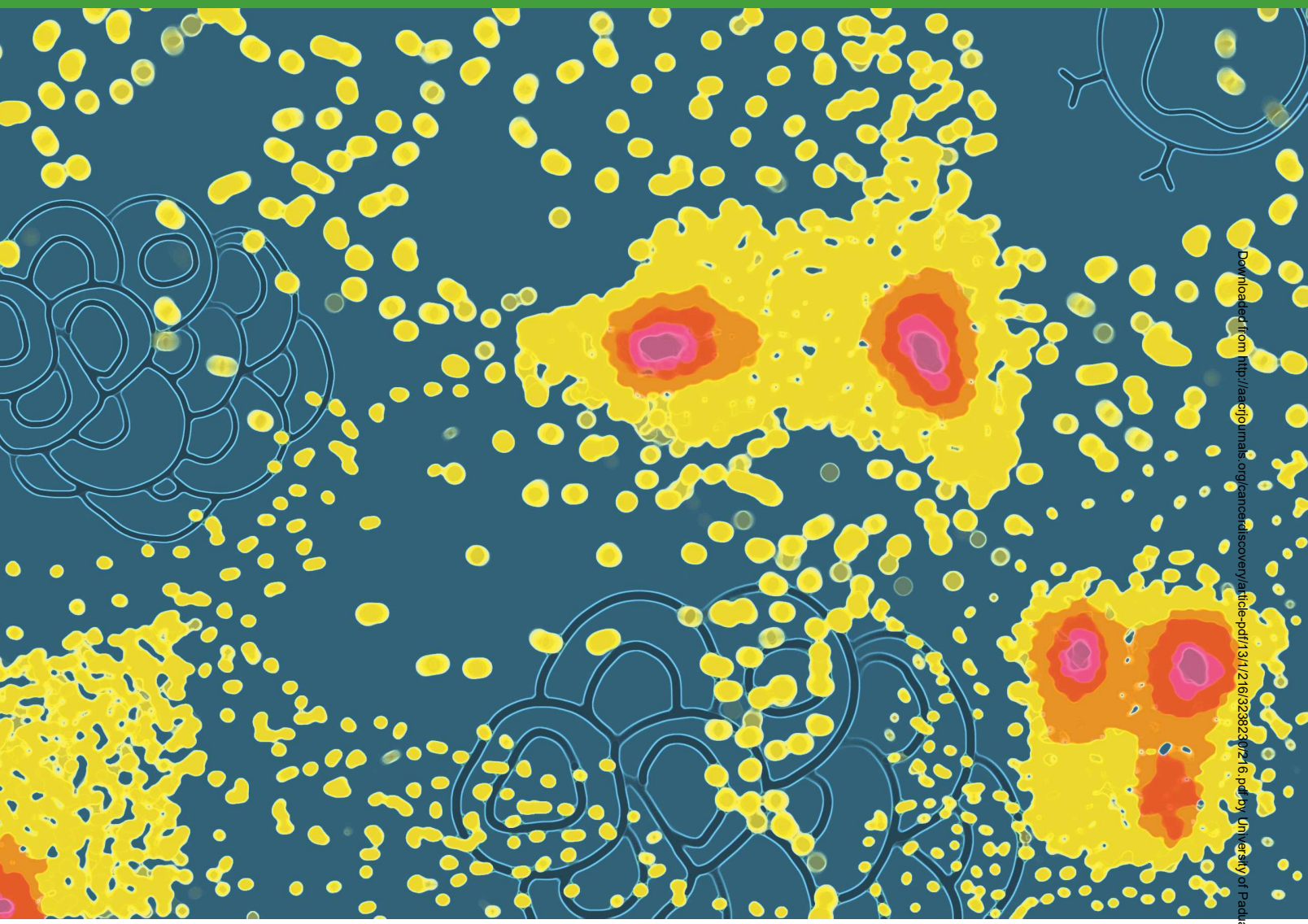

INTRODUCTION

Diffuse large B-cell lymphomas (DLBCL) are biological and clinically heterogeneous diseases that develop from mature activated B cells (1). Under normal circumstances, B-cell activation requires stimulation of the B-cell receptor (BCR) by a cognate antigen and costimulation from specialized T cells (2). Fully activated B cells can form transient structures called germinal centers (GC), in which they undergo somatic hypermutation (SHM) and compete for T-cell help to promptly expand and improve the affinity of their BCR against foreign antigens, before differentiating into effector cells, namely, plasma cells (PC; antibody-secreting cells) or memory B cells (MBC; long-lived cells that activate upon antigen reencounter, enabling faster and enhanced responses; ref. 3). These fine-tuned processes require B cells to be transiently endowed with tumorigenic-like features (heightened proliferation, genomic instability, tolerance to DNA damage, dysregulated metabolism, cell death escape, etc.), which are hijacked and perpetuated by mutations in lymphomas (4). These mutations are believed to largely arise as aberrant by-products of SHM, a process catalyzed by the enzyme activation-induced cytidine deaminase (AID/*AICDA*; ref. 3).

Although DLBCLs frequently initiate from, and localize to, the lymph nodes, one third of patients present with extranodal tumors in nonlymphoid organs, including immune-privileged sites, with an often fatal outcome (5–7). Extranodal DLBCLs manifest in advanced stages of the nodal disease or occur as primary events. The localization of these aggressive tumors and their elevated relapse rates (5) create significant clinical challenges. Standard DLBCL treatments (ref. 1; chemotherapy, anti–B-cell antibodies, and radiotherapy) are insufficient to cure most patients and carry significant toxicity. Moreover, there is no way to identify their onset at early stages, when they may be more susceptible to targeted therapies.

Recent large-scale profiling efforts have yielded a genetically defined classification for DLBCLs, including the identification of a highly aggressive subtype called "C5"/"MCD" (hereafter MCD) with the highest frequency of extranodal dissemination (8, 9). MCD and primary extranodal tumors in

immune-privileged sites share founder mutations targeting *MYD88* [core Toll-like-receptor (TLR) signaling mediator], *CD79B* (BCR complex component), *TBL1XR1* (transcriptional repression complexes component), and others (8, 9). Approximately 70% of these carry an *MYD88*^{L265P} gain-of-function missense mutation (9) that facilitates proliferation and survival through constitutive NF-κB signaling (10). This same mutation occurs in other B-cell malignancies, including Waldenstrom macroglobulinemia (WM) and chronic lymphocytic leukemia (11, 12), highlighting its widespread biological relevance. Mice expressing *Myd88*^{L252P} (murine equivalent to *MYD88*^{L265P}) in all B cells develop lymphadenopathy and occasional lymphomas with old age (13). A combination of *Myd88*^{L252P} with BCL2 overexpression, a common feature in MCD-DLBCLs (8, 9), results in a higher incidence of lymphomas that closely resemble their human counterparts (14). However, the mechanisms through which these tumors arise from the immune system and progress to an overt and advanced disease remain unknown.

MCD tumors show the highest AID activity footprint, suggesting that these have transited through the GC during transformation (8). Still, *AICDA* is expressed in activated B cells before entering the GC (15), and even in proliferating B cells outside of lymphoid follicles (16), suggesting that MCD precursors could resort to alternative activated states to accumulate mutations (17). Because the immune system keeps a tight control on B-cell activation through selective costimulation, we hypothesized that MCD founder mutations altered these requirements, enabling the progressive transformation and expansion of lymphoma precursors. Here, we explore the evolutionary advantage conferred to mature B cells by the hallmark mutation *MYD88*^{L265P}, as well as the pathogenic trajectories delineated by this mutation, to provide critical insight into extranodal lymphoma transformation and the precursor populations involved.

RESULTS

Myd88 Mutations Confer a Competitive Advantage to GC B Cells

To dissect how MCD founder mutations shape pathogenic trajectories, we first explored the impact of the class-defining lesion *MYD88*^{L265P} on the GC. We crossed an existing Cre-inducible *Myd88*^{L252P} mouse model (13) to the Cγ1Cre strain (18), restricting MYD88-mutant expression to (pre-) GC B cells (GCB) and GC-derived cells. We immunized young *Cγ1Cre;Myd88*$^{L252P/WT}$ or *Cγ1Cre;Myd88*$^{WT/WT}$ [wild-type (WT)] mice with the T cell–dependent antigen sheep red blood cells (SRBC) and profiled spleens at the peak of the GC. Although B-cell levels were unaltered (Fig. 1A; Supplementary Fig. S1A), *Myd88*$^{L252P/WT}$ mice showed a significant increase in the fraction (Fig. 1B) and absolute number (Supplementary Fig. S1B) of FAS$^+$GL7$^+$ GCBs. This expansion extended to GCBs with a mature phenotype (FAS$^+$CD38$^-$; Supplementary Fig. S1C). An alternative T cell–dependent antigen yielded similar results (Supplementary Fig. S1D). In line with these findings, IHC staining for B cells (B220) and GCBs [peanut agglutinin (PNA)] revealed intact follicles harboring an increase in GC number and size in *Myd88*$^{L252P/WT}$ mice (Fig. 1C–E).

To test whether *Myd88*^{L252P} enhanced the competitive fitness of GCB, we conducted mixed chimera experiments in which equal numbers of *Cd45.2;Myd88*$^{L252P/WT}$ or *Cd45.1/2;Myd88*$^{WT/WT}$ bone marrow (BM) cells were transplanted into irradiated WT recipients. Following immunization, *Myd88*^{L252P} GCBs manifested a significant competitive advantage, whereas the proportions of CD45.2$^+$ and CD45.1/2$^+$ total B cells were comparable (Fig. 1F). To dissect the kinetics of this advantage, we investigated additional time points following immunization. Although the GC response in chimeric mice showed the expected profile and duration (Fig. 1G, left), *Myd88*^{L252P} GCBs were consistently expanded and developed cumulative dominance over time (Fig. 1G, center and right). These results indicate that GCBs harboring *MYD88* mutations are endowed with a significant competitive advantage.

Myd88-Mutant GCB Exhibit Increased Proliferative Capacity

The size of the GC is determined through a fine-tuned balance between proliferation and cell death (3). Notably, the fraction of apoptotic GCBs was comparable in WT and *Myd88*$^{L252P/WT}$ mice, as assessed by cleaved caspase (Supplementary Fig. S2A) or Annexin V/DAPI (Supplementary Fig. S2B) staining, suggesting aberrant survival does not explain *Myd88*^{L252P} GCB fitness. On the other hand, *Myd88*^{L252P} GCB showed increased levels of the proliferation marker Ki-67 as compared with WT (Fig. 2A). Similarly, mutant GCBs exhibited higher incorporation of 5-ethynyl-2-deoxyuridine (EdU; Fig. 2B), indicative of increased DNA synthesis and proliferation. Notably, although the fraction of proliferating WT GCBs progressively decreased over the GC as expected (19), the proportion of Ki-67$^+$ *Myd88*^{L252P} GCBs remained elevated and fairly constant (Fig. 2C). These differences align with the observed cumulative expansion of *Myd88*$^{L252P/WT}$ GCBs (Fig. 1G).

To gain insight into the proliferative capacity of *Myd88*$^{L252P/WT}$ B cells, we used an established culture system in which naïve B cells (NB) exposed to high levels of costimulatory signals develop a GC-like phenotype (iGCB; refs. 20, 21). To avoid artifactual effects related to the extent and timing of Cγ1Cre-induced recombination *ex vivo*, we isolated NB from *CD19Cre;Myd88*$^{L252P/WT}$ or *CD19Cre;Myd88*$^{WT/WT}$ mice. Although both WT and mutant B cells acquired an iGCB profile to a similar extent (see below), *Myd88*$^{L252P/WT}$ iGCB divided faster, as revealed by accelerated proliferation dye dilution (Supplementary Fig. S2C). These results suggest that the proliferative advantage of *Myd88*$^{L252P/WT}$ GCB is supported, at least in part, through a cell-intrinsic effect.

Myd88 Mutations Blur the Separation between GC Cell Compartments

The GC reaction is made up of anatomically and functionally specialized compartments; the dark zone (DZ; CXCR4$^+$CD86$^-$) and light zone (LZ; CXCR4$^-$CD86$^+$). Positively selected GCBs undergo repeated rounds of division in the DZ (3). In line with the increase in proliferating GCBs, *Myd88*^{L252P} mice showed relative expansion of DZ GCBs (Supplementary Fig. S2D), and *Myd88*^{L252P} GCBs preferentially acquired a DZ profile in chimeric mice (Fig. 2D). This became more pronounced at later stages in the GC

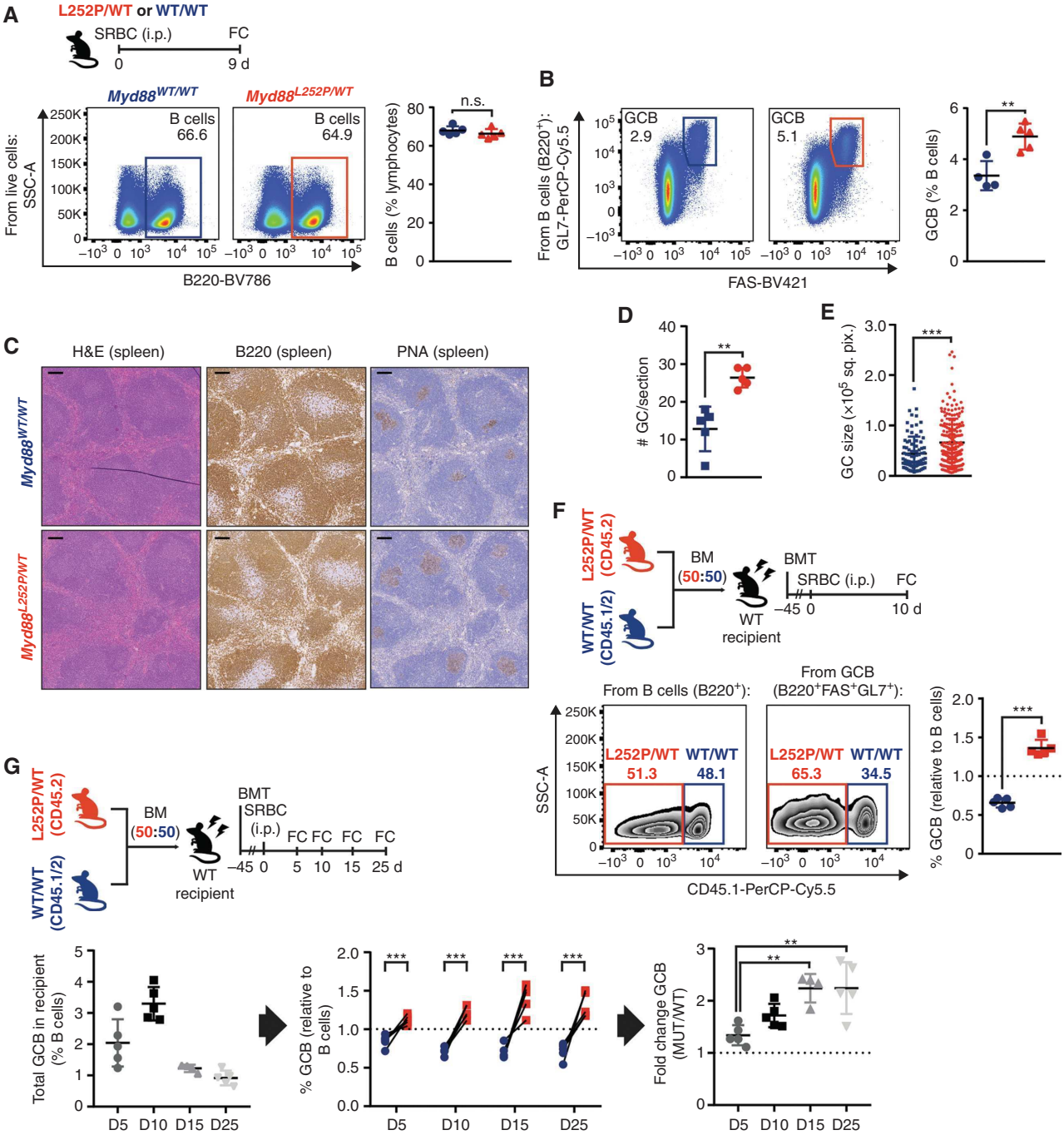

Figure 1. *Myd88* mutations increase the competitive fitness of GCB. **A** and **B,** Flow cytometry (FC) analysis of splenic B cells (**A**) or GCBs (**B**). SSC-A, side scatter area. **C,** Hematoxylin and eosin (H&E), B220 IHC, and PNA IHC in consecutive splenic sections from animals treated as in **A**. Scale bars, 100 m. **D** and **E,** GC numbers (**D**) or individual area (**E**), based on PNA staining. Dots represent individual animals (**D**) or GCs (**E**). Results for 5 animals per genotype. **F,** FC analysis of $Myd88^{L252P/WT}$ and $Myd88^{WT/WT}$ relative contribution to B cells and GCBs, based on CD45 allele frequencies. BMT, bone marrow transplant. **G,** FC analysis of splenic GCBs. Values represent mean ± SEM. Data reproducible with 2 repeats. n.s., not significant; **, $P<0.01$; ***, $P<0.001$, using unpaired (**A**, **B**) or paired (**F**, **G**) two-tailed Student *t* test with the two-stage step-up method of Benjamini, Krieger, and Yekutieli where applicable or Mann–Whitney *U* test (**D**, **E**).

reaction (Supplementary Fig. S2E). However, the fraction of proliferating cells (Fig. 2E) and the relative expression of Ki-67 among them (Fig. 2F) were higher in both compartments for $Myd88^{L252P}$ GCB than for WT. Thus, the increase in proliferating mutant GCBs does not simply reflect an abnormal distribution across zones but rather appears as a core feature conferred by $Myd88^{L252P}$ to all GCB, which obscures canonical compartmentalization.

To explore this, we sorted $Myd88^{L252P/WT}$ or WT GCBs from each compartment and conducted RNA sequencing

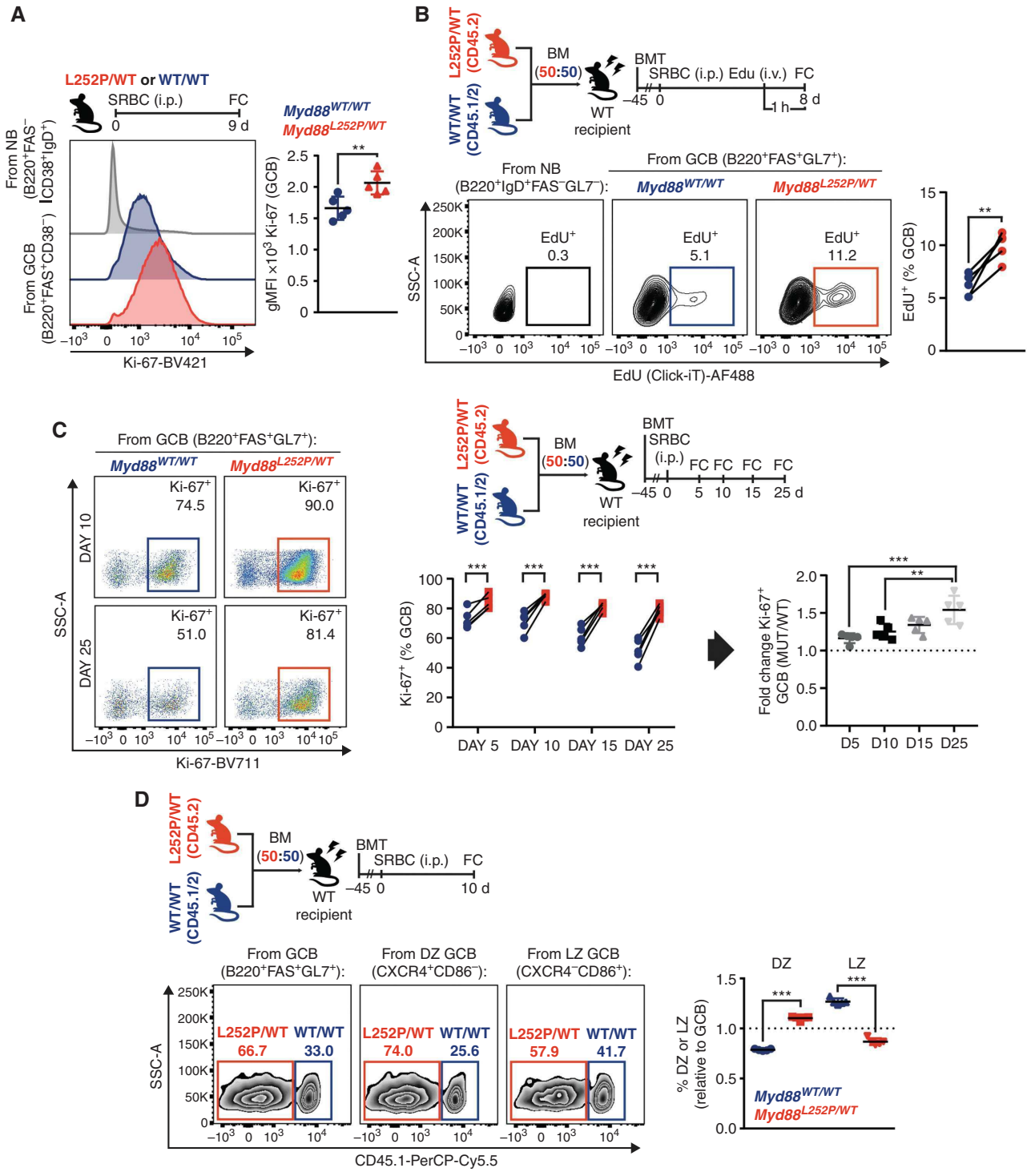

Figure 2. *Myd88* mutations confer a proliferative advantage to GCBs. **A,** Geometric mean fluorescence intensity (gMFI) of Ki-67 in splenic GCBs. **B,** Flow cytometry (FC) analysis of EdU incorporation by GCBs. NBs illustrate nonproliferating cells. BMT, bone marrow transplant; SSC-A, side scatter area. **C,** FC analysis of Ki-67+ GCBs. **D,** FC analysis of *Myd88*$^{L252P/WT}$ and *Myd88*$^{WT/WT}$ relative contribution to total, DZ, or LZ GCBs. (*continued on following page*)

(RNA-seq). Hierarchical clustering and principal component analysis revealed segregation by both *Myd88* status and cell type (Fig. 2G; Supplementary Fig. S2F). Interestingly, despite the phenotypic DZ/LZ asymmetry observed by flow cytometry (FC), *Myd88*$^{L252P/WT}$ DZ and LZ GCBs were transcriptionally closer to prototypical LZ GCBs (Fig. 2H; Supplementary Fig. S2G) and further away from prototypical DZ GCBs (Fig. 2I; Supplementary Fig. S2G) than their WT

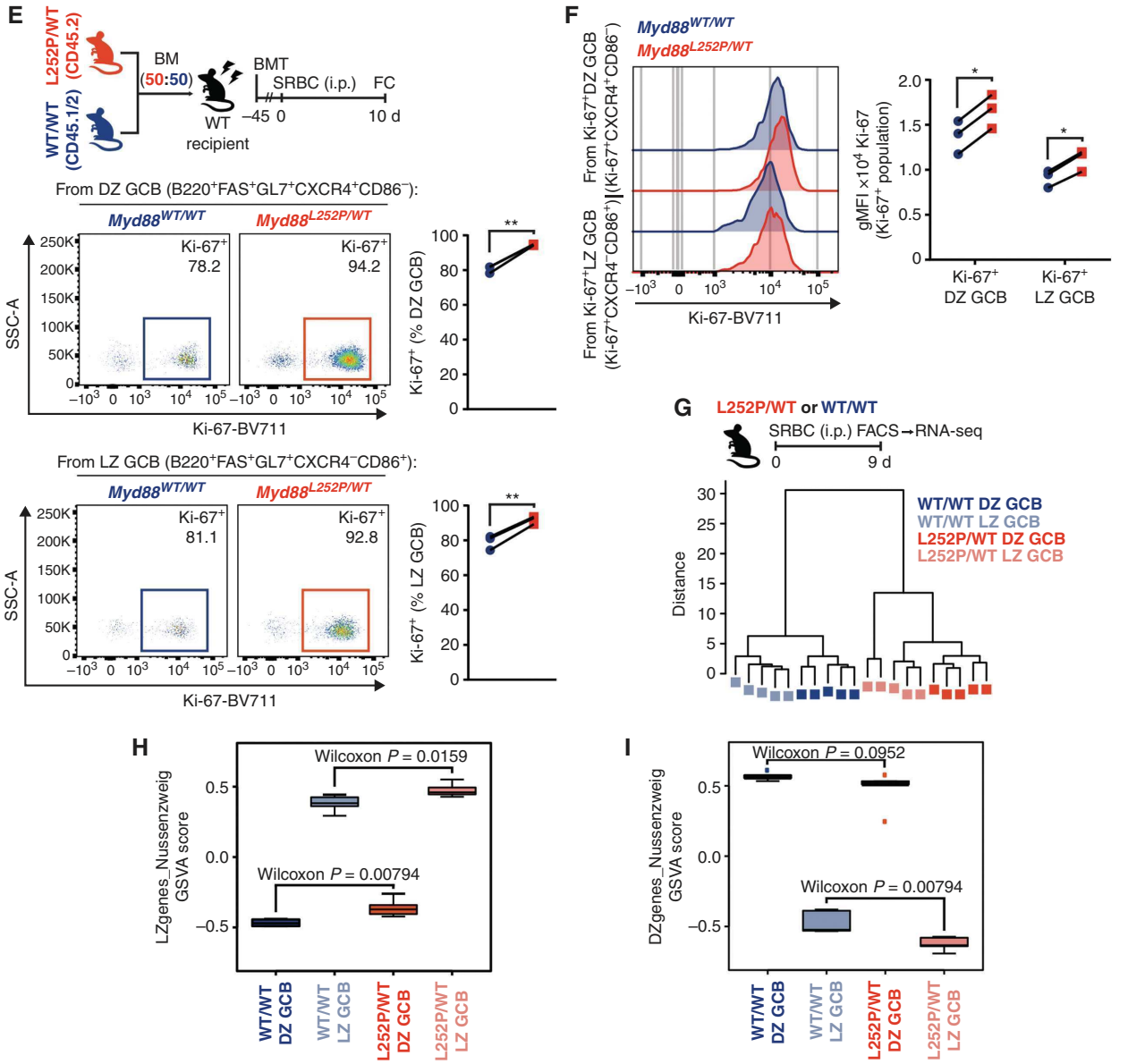

Figure 2. ***(Continued)*** **E,** FC analysis of Ki-67+ DZ and LZ GCBs from **D**. **F,** FC analysis of Ki-67 expression in Ki-67+ DZ and LZ GCBs from **E**. **G,** Hierarchical clustering, based on Euclidean distance, for RNA-seq samples from sorted GCBs. **H** and **I,** Gene set variation analysis (GSVA) for samples in **G**, relative to canonical LZ (**H**) or DZ (**I**) GCB signatures (GSE38696). Values represent mean ± SEM. *, $P < 0.05$; **, $P < 0.01$; ***, $P < 0.001$. *P* values calculated using unpaired (**A**, **D**) or paired (**B**, **C**, **E**, **F**) two-tailed Student *t* test with the two-stage step-up method of Benjamini, Krieger, and Yekutieli where applicable.

counterparts. Hence, although *Myd88*^{L252P} DZ GCBs portray canonical features, such as their proliferative status, their transcriptional identity appears more ambiguous.

Myd88 Mutations Reduce the Threshold for T cell–Derived Costimulatory Signals

B cells require costimulation to fully activate, escape cell death, and differentiate (2). In the GC, specialized follicular helper T cells (T_{FH}) provide membrane-bound (e.g., CD40L) and soluble (e.g., IL4) signals to B cells (3). Interestingly, the transcriptional profile of MCD tumors is depleted of GC T_{FH} signatures (9), which may reflect their immune evasive nature but could also suggest lower reliance on T-cell help. *Myd88*^{L252P} and WT mice showed comparable levels of CD4+ cells (Fig. 3A). *Myd88*^{L252P} mice presented an expansion of GC T_{FH} (Fig. 3B), proportional to that of GCB (Fig. 3C), suggesting that T_{FH} dosage in *Myd88*^{L252P} GCs is adequate.

On the other hand, NF-κB priming by *MYD88*^{L265P} (13) could lower signaling thresholds in B cells, enabling heightened responses with minimal T-cell help. To test whether GCB–T_{FH} cross-talk was essential for MYD88-mutant B cells, as is for WT, we administered CD40L-blocking or control antibodies to SRBC-immunized chimeric mice (Fig. 3D). In IgG control–treated mice, *Myd88*^{L252P} GCB

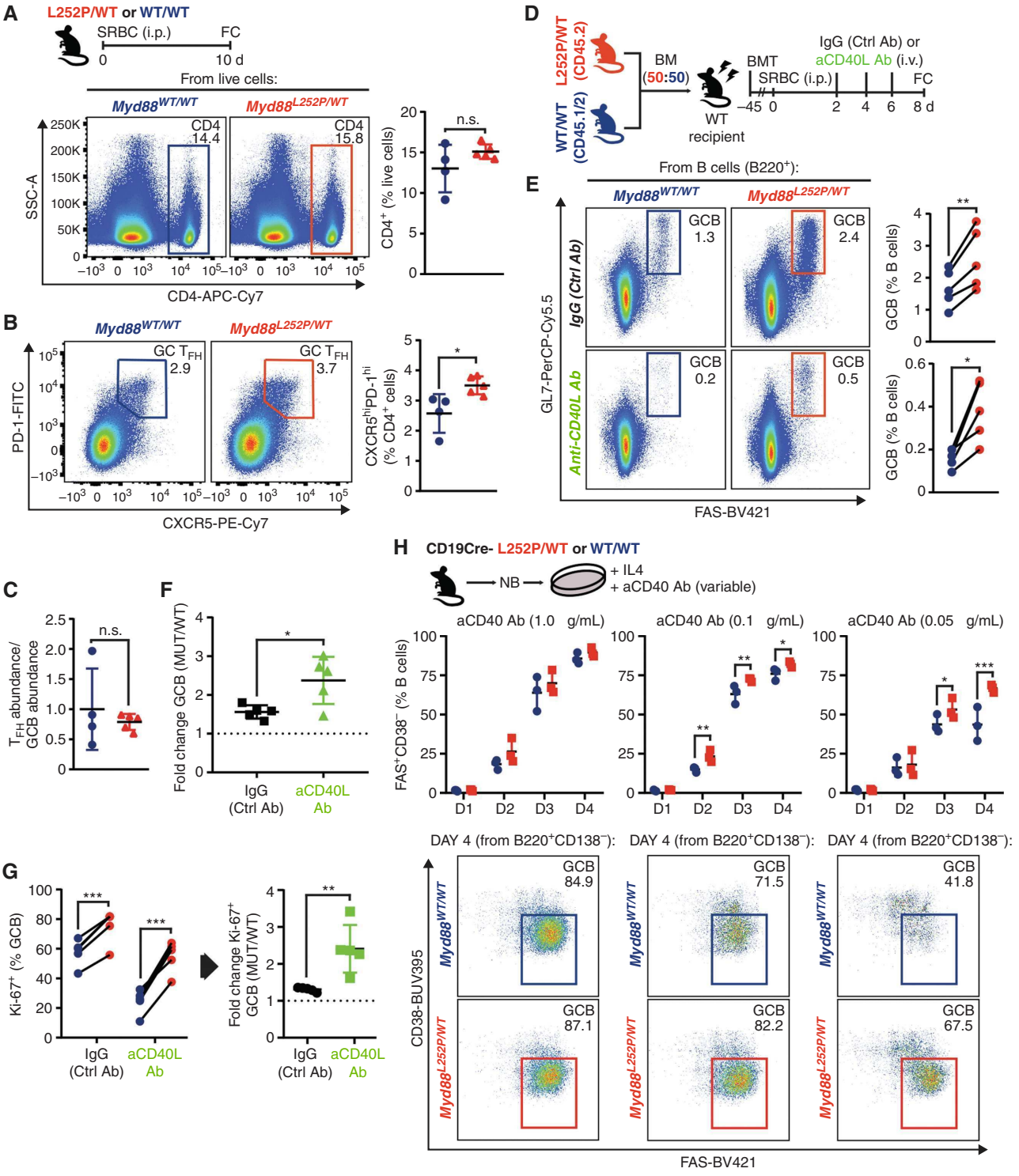

Figure 3. *Myd88* mutations lower the requirement for T cell–derived costimulatory signals. **A–C,** FC analysis of CD4+ (**A**) or GC T_{FH} (**B**) cells. SSC-A, side scatter area. **C,** GC T_{FH} abundance relative to GCB in the same animals. **D,** Experimental scheme for **E**–**G**. BMT, bone marrow transplant. **E** and **F,** FC analysis of GCBs as percentage of B cells (**E**) or change between conditions (**F**). **G,** FC analysis of Ki-67 expression in GCBs from **E**. **H,** FC analysis of iGCB with variable CD40 stimulation. (*continued on following page*)

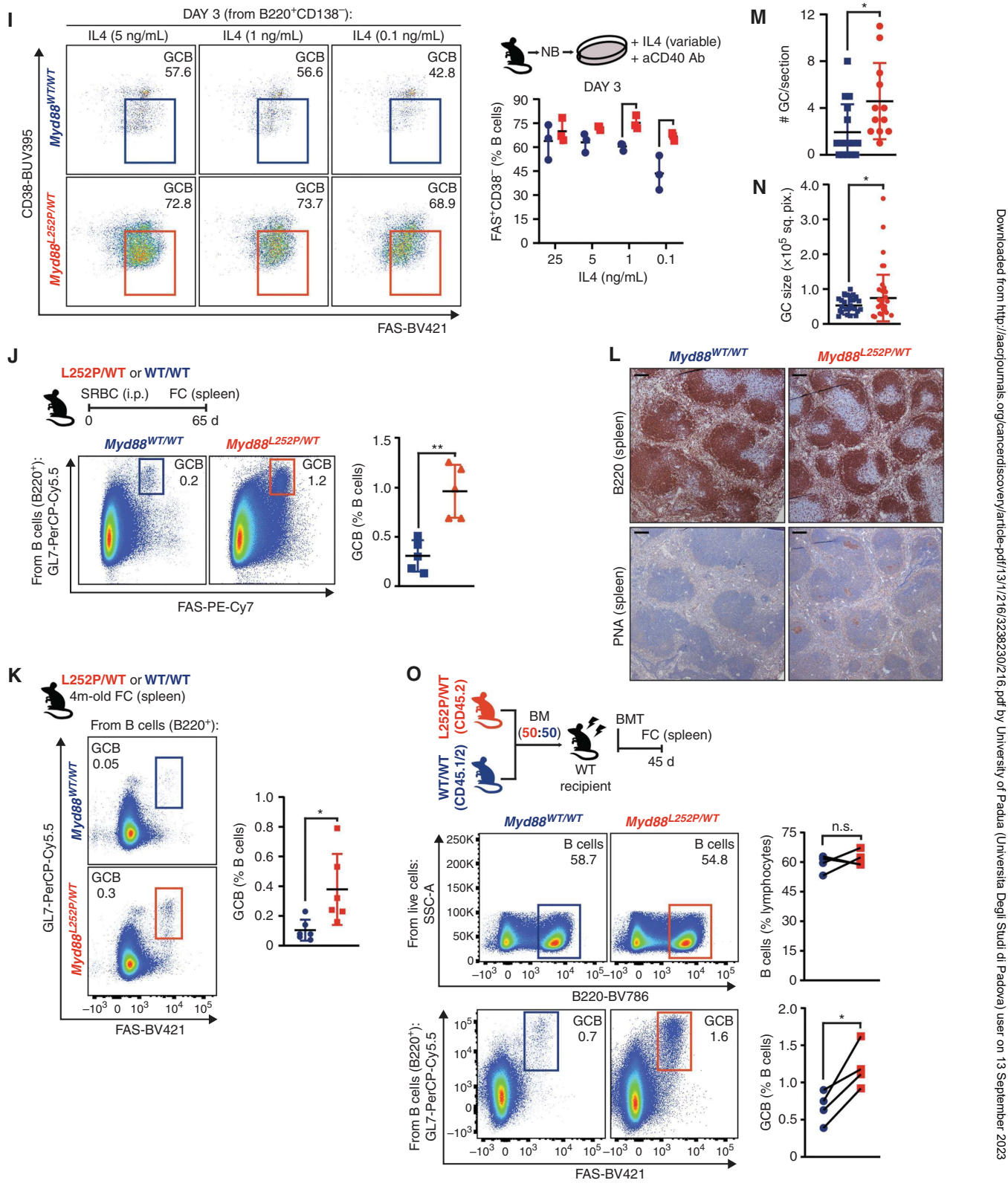

Figure 3. ***(Continued)*** **I,** FC analysis of iGCB with variable IL4 stimulation. **J,** FC analysis of splenic GCBs. **K,** FC analysis of GCBs in nonimmunized mice. **L,** B220 and PNA IHC in consecutive sections from animals treated as in **K**. Scale bars, 100 m. **M** and **N,** GC numbers (**M**) or individual area (**N**) in naïve mice. Dots represent individual animals (**M**) or GCs (**N**). Results for 12 to 18 animals per genotype from 2 experiments. **O,** FC analysis of *Myd88*$^{L252P/WT}$ and *Myd88*$^{WT/WT}$ relative contribution to B cells and GCBs. Values represent mean ± SEM. n.s., not significant; *, $P < 0.05$; **, $P < 0.01$; ***, $P < 0.001$. *P* values calculated using unpaired (**A**–**C**, **F**, **G**, **J**, **K**) or paired (**E**, **G**, **O**) two-tailed Student *t* test, Mann–Whitney *U* test (**M**, **N**), or two-way ANOVA with Tukey posttest (**H**, **I**).

showed the expected advantage (Fig. 3E, top row). Strikingly, whereas anti-CD40L treatment almost completely abrogated WT GCBs, there was significantly less reduction of *Myd88*^{L252P} GCBs (Fig. 3E, bottom row). *Myd88*^{L252P} GCBs resisting CD40L blockage still grouped in clusters within follicles (Supplementary Fig. S3A). Similar results were obtained using a strictly T cell–dependent antigen (Supplementary Fig. S3B). These results suggest that, although *Myd88*^{L252P} B cells benefit from T-cell help, their lower signaling threshold allows them to fully activate, become GCBs, and expand with minimal costimulation. In fact, the relative *Myd88*^{L252P} GCB expansion was more pronounced after blocking CD40L (Fig. 3F; Supplementary Fig. S3C), suggesting that normal T-cell help partially masks the advantage conferred by *Myd88*^{L252P}. Differences in proliferation were also magnified after blocking CD40L, with a large proportion of *Myd88*^{L252P} GCBs retaining their Ki-67^{+} status (Fig. 3G; Supplementary Fig. S3D).

To validate our findings, we assessed the impact of limited stimulation on iGCB formation. When exposed to high concentrations of a CD40-activating antibody, WT and *Myd88*$^{L252P/WT}$ activated and differentiated into mature iGCB at similar rates (Fig. 3H, left column). However, when the dosage was reduced by 10- or 20-fold, a larger fraction of *Myd88*$^{L252P/WT}$ B cells acquired an iGCB phenotype compared with WT (Fig. 3H, center and right columns), supporting that the activation threshold for mutant cells is significantly lower. Accordingly, *Myd88*$^{L252P/WT}$ B cells showed higher relative IκBα phosphorylation levels, and reduced total IκBα levels, compared with WT, upon acute CD40 stimulation (Supplementary Fig. S3E–S3G).

Activated B-cell DLBCL (ABC-DLBCL) tumors carrying *MYD88*^{L265P} harbor increased p-STAT3 levels, and *MYD88* silencing in MCD cell lines impairs STAT3 phosphorylation (10). Such an increase in p-STAT could enhance the response to IL4. Thus, we conducted additional *ex vivo* stimulation assays limiting IL4 concentration. Again, *Myd88*$^{L252P/WT}$ B cells managed to proliferate and acquire a fully mature iGCB phenotype even with highly restrictive IL4 concentrations that were detrimental to WT B-cell expansion/activation (Fig. 3I). In all, our data show that *MYD88*-mutant B cells can thrive with minimal T cell–derived costimulation.

Myd88 Mutations Favor Spontaneous GC Reactions

The lower reliance of *Myd88*^{L252P} B cells on T-cell help could facilitate their recurring or persistent activation, a requirement for MCD pathogenesis (22) and tumor cell survival (23). To explore this, we profiled *Myd88*$^{L252P/WT}$ and WT mice two months after SRBC immunization, a time point at which GCs should be fully resolved. Akin to the GC peak, *Myd88*^{L252P} mice exhibited significantly more GCB than WT, which only presented a residual population (Fig. 3J). Detected *Myd88*^{L252P} GCBs could represent aberrantly long-lasting cells derived from the immunization, and/or originate from spontaneous GCs (24). To explore whether *Myd88*^{L252P} exacerbated spontaneous GC formation/expansion, we profiled adult naïve mice housed in our specific pathogen–free facility. Indeed, *Myd88*^{L252P} animals presented significantly more spontaneous splenic GCBs by FC (Fig. 3K; Supplementary Fig. S3H) or IHC (Fig. 3L–N). A similar phenotype was observed in inguinal lymph nodes (Supplementary Fig. S3I). To exclude potential artifactual environmental variables—despite animals with different genotypes being housed as cagemates—we profiled naïve chimeric mice and observed comparable phenotypes (Fig. 3O; Supplementary Fig. S3J). This lower threshold to form GCBs shown by MYD88-mutant B cells could facilitate the aberrant reactivation of MCD precursor populations.

Myd88 Mutations Enable an Aberrantly Increased and Pervasive GC Output

TBL1XR1 mutations in GCBs bias them toward MBCs and away from PCs (22), which prompted us to explore whether this was a common theme among MCD founder mutations. First, we conducted a supervised analysis of the *Myd88*$^{L252P/WT}$ LZ GCB transcriptome (Fig. 2G) and, indeed, found strong enrichment for GCB-to-MBC transition signatures (Fig. 4A; ref. 25), and a depletion for genes associated with the PC fate (Fig. 4B). Differentially upregulated genes in mutant LZ GCBs included MBC-associated markers (26, 27), including *Bcl2*, *Il9r*, and *Ccr6* (Supplementary Table S1). We then aimed to validate whether the transcriptional deviation from the PC fate resulted in constrained plasmacytic differentiation, using our *ex vivo* system (Supplementary Fig. S2C). The frequency (Fig. 4C) and absolute number (Fig. 4D) of CD138^{+} cells produced by *Myd88*$^{L252P/WT}$ B cells were moderately but significantly lower than for WT. Interestingly, although *Myd88*$^{L252P/WT}$ B cells lost IgD surface expression (reflective of activation) before WT did (Supplementary Fig. S4A), and underwent more division rounds per unit of time (Supplementary Fig. S4B), the relative CD138^{+} cell output was consistently inferior after each cell cycle (Fig. 4E).

Currently, there are no equivalent systems to induce and compare MBC formation. Thus, to assess whether the transcriptional bias translated into MBC expansion, we used a Cre-inducible fluorescent reporter (*Rosa26YFP*; ref. 28) to track (pre)GC-derived MBCs *in vivo* (Supplementary Fig. S4C). Following immunization, *Rosa26YFP*;*Cγ1Cre*;*Myd88*$^{L252P/WT}$ mice exhibited a significant increase in GC-derived (YFP^{+}) MBC, compared with controls (Fig. 4F; Supplementary Fig. S4D). This expansion was disproportionately higher than that of GCBs (Fig. 4G), suggesting that *MYD88*$^{L265P/WT}$ GCs generate a significantly greater abundance of MBC. This exacerbated output could produce an abnormal "drainage" of LZ GCBs, and relative DZ GCB overrepresentation (Fig. 2D). Next, to determine whether the MBC expansion depended on T-cell costimulation, we generated *Rosa26YFP*-harboring chimeric animals and administered CD40L-blocking antibodies following immunization (Fig. 4H). Similar to GCBs (Fig. 3E), mutant YFP^{+} MBCs were significantly expanded in control conditions and upon impairment of GCB–T_{FH} cross-talk (Fig. 4H). Thus, the aberrant phenotypes caused by *MYD88* mutation appear hardwired into B cells and show little dependence on costimulation.

T_{FH} fulfill a gatekeeper function ensuring that GCBs that develop a high affinity for the antigen are preferentially selected to survive, expand, and exit as long-lived effectors (2, 29). Given the observations above, we assessed antigen specificity in our *Rosa26YFP*-harboring models. NP-OVA–immunized chimeric mice showed the expected overrepresentation

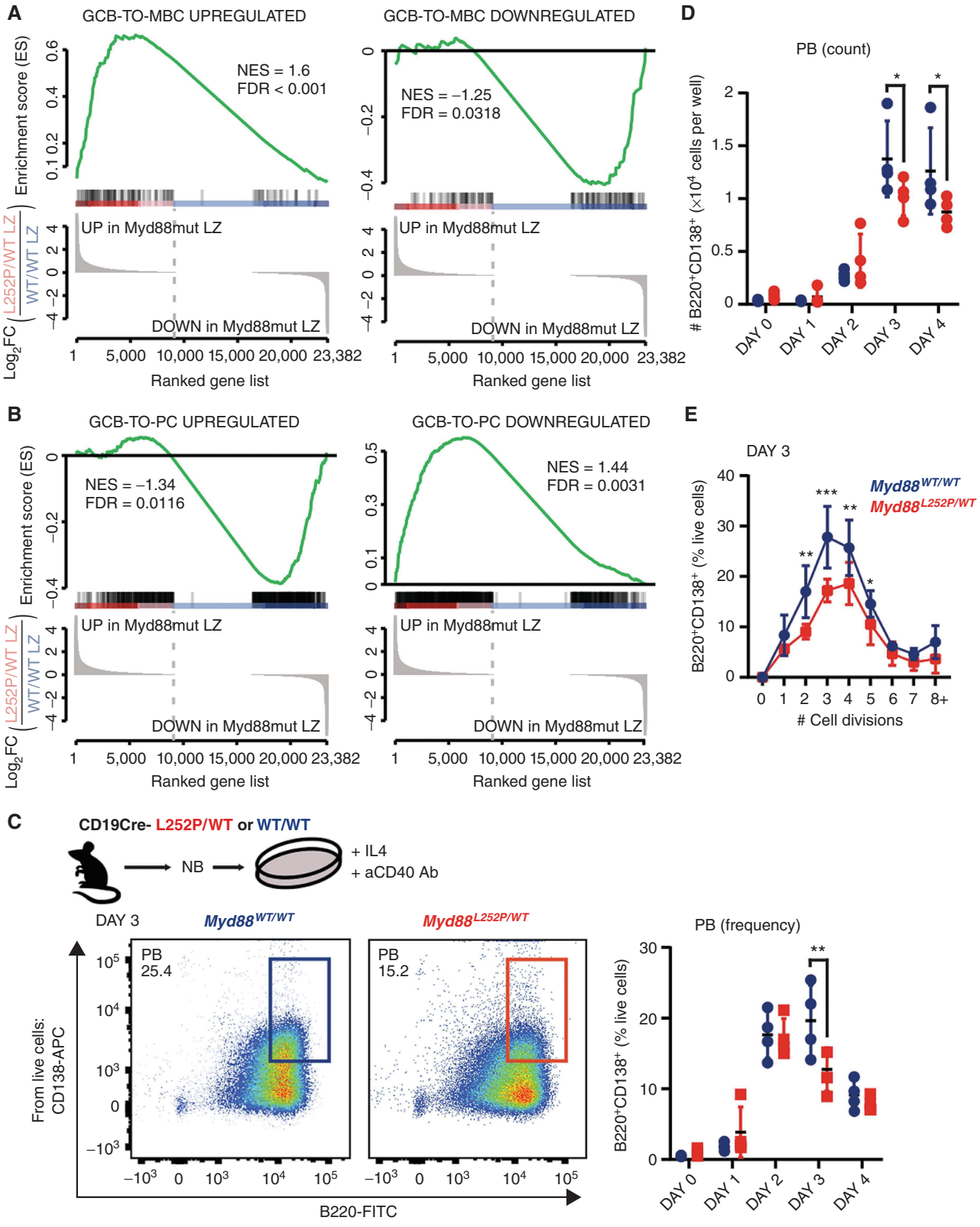

Figure 4. *Myd88* mutations enable an aberrantly increased and pervasive GC output. **A** and **B,** Gene set enrichment analysis of MBC (**A**) or PC (**B**) signatures (GSE4142) against *Myd88*$^{L252P/WT}$ LZ GCB. NES, normalized enrichment score. **C** and **D,** FC analysis of CD138$^+$ cells relative (**C**) or absolute (**D**) abundance. PB, plasmablasts. **E,** FC analysis of the relative fraction of CD138$^+$ cells per cell division, determined by proliferation dye dilution, in cells from **C**. Results for 3 animals per genotype. (*continued on next page*)

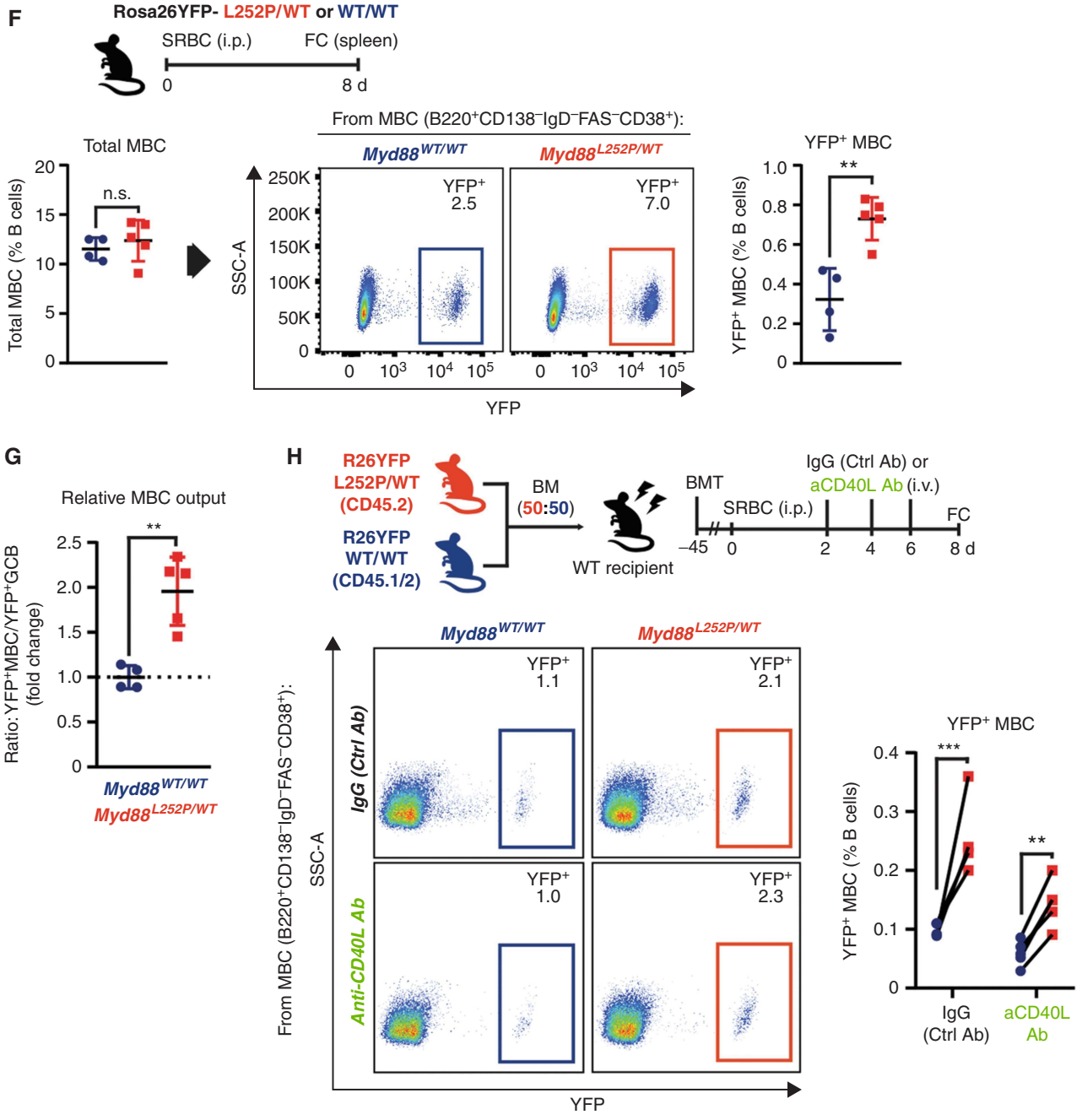

Figure 4. ***(Continued)*** **F,** FC analysis of total (left) or YFP+ (right) MBCs. SSC-A, side scatter area. **G,** YFP+ MBC abundance relative to YFP+ GCB in the same animals. **H,** FC analysis of YFP+ MBCs. BMT, bone marrow transplant. (*continued on following page*)

of total mutant GCBs (Fig. 4I, left). However, the relative frequency of cells with high affinity for the antigen (NP+) was significantly lower among mutant GCB than for WT (Fig. 4I, right). More importantly, among the expanded GC-derived mutant MBC pool, there was a dramatically lower fraction of cells with detectable NP affinity (Fig. 4J). These data suggest that *MYD88* mutations enable highly permissive GC transit and exit, which could facilitate the spurious expansion and persistence of B-cell clones.

Myd88 Mutations Trigger an Aged/Autoimmune-like Program in GCBs

To gain mechanistic insight into the observed phenotypes, we conducted further analysis of RNA-seq profiles (Fig. 2G). Differential expression analysis identified *Myd88*^{L252P}-driven signatures in DZ and LZ GCBs (|FC|>1.5; FDR<0.05), which were skewed toward gene activation (Fig. 5A; Supplementary Fig. S5A; Supplementary Table S1). Pathway analysis revealed enrichment for ABC-DLBCL, advanced-stage DLBCL, and

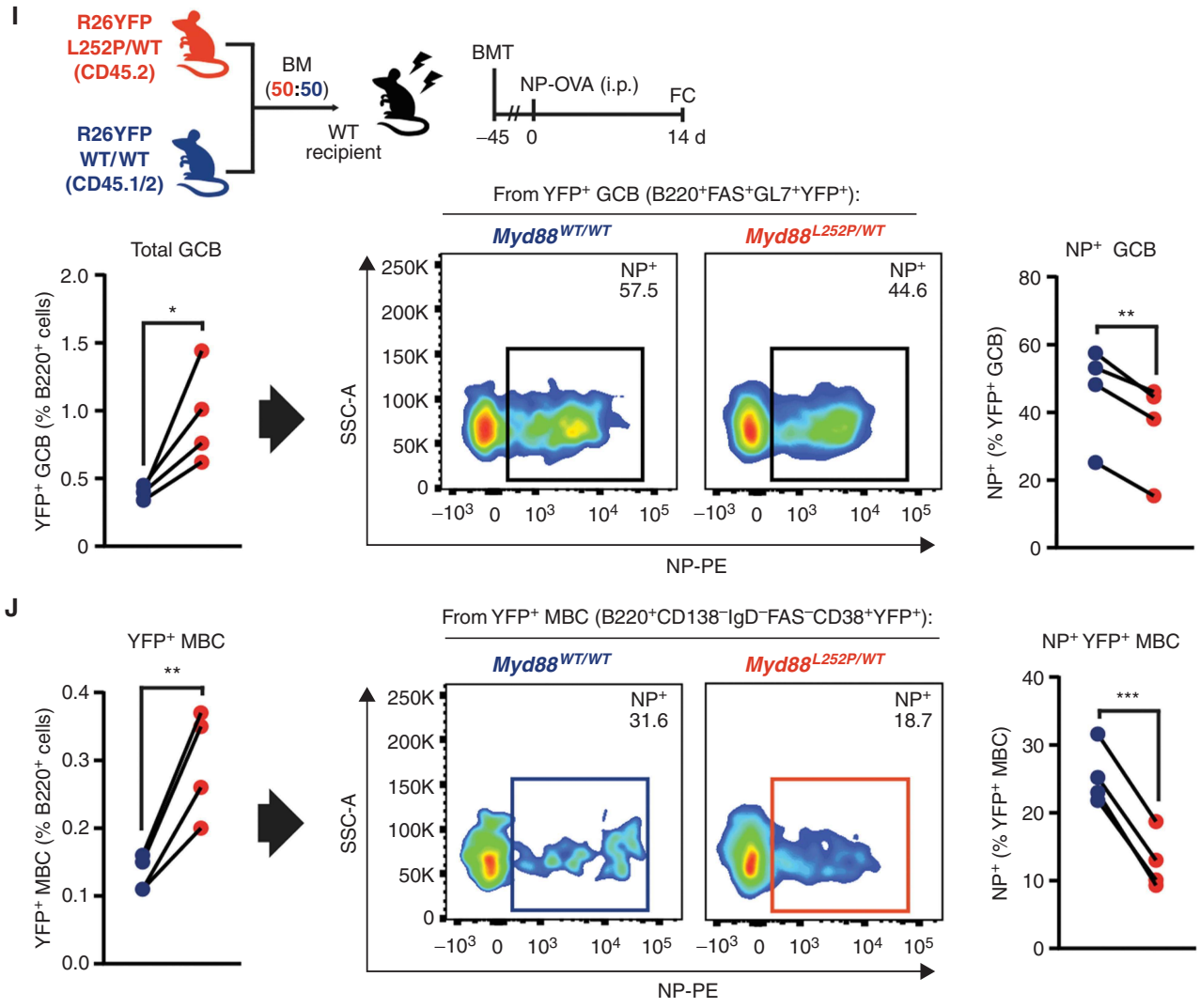

Figure 4. ***(Continued)*** **I** and **J,** FC analysis of total (left) or NP-specific (right) YFP+ GCBs (**I**) or YFP+ MBCs (**J**). Values represent mean ± SEM. n.s., not significant; *, $P < 0.05$; **, $P < 0.01$; ***, $P < 0.001$. *P* values were calculated using unpaired (**F**, **G**) or paired (**H**–**J**) two-tailed Student *t* test or two-way ANOVA with Tukey posttest (**C**–**E**).

WM signatures, supporting that our models recapitulate *MYD88*^{L265P} effects in human lymphomas (Fig. 5B; Supplementary Fig. S5B; Supplementary Table S1). Accordingly, we saw enrichment for NF-kB–regulated genes, the central cascade activated by *MYD88*^{L265P} (Fig. 5B; Supplementary Fig. S5B; ref. 30). We further saw depletion of T_{FH} signatures (Fig. 5B; Supplementary Fig. S5B), partly driven by downregulation of the transcription factors *Jun* and *Fos*. We also observed enrichment for cell migration and chemotaxis signatures (Fig. 5B; Supplementary Fig. S5B), which could relate to the MBC-like program in GCBs (Fig. 4A), but also to the highly prevalent extranodal presentation of *MYD88*^{L265P} tumors. Related to cell motility, *Myd88*^{L252P} LZ GCB downregulated *Rgs13* (Fig. 5A), a negative modulator of CXCR4 function (31), which could contribute to the observed DZ skew (Fig. 2D). *Myd88*^{L252P} LZ GCBs also upregulated *Il13ra1* (Supplementary Table S1), which pairs with the IL4 receptor and signals through overlapping effectors (32), providing a plausible mechanistic explanation to the enhanced response to IL4 by *Myd88*^{L252P} B cells (Fig. 3I).

Beyond the aforementioned profiles, the most prominent signal in *Myd88*^{L252P} GCBs related to IFN signaling and IFNγ in particular (Fig. 5B; Supplementary Fig. S5B). IFNγ not only instructs B-cell function against infections but also drives autoimmune phenotypes (33, 34). Indeed, our analysis showed enrichment for signatures related to immune responses and the autoimmune disorder systemic lupus erythematosus (Fig. 5B). IFNγ induces the expression of the transcription factor T-BET in B cells and drives the formation of "aged/autoimmune" B cells (AiBC; refs. 35–37). AiBCs are an MBC subpopulation, phenotypically distinguishable as T-BET+ and/or CD11c+ (38), that expand and differentiate into PCs responsible for pathogenic autoantibody production (36). B cells with similar phenotypes accumulate during viral/parasitic infections and in aged healthy females (38). Interestingly, *Myd88*^{L252P} GCBs showed *Tbx21* (T-BET) and

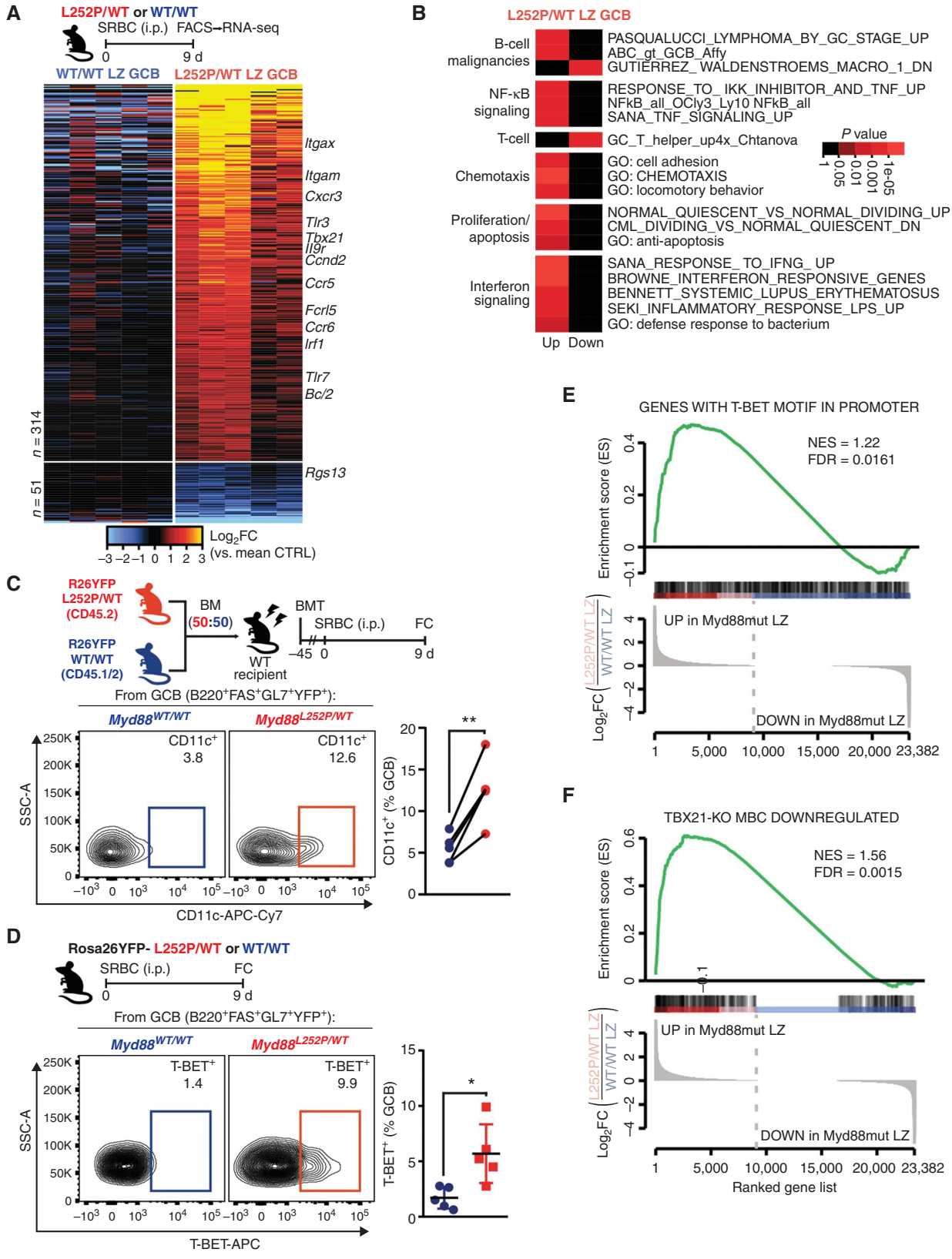

Figure 5. MCD mutations trigger an aged/autoimmune-like program in GCBs. **A,** Differentially expressed genes in *Myd88*$^{L252P/WT}$ LZ GCBs. **B,** Pathway analysis for genes in **A**. **C** and **D,** FC analysis of CD11c$^+$ (**C**) or T-BET$^+$ (**D**) GCBs. BMT, bone marrow transplant; SSC-A, side scatter area. **E,** Gene set enrichment analysis (GSEA) of genes with a T-BET binding motif in their promoter (HOCOMOCO v11; >90% match within −5 kb:TSS:+2 kb) against *Myd88*$^{L252P/WT}$ LZ GCBs. NES, normalized enrichment score. **F,** GSEA of T-BET knockout (KO) MBC (GSE81189) against *Myd88*$^{L252P/WT}$ LZ GCBs. (*continued on following page*)

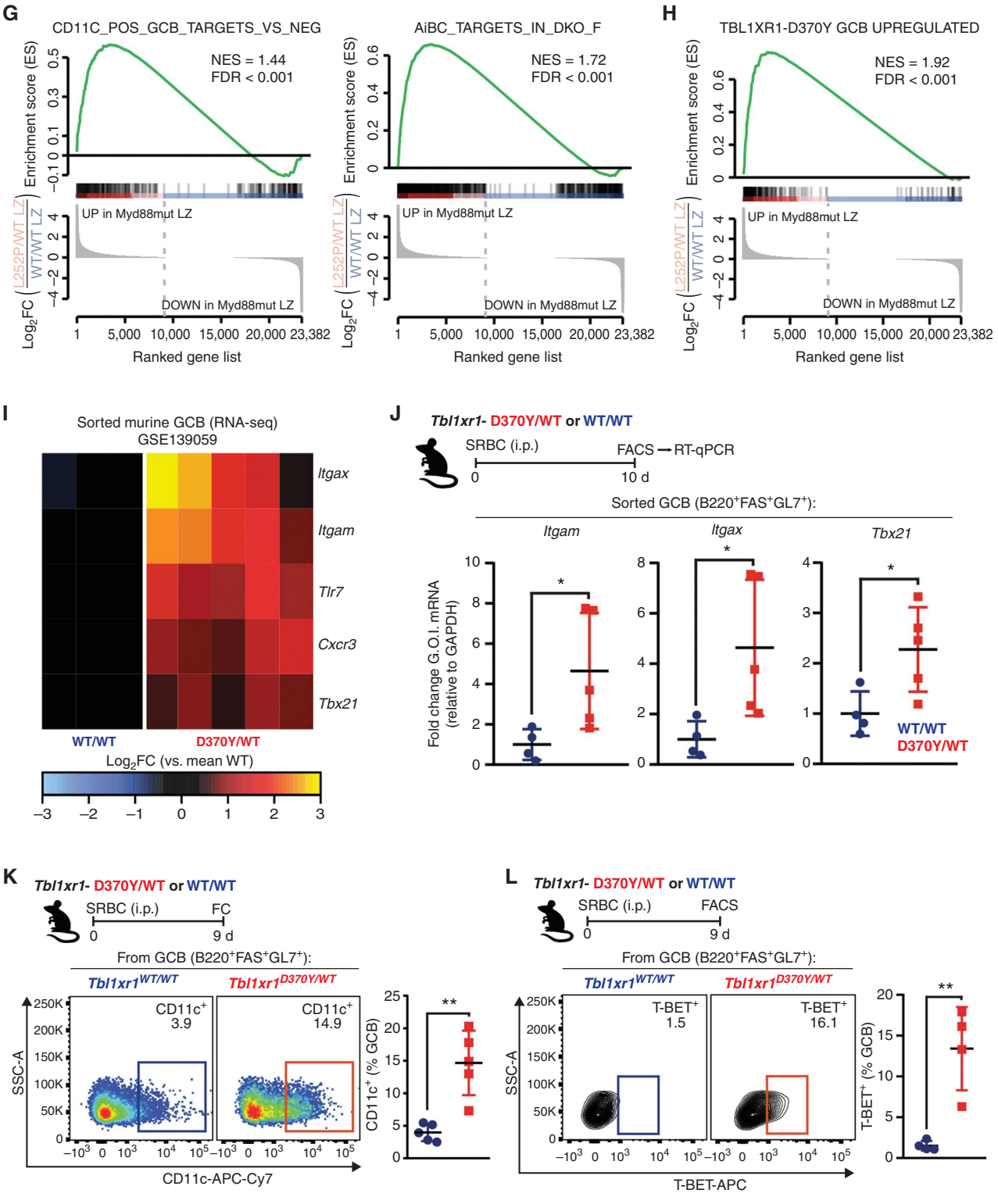

Figure 5. ***(Continued)*** **G,** GSEA of canonical murine AiBC signatures (GSE175365) against *Myd88*$^{L252P/WT}$ LZ GCB. **H,** GSEA of *Tbl1xr1*-mutant GCBs (GSE139059) against *Myd88*$^{L252P/WT}$ LZ GCBs. **I,** RNA-seq–based expression of genes of interest (G.O.I.) in *Tbl1xr1*-mutant (D370Y/WT) or WT GCBs (GSE139059). **J,** RT-qPCR validation of selected genes from **I** on independent animals. **K** and **L,** FC analysis of CD11c$^+$ (**K**) or T-BET$^+$ (**L**) GCBs in *Tbl1xr1*-mutant mice. (*continued on next page*)

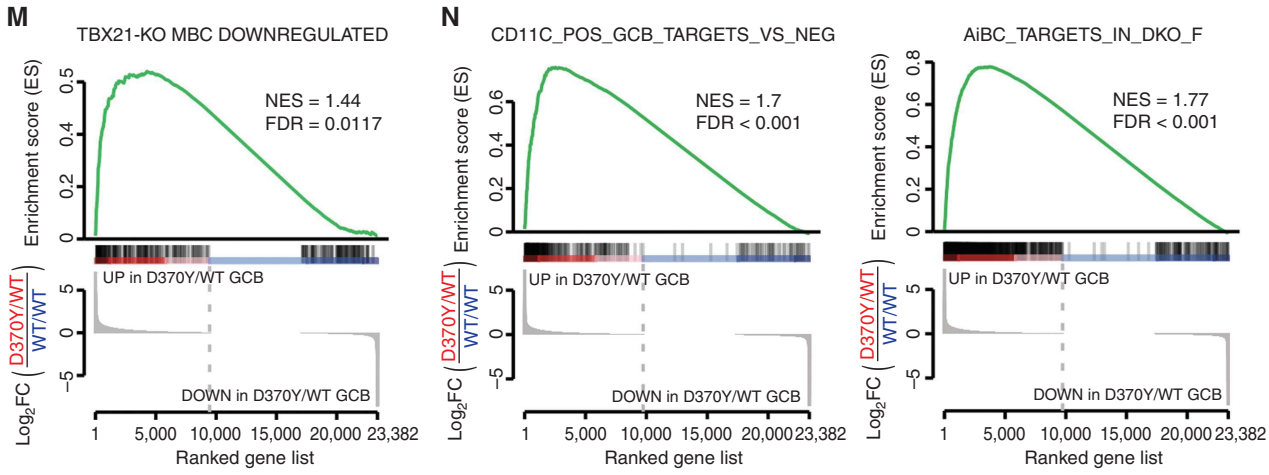

Figure 5. ***(Continued)*** **M,** GSEA of T-BET-KO MBCs (GSE81189) against *Tbl1xr1*-mutant GCBs. **N,** GSEA of canonical murine AiBC signatures against *Tbl1xr1*-mutant GCBs. Values represent mean ± SEM. *, $P < 0.05$; **, $P < 0.01$; ***, $P < 0.001$. *P* values were calculated using unpaired (**D**, **J**–**L**) or paired (**C**) two-tailed Student *t* test.

Itgax (CD11c) upregulation (Fig. 5A; Supplementary Fig. S5A) by RNA-seq, a finding confirmed by RT-qPCR in independent mice (Supplementary Fig. S5C). Enhanced CD11c (Fig. 5C) and T-BET (Fig. 5D) protein expression was further observed in *Myd88*^{L252P} GCBs driven by SRBC or alternative antigens (Supplementary Fig. S5D). In line with T-BET induction, genes with T-BET binding motifs in their promoter were overrepresented among upregulated genes in *Myd88*^{L252P} LZ GCBs (Fig. 5E). Similarly, these genes matched those downregulated in T-BET knockout MBCs (Fig. 5F; ref. 39). These findings suggest that aberrant T-BET expression induces transcriptional rewiring of *Myd88*^{L252P} GCB. *Myd88*^{L252P} GCBs showed upregulation of other AiBC-related genes, including *Itgam* (CD11b), *Fcrl5*, *Tlr7*, and *Cxcr3* (Fig. 5A; Supplementary Fig. S5E; refs. 38–40). Beyond individual markers, *Myd88*^{L252P} GCBs showed significant enrichment for canonical AiBC signatures (Fig. 5G; Supplementary Fig. S5F; ref. 41). In all, *Myd88*^{L252P} induced a program in GCBs that closely resembles that of pathogenic B cells driving autoimmune disorders.

Induction of an AiBC Program Is a Common Feature among MCD Founder Mutations

In addition to IFNγ, TLR activation is typically required to generate AiBCs (40). Because MYD88 is a critical signaling hub for most TLRs, the AiBC-related phenotype could pertain to *MYD88*^{L265P} but not to MCDs as a class. Hence, we explored whether *TBL1XR1* mutations would have similar effects. TBL1XR1 is a structural component of the SMRT/HDAC3 corepressor complex (22) with no evident functional link to MYD88. However, the transcriptome of *Myd88*^{L252P} GCB showed significant enrichment for that of *Tbl1xr1*^{MUT} GCB (Fig. 5H; Supplementary Fig. S5G). Further analysis of RNA-seq data from *Tbl1xr1*^{MUT} GCB (22) revealed differential upregulation of AiBC markers, including *Tbx21*, *Itgax*, and *Itgam* (Fig. 5I), a finding confirmed by RT-qPCR in independent mice (Fig. 5J). Accordingly, *Tbl1xr1*^{MUT} GCBs showed protein-level upregulation of T-BET (Fig. 5K), CD11c (Fig. 5L), and TLR7 (Supplementary Fig. S5H). Furthermore, as observed for *Myd88*^{L252P}, *Tbl1xr1*^{MUT} GCBs exhibited transcriptional enrichment for genes downregulated upon T-BET knockout (Fig. 5M) and for canonical AiBC signatures (Fig. 5N). These data suggest that the acquisition of an AiBC-like program is a common prevalent feature in MCD transformation, which is triggered by mechanistically distinct founder mutations.

MCD Mutations Cause a Cumulative Expansion of AiBC-like MBC

Given the transcriptional imprint exerted by T-BET in GCBs harboring MCD founder mutations, we explored whether this resulted in the generation of AiBC-like MBCs, something of particular relevance considering that these mutations aberrantly increase MBC output (ref. 22 and results herein). Notably, a significantly higher fraction of GC-derived MBCs coexpressed the canonical AiBC markers CD11b/CD11c in *Myd88*^{L252P} mice (Fig. 6A). Accordingly, a higher proportion of *Myd88*^{L252P} MBCs expressed T-BET (Fig. 6B). Studies in *Rosa26YFP;Cγ1Cre;Tbl1xr1*^{MUT} animals revealed a similar expansion of CD11b^{+}CD11c^{+} (Fig. 6C) and T-BET^{+} (Fig. 6D) MBCs.

Although AiBC generation was first described as absolutely dependent on CD40 signaling (42), recent studies suggest this could be context-dependent (43). Given the observed lower dependency on CD40 stimulation among *Myd88*^{L252P} B cells, we asked whether the AiBC-like MBC expansion would occur under poor costimulation. CD40L-blocking antibodies reduced WT CD11c^{+} MBCs by ~50%, whereas mutant CD11c^{+} MBC abundance remained elevated and comparable to that in IgG control–treated mice (Fig. 6E; Supplementary Fig. S6A), suggesting little-to-no costimulation is needed for mutant B cells to follow this cell fate.

CD19Cre;Myd88^{L252P} mice, which express the mutation in all B cells, develop lymphadenopathy and occasional lymphomas with old age (median survival ~70 weeks; ref. 13). We explored whether AiBC-like MBCs would also expand in this model. At 25 weeks of age, a time point at which *CD19Cre;Myd88*^{L252P} mice do not show evidence of lymphoproliferative disease (13), total MBCs were expanded, and, within

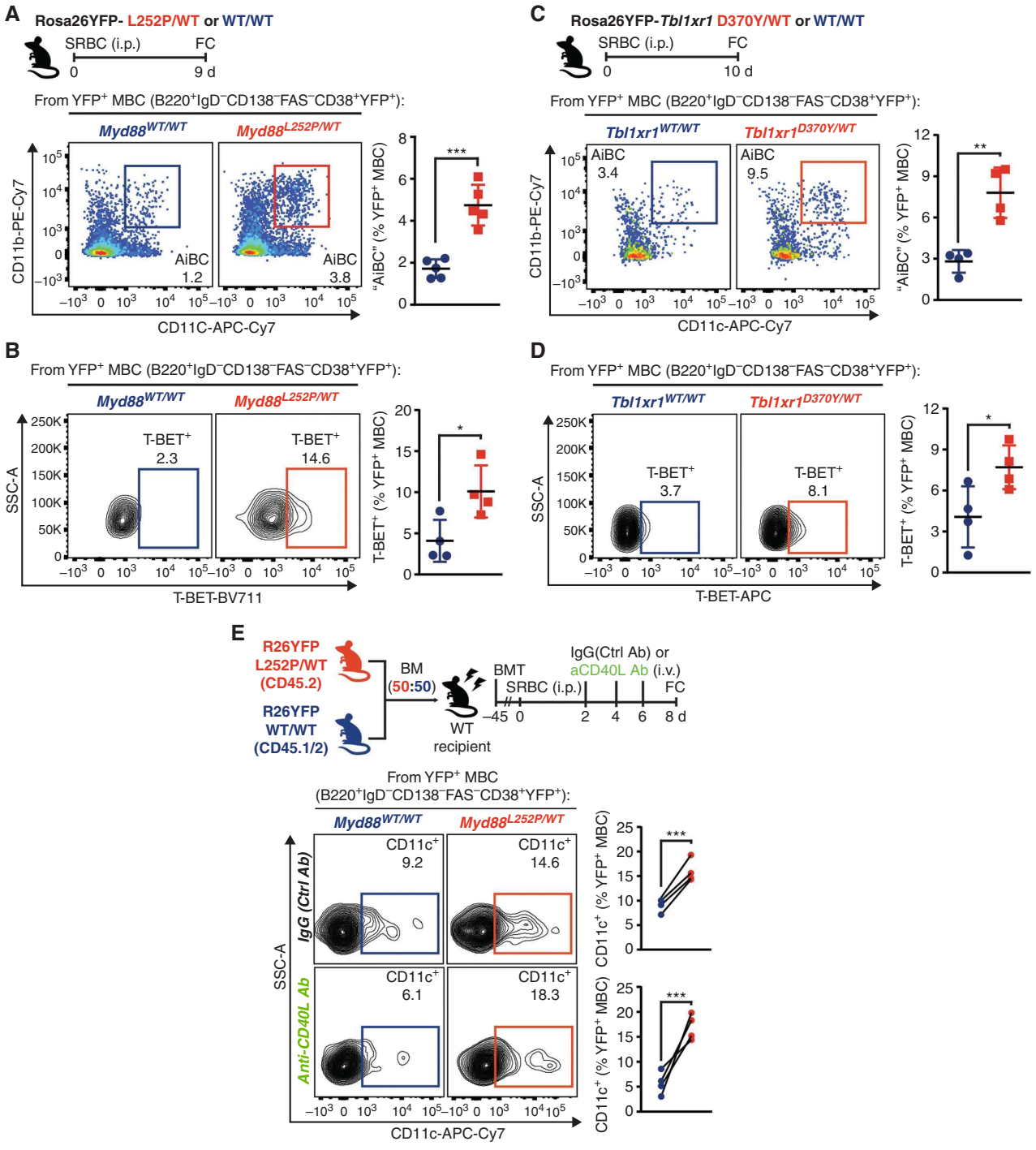

Figure 6. MCD mutations cause a cumulative expansion of AiBC-like MBCs. **A–D,** FC analysis of CD11b+ CD11c+ (**A**, **C**) or T-BET+ YFP+ (**B**, **D**) MBCs. SSC-A, side scatter area. **E,** FC analysis of CD11c+ YFP+ MBCs. BMT, bone marrow transplant. (*continued on next page*)

this population, there was a significant overrepresentation of AiBC-like (T-BET+CD11c+) phenotypes (Fig. 6F; Supplementary Fig. S6B). NBs did not express these markers, suggesting the phenotype was acquired only after activation (Supplementary Fig. S6C). Notably, mutant AiBC-like MBCs manifested a more active proliferative phenotype than WT counterparts, as per Ki-67 staining (Fig. 6G). Such differences were absent in non–AiBC-like MBCs (Supplementary Fig. S6D). This prompted us to explore whether AiBC-like MBCs progressively accumulated during malignant transformation. Hence, we conducted longitudinal tracking of B cells in *Myd88*^{L252P} aging mice (20–90 weeks). Strikingly, mutant mice showed increasing accumulation of T-BET+CD11c+ MBCs (Fig. 6H), whereas there was little change in sex- and age-matched

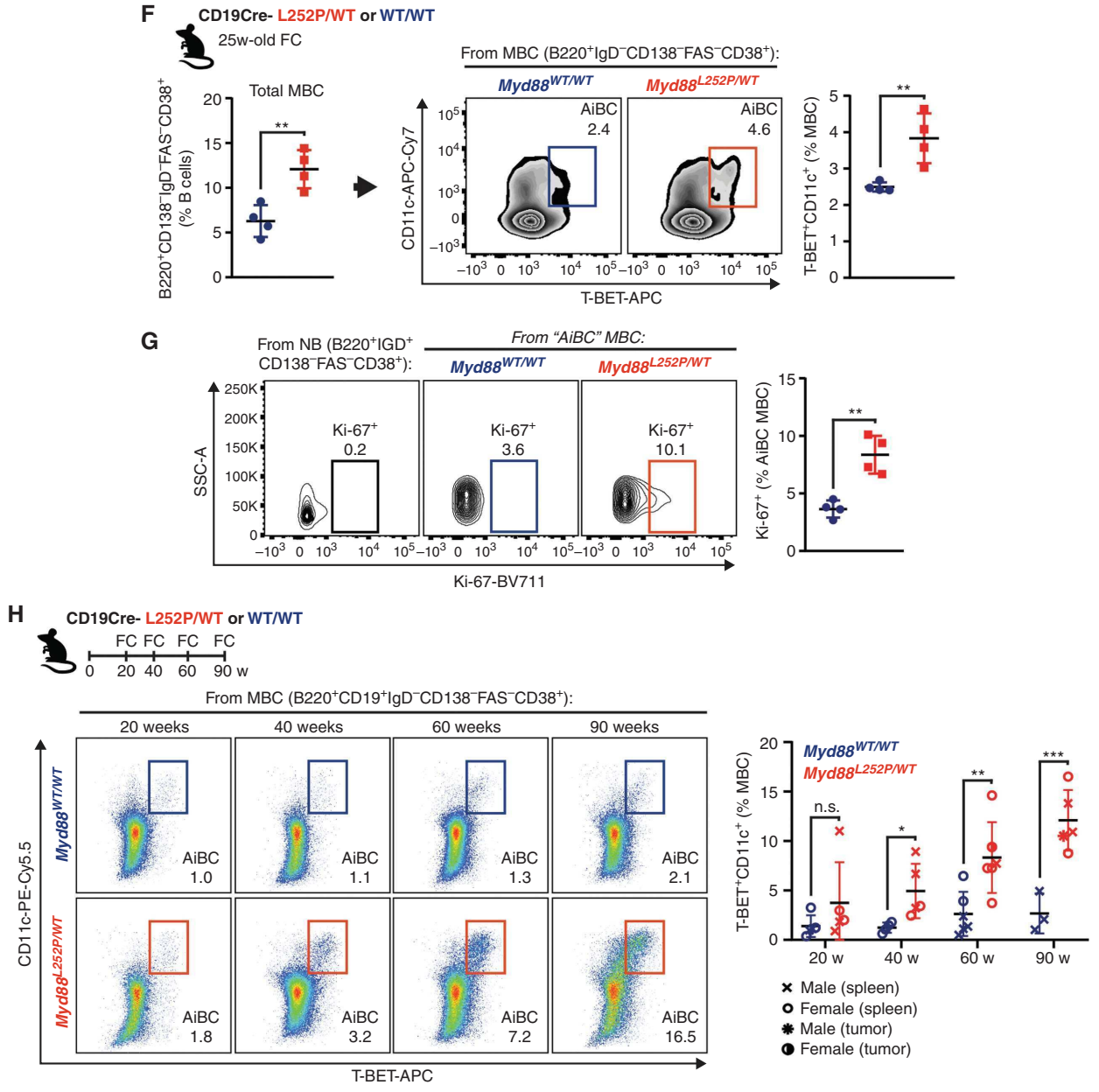

Figure 6. ***(Continued)*** **F,** FC analysis of total (left) or T-BET$^+$CD11c$^+$ (right) MBCs in nonimmunized young animals. **G,** FC analysis of Ki-67$^+$ AiBC-like MBCs in mice from **F**. NB illustrates nonproliferating cells. **H,** FC analysis of splenic T-BET$^+$CD11c$^+$ MBCs in nonimmunized mice. Tumor samples are plotted but not considered for statistical analysis. (*continued on following page*)

WT animals. Similar results were obtained when defining AiBC-like MBCs as CD11b$^+$CD11c$^+$ or CD11b$^+$T-BET$^+$ (Supplementary Fig. S6E and S6F). Conversely, we found little splenic plasmacytic differentiation (CD138$^+$ cells), even at old age (Fig. 6I), suggesting these cells do not play a leading role in the longitudinal transformation.

To gain insights into the origin and trajectory of AiBC-like MBCs, we isolated this and other B-cell subsets from *CD19Cre*;*Myd88*$^{L252P/WT}$ mice at 40 weeks of age (Supplementary Fig. S6G) and performed targeted BCR sequencing. Despite reports that *Aicda* can activate in developing B cells under BCR/TLR costimulation (44), NBs from mutant mice showed largely undetectable SHM levels (Fig. 6J). On the other hand, AiBCs exhibited elevated SHM levels (Fig. 6J), suggesting these transited through the GC or acquired a GCB-like phenotype during their formation/expansion. SHM in AiBCs was significantly higher than that in other MBCs, but still lower than in (spontaneous) GCBs in the same animals (Fig. 6K). Notably, AiBCs showed the highest clonality across all studied populations, as would be expected from prospective lymphoma precursors. Two animals in our longitudinal study presented overt B-cell lymphomas at the time of necropsy, one of which had extranodal peritoneal localization (Supplementary Fig. S6H). Although a fraction

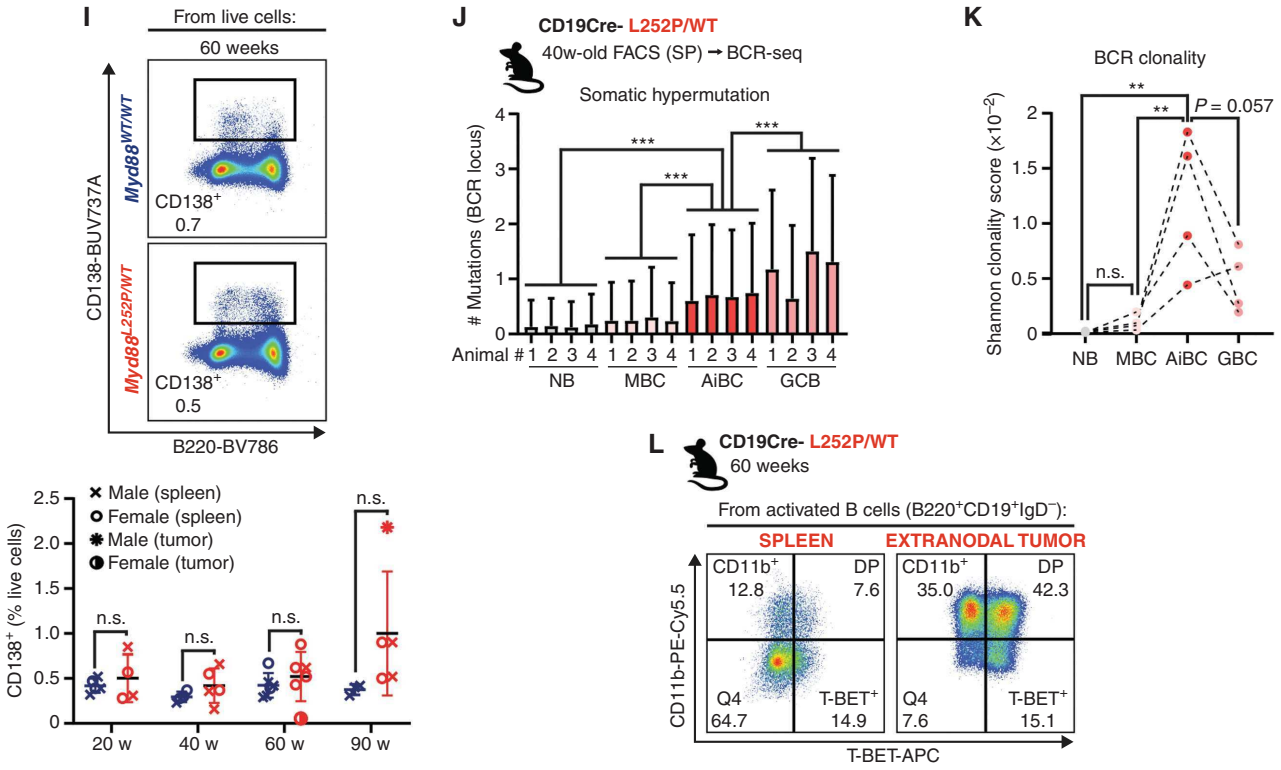

Figure 6. ***(Continued)*** **I,** FC analysis of CD138+ cells in animals from **H**. **J,** BCR mutation burden in splenic B cells. BCR-seq, BCR sequencing. Values, mean ± SD. **K,** Clonality based on productive VDJ combinations. Datasets were downsampled to a common minimum to prevent size-based bias. **L,** FC analysis of T-BET and CD11b expression in activated B cells from the spleen or extranodal tumor from an animal in **H**. Values represent mean ± SEM. n.s., not significant; *, $P < 0.05$; **, $P < 0.01$; ***, $P < 0.001$. *P* values were calculated using unpaired (**A**–**D**, **F**, **G**–**J**) or paired (**E**) two-tailed Student *t* test with the two-stage step-up method of Benjamini, Krieger, and Yekutieli where applicable or a Kruskal–Wallis test (**J**, **K**).

of all splenic activated (IgD−) B cells expressed CD11b and/or T-BET in this animal, more than 90% of tumor cells expressed one or both of these (Fig. 6L). In all, these observations support a role for AiBC-like MBCs as prospective precursor populations for MCD lymphomas.

T-BET Supports the Fitness of MYD88-Mutant B Cells

As the master regulator of canonical AiBC, T-BET ablation results in the loss of this population and amelioration of autoimmune disease severity in animal models (36). The observed T-BET–driven GCB transcriptional program and AiBC-like MBC expansion in our models suggest a similar dependency may exist in MCD precursors. To test this, we ablated T-BET in nontransformed primary *Myd88*^{L252P} B cells using CRISPR/CAS9 and assessed their fitness to form GCBs after transplantation into immunocompetent recipients. Only a minimal fraction of NBs from donor mice would be expected to recognize a given antigen, greatly limiting our capacity to study transferred cells. To overcome this, we crossed our models to incorporate an engineered BCR with defined specificity for NP (*B1-8hi* strain; ref. 45). Briefly, NP-specific NBs from *B1-8hi;Cd45.1;Myd88*^{L252P} or *B1-8hi;Cd45.1;Myd88*^{WT} mice were first primed to enable editing (46), nucleofected with CAS9 complexes carrying control or *Tbx21* guide RNAs (gRNA), and adoptively transferred into WT recipients (Fig. 7A). A fluorescently labeled trans-activating RNA was used to track effective nucleofection with CAS9 complexes (Supplementary Fig. S7A). Targeted sequencing 24 hours after nucleofection confirmed the presence of disruptive lesions at the intended loci (Supplementary Fig. S7B). Recipient animals were immunized with an NP–protein conjugate the day after cell transfer and profiled at the peak of the NP-induced GC. Approximately 10% of GCBs in recipients derived from *gCtrl*-treated *B1-8hi;Cd45.1;Myd88*^{L252P} transferred B cells (Fig. 7B; Supplementary Fig. S7C). Strikingly, *gTbx21*-treated mutant donors manifested significantly impaired expansion, similar to that of *B1-8hi;Cd45.1;Myd88*^{WT} donor B cells (Fig. 7B). As expected, *Myd88*^{L252P} GCBs featured higher T-BET expression compared with WT (Fig. 7C). However, GCBs derived from *gTbx21*-treated *B1-8hi;Cd45.1;Myd88*^{L252P} cells showed minimal T-BET expression, confirming efficient editing (Fig. 7C). In line with the observed loss of competitive fitness, *gTbx21*-treated cells showed a significant reduction in Ki-67 expression, reflecting their impaired proliferative status (Fig. 7D). T-BET ablation also significantly impaired the expansion of AiBC-like (CD11c+) MBCs derived from transferred cells (Fig. 7E). Conversely, WT B-cell fitness was unaltered by *Tbx21* knockout (Supplementary Fig. S7D–S7G). In all, these results show that T-BET supports the competitive fitness of B cells harboring founder MCD mutations.

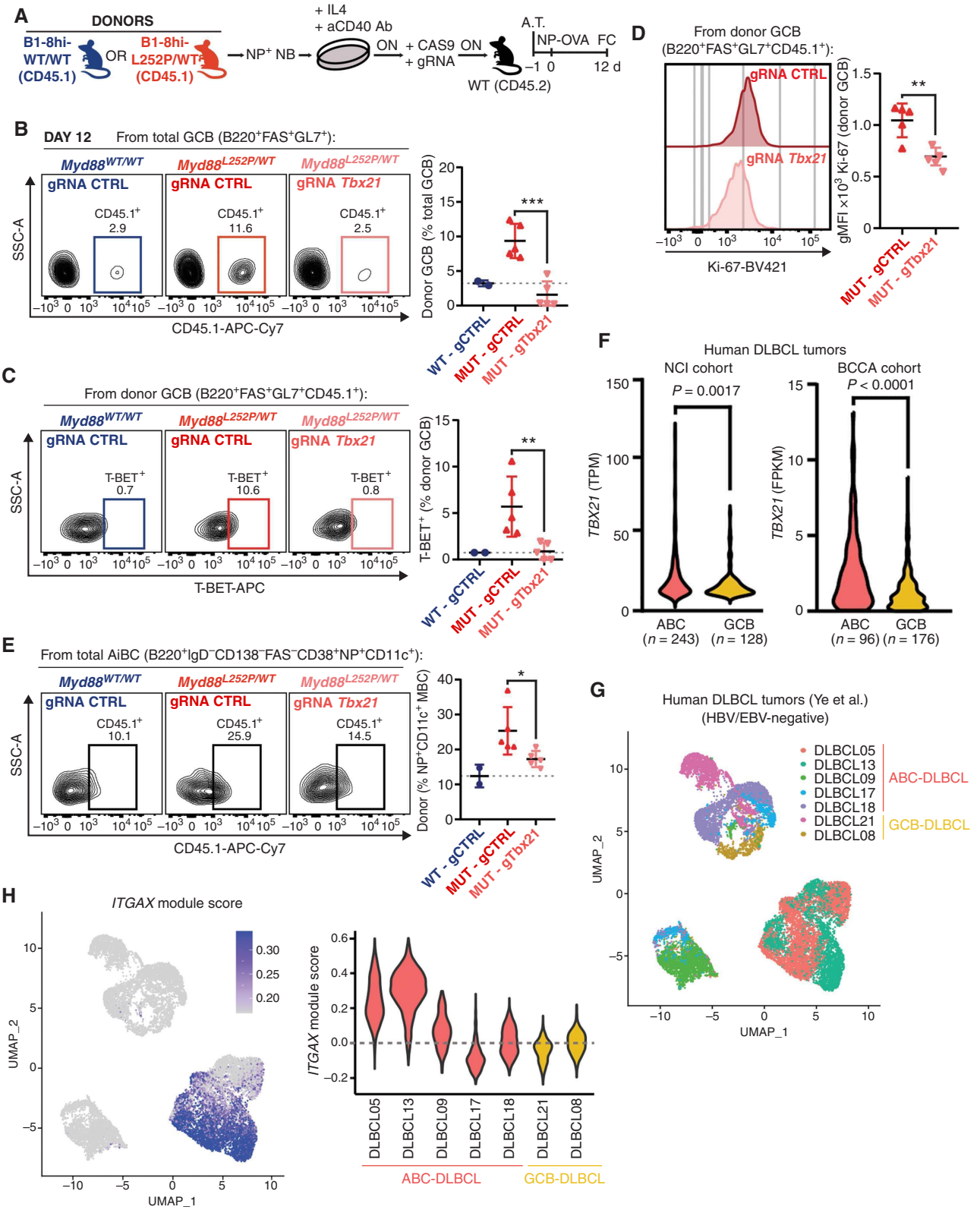

Figure 7. T-BET supports the fitness of MYD88-mutant B cells. **A,** Experimental scheme for **B**–**E**. A.T., adoptive transfer; ON, overnight; SSC-A, side scatter area. **B,** FC profiling of donor B-cell contribution to total GCBs. **C,** FC analysis of T-BET+ donor-derived GCBs. **D,** FC analysis of Ki-67 expression in donor-derived GCBs. gMFI, geometric mean fluorescence intensity. **E,** FC analysis of donor B-cell contribution to AiBC-like MBCs. **F,** RNA-seq–based *TBX21* expression in primary specimens from NCI (left; ref. 47) or BCCA (right; refs. 48, 49) cohorts. FPKM, fragments per kilobase of exon per million mapped fragments; TPM, transcripts per million. **G,** Uniform manifold approximation and projection (UMAP) depiction of single-cell RNA-seq data from Epstein–Barr virus (EBV)/hepatitis B virus (HBV)–negative DLBCL tumors (50). **H,** Relative expression of the *ITGAX* module among specimens in **G**. (*continued on following page*)

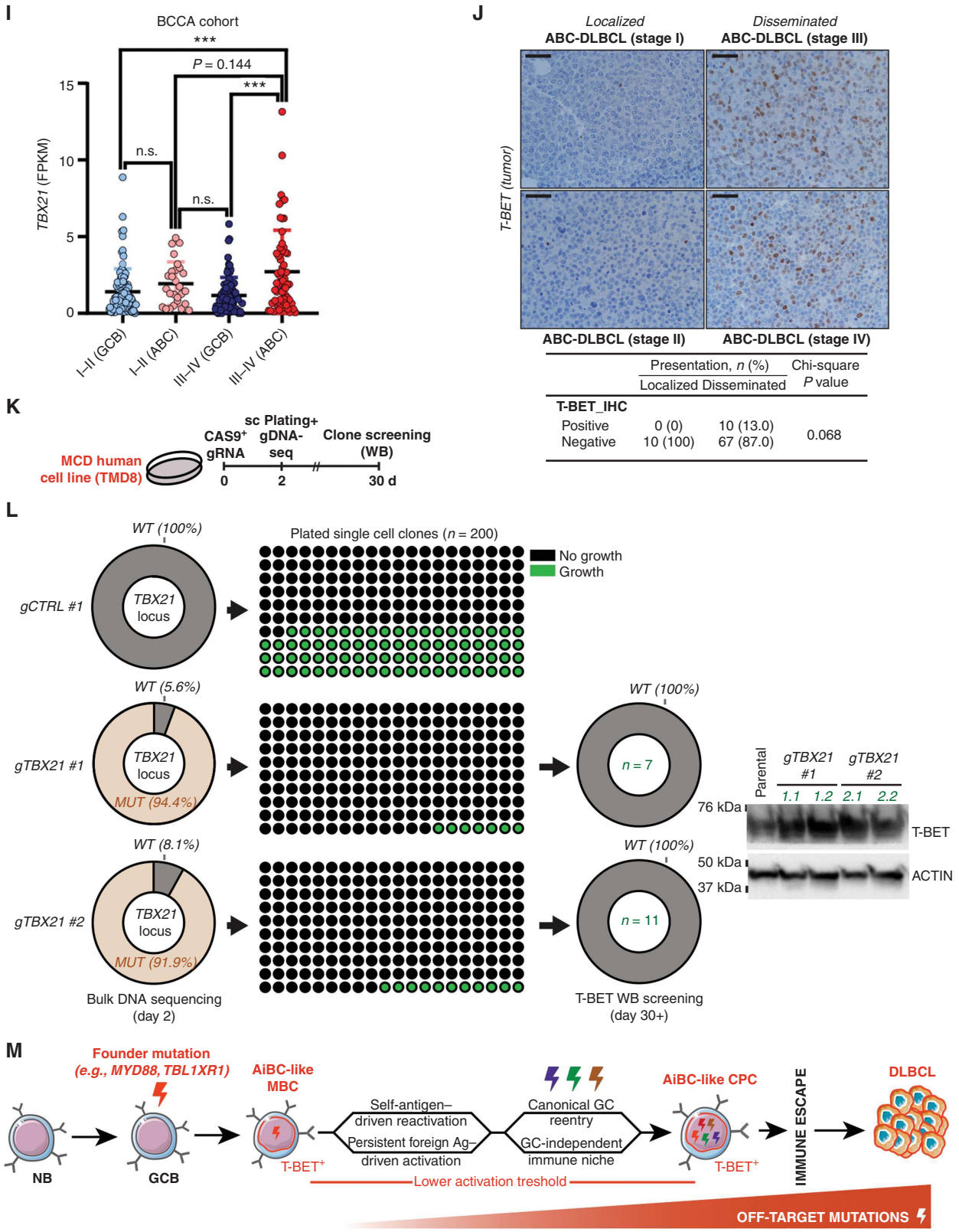

Figure 7. ***(Continued)*** **I,** RNA-seq-based *TBX21* expression in primary human DLBCL specimens. **J,** Representative images and quantification of T-BET IHC in specimens from the BCCA cohort (52). Scale bars, 20 m. **K,** Experimental scheme for **L**. gDNA, genomic DNA; WB, Western blot. **L,** Left, penetrance of targeted genomic alterations at the time of cell plating. Center, number of detectable clonal outgrows 30 days after plating. Right, WB-based T-BET expression in clonal outgrows. Representative blots for 2 clones per gRNA. **M,** Schematic representation of the proposed transformation model. Values represent mean ± SEM. n.s., not significant; *, $P < 0.05$; **, $P < 0.01$; ***, $P < 0.001$. *P* values were calculated using unpaired two-tailed Student *t* test (**B**–**F**) or one-way ANOVA with Tukey posttest (**I**).

Human ABC-DLBCL Tumors Exhibit AiBC-like Features

In the context of autoimmune disorders, some AiBCs retain their transcriptional and phenotypic profiles despite T-BET downregulation following disease onset (41). To assess whether T-BET expression could be detected in human DLBCL, we first analyzed transcriptional profiles of primary tumors from the NCI (47) and British Columbia Cancer Agency (BCCA; refs. 48, 49) cohorts and found that ABC-DLBCLs showed significantly higher *TBX21* expression than GCB-DLBCLs (Fig. 7F). When narrowing down to MCD-DLBCL, the significant difference was upheld (Supplementary Fig. S7H) despite the limited number of MCD cases. MCD showed the highest levels of *TBX21* among ABC-DLBCL only after N1 tumors (another subtype thought to originate from MBC; ref. 9). RT-qPCR and Western blot (WB) profiling of *TBX21*/T-BET in human cell lines supported these findings (Supplementary Fig. S7I–S7K). These observations in clinical specimens are consistent with the accumulation of T-BET$^+$ B cells in our preclinical models (Fig. 6H).

To provide greater evidence that AiBC-like phenotypes exist in human ABC-DLBCL, beyond *TBX21*, we analyzed published single-cell RNA-seq profiles from primary tumors (50). Most cases in that study (n = 10/17) were Epstein–Barr virus/hepatitis B virus–positive, which could drive the expansion of AiBC (38). After excluding these to avoid confounding effects (Fig. 7G), most ABC-DLBCLs (n = 5/7) showed a high proportion of cells with elevated expression of *ITGAX* and other canonical AiBC markers (e.g., *CD22*, *FCRL5*; ref. 51), whereas only a minor fraction of cells expressed these in GCB-DLBCLs (n = 2; Fig. 7H; Supplementary Fig. S7L and S7M).

Our models strongly suggest that the AiBC phenotype is linked to dissemination-prone DLBCLs. Disseminated ABC-DLBCL (stages III–IV; n = 60) showed a trend toward higher *TBX21* expression than localized tumors did (stages I–II; n = 30; Fig. 7I). Given the small number of cases in the latter category, this analysis was likely underpowered to reach statistical significance. Still, disseminated ABC-DLBCL (but not localized cases) showed significantly higher *TBX21* levels than localized (n = 100) or disseminated (n = 80) GCB-DLBCL (Fig. 7I). To complement this, we conducted T-BET IHC staining of ABC-DLBCL tissue microarrays (52). T-BET expression in tumor cells was variable and generally lower than in T cells in the same sections (Supplementary Fig. S7N). Still, in line with the mRNA data, we found that a fraction of disseminated ABC-DLBCL harbored T-BET$^+$ tumor cells, whereas these were not detected in limited-stage cases (Fig. 7J).

T-BET Supports the Self-Renewal Capacity of MCD Tumor Cells

To test whether T-BET influences the fitness of fully transformed MCD-DLBCL, we ablated T-BET in cell lines using CRISPR/CAS9 and assessed their ability to outgrow from single cells as a measure of self-renewal capacity (Fig. 7K). Bulk sequencing 48 hours after the delivery of *TBX21*-directed CAS9 complexes revealed extremely high penetrance of targeted disruptive mutations (Fig. 7L, left column). Only a minor fraction of plated cells (7/200 and 11/200, for two independent gRNAs) underwent clonal expansion as compared with *gCTRL*-treated cells (78/200 outgrows; Fig. 7L, center column). Importantly, the few *gTBX21*-treated clones that did expand showed T-BET levels comparable to parental, suggesting these derived from cells that escaped *TBX21* editing (Fig. 7L, right column). Conversely, *TBX21* ablation in a GCB-DLBCL model only had a mild nonsignificant effect on clonal fitness (Supplementary Fig. S7O–S7R). These findings suggest that T-BET retains an important role beyond lymphomagenesis by supporting the clonogenic potential of fully transformed MCD tumor cells.

DISCUSSION

During an adaptive immune response, lack of costimulation results in B-cell death, preventing the misfiring and inappropriate engagement of B cells in inflammatory responses (2, 29). Here, we found that *MYD88*^{L256P} alleviates this requirement, enabling B cells to activate, proliferate, and differentiate into long-lived MBCs even under poor costimulation. *TBL1XR1* mutations also imprint pathogenic trajectories on B cells despite limited costimulation (22), highlighting a common theme in MCD lymphomagenesis. Such autonomous programs illustrate how B cells normally attuned to their niche and under strict surveillance may initiate and sustain transformation. Moreover, although T-cell help may be readily available to B cells undergoing transformation in lymphoid tissues, this may not be the case at extranodal sites. Immune-privileged sites, which are targeted by *MYD88*^{L256P} lymphomas (53), represent an extreme scenario, in that they offer a significantly different stromal landscape and greatly restrict lymphocytic infiltration, so they are likely ill-equipped to support transformation programs reliant on extensive B/T-cell cross-talk. Our results suggest that *MYD88* mutations would still enable lymphomagenesis in such contexts. This is different from lymphomas such as classic Hodgkin, in which transformation and tumor maintenance rely on strong costimulation (54).

Our results show that *MYD88* mutations endow B cells with a lower threshold and even semiautonomous capacity to engage in proliferative responses to external signals, consistent with studies showing increased proliferation of *MYD88*^{MUT} B cells (55, 56). We find that this property leads to increased competitive fitness against WT B cells. Along these lines, we observed that mutant GCB formation and expansion occurred even in the absence of immunization. Age-associated spontaneous GC formation can be supported by TLR signaling (24). Beyond the direct effects of the *MYD88* mutation downstream of TLRs, *Myd88*^{L252P} GCB exhibited upregulation of *Tlr3* and *Tlr7*, which could further contribute to these phenomena. TLRs not only activate by sensing conserved molecular patterns in pathogens but can also become aberrantly stimulated by self-antigens (57). Notably, MCD and primary extranodal DLBCLs distinctively harbor BCRs that solely or promiscuously recognize self-antigens (9, 58). Accordingly, MCD cell lines depend on autoreactive BCR signaling for their survival *in vitro* (23). Self-reactivity could also serve as a source of continuous or repeated activation for lymphoma precursors. Self-reactive antibodies have been detected in aged mice expressing *Myd88*^{L252P} in all B cells (14). Although the early introduction of the mutation could artifactually alter central tolerance

mechanisms in the BM, recent findings showed that spontaneous GCBs from animals where *Myd88*^{L252P} was expressed in mature B cells harbored BCRs with similar properties to the self-reactive receptors in MCD cell lines (59). Here, we largely limited *Myd88*^{L252P} expression to activated mature B cells, in line with the current understanding that founder mutations most likely arise as aberrant SHM by-products (8). Normally, lack of costimulation further prevents the expansion of self-reactive B cells that escaped central tolerance checkpoints (2), and even anergic self-reactive B cells awakened by antigen mimicry need to mutate their BCRs away from self to "redeem" themselves and be positively selected (29). Here, we show that MYD88-mutant GCs are significantly more permissive in terms of antigen specificity, which could set the stage for the aberrant activation and selection of clonal precursors driven by self-reactivity.

Previous studies on the effects of *MYD88* mutations focused exclusively on plasmacytic fates, reporting abnormally elevated IgM antibodies and increased plasmablast proliferation in aged animal models (55, 60). Although informative, these did not delineate transformation trajectories or elucidate the selective advantage conferred by *MYD88*^{L265P} as a founder mutation. We and others recently showed that MBCs are the most likely MCD precursor (22, 61), challenging the long-held belief that these arise from plasmablasts (17). Similarly, WM, a disease in which >90% of tumors carry *MYD88*^{L265P} and tumor cells exhibit plasmacytic features, is thought to derive from MBC (62). In line with this revised framework, we now show that *MYD88* mutation not only provides a competitive advantage to B cells but also shepherds them toward the MBC fate. The fact that early mutations in two functionally unrelated genes, namely, *TBL1XR1* and *MYD88*, harness overlapping pathogenic trajectories, is a bona fide example of convergent evolution during lymphomagenesis.

MBCs represent a heterogeneous and largely uncharted population. Here, we found that MCD founder mutations introduce a T-BET–driven transcriptional program in GCBs and cause the cumulative expansion of AiBC-like MBCs. Unlike other MBCs, AiBC reactivation can be supported not only through BCR engagement and canonical costimulation (63) but also through TLR activation (35). TLR stimulation *ex vivo* is enough to induce T-BET expression in B cells, and increased TLR7 dosage promotes AiBC expansion (41). In turn, T-BET induces *AICDA* expression in MBC (39), which may favor the accumulation of mutations outside of a canonical GC context. Such plasticity and increased autonomy make AiBCs ideal vectors for driving pathogenic processes, as first described for autoimmune disorders (35–37). Notably, mutations similar to those in ABC-DLBCLs were identified in self-reactive pathogenic MBC in patients with Sjogren syndrome (SS; ref. 64), a rheumatic disease. Ours is the first demonstration that lymphoma mutations directly promote the generation of AiBC-like MBC in response to foreign antigens or even in the absence of immunization. A relationship between autoimmune disorders and lymphomas has been extensively reported (65), whereby patients with lupus, SS, or other autoimmune disorders show increased risk of developing aggressive lymphomas. One study on patients with lupus who developed DLBCL found most tumors corresponded to the non-GCB subtype (66). Also, a third of patients had only extranodal involvement at DLBCL diagnosis, and their onset was significantly shorter than for nodal disease alone. Given that MCDs fall into the non-GCB subclass (9), show significant association with extranodal disease (8, 47), and share a mutational landscape with primary extranodal tumors (9, 53), it is tempting to speculate that MCD-DLBCL may be disproportionately prevalent among patients with autoimmune disorders. Our finding that lymphomas and autoimmune disorders harness similar pathogenic populations provides a rationale for these clinical observations and prompts us to think of them as a spectrum rather than separate entities. Although our findings more directly support such conceptual framework for MCD and primary extranodal DLBCLs, BN2- and A53-DLBCLs also harbor self-reactive-prone BCRs (9), suggesting this may be a common theme among ABC-DLBCLs. Alternative stimuli, such as chronic infections, could similarly drive the production and restimulation of AiBC-like MBCs involved in lymphomagenesis. A clinical association between chronic viral infections and DLBCL has been made (67–69), although this appears specific to BN2-DLBCLs (70).

DLBCLs are most frequently diagnosed among people in their seventh decade, and the incidence of ABC-type tumors increases with age (71). It has been hypothesized that this skew reflects a change in normal B-cell populations during aging (71). Clonal expansion of B cells, overall reduction in B-cell diversity (72), and increased usage of the self-reactive-prone VH4-34 BCR (73) have been observed in aged individuals with no evident hematologic malignancies. This further supports a model in which a clonal and potentially autoreactive B-cell population, such as AiBC, is directly involved in lymphomagenesis. Our findings indicate that MCD founder mutations instruct these phenotypes. The incidence of *MYD88*^{L265P} was also significantly higher in tumors from older individuals (74). Mutations targeting *MYD88* have also been recently reported in lymphoid clonal hematopoiesis of indeterminate potential (L-CHIP; ref. 75), and normal precursors and mature B cells from patients with lymphoma (76), supporting the idea that MCD transformation involves a longitudinal process (Fig. 7M). Although these observations also indicate that MCD founder mutations can be acquired early in the B-cell lineage, our findings suggest that AiBC phenotypes manifest at the mature B-cell stage and support the idea that these cells acquire a GC-like state at some point during transformation.

The identification of precursor populations for aggressive and potentially incurable lymphomas remains a long sought-after but elusive goal. Here, we show that founder mutations associated with extranodal DLBCL give rise to a phenotypically distinguishable MBC subpopulation that differentially accumulates in time. In line with their prospective role as precursor cells, canonical AiBCs disseminate and can be found in circulation and distributed to many tissues (77). These observations raise the provocative idea that an accumulation of AiBC-like MBCs may be detectable in patients with lymphoma preceding primary tumor onset and/or ensuing relapses, paving the way for risk-based stratification and prophylactic interventions. This could further apply to premalignant conditions known

to harbor *MYD88*^{L265P}, such as monoclonal gammopathy of undetermined significance (78) or L-CHIP (75). Given their dismal outcome, patients at risk of developing central nervous system relapses routinely receive prophylactic treatment with methotrexate, a broad immunosuppressant, but recent studies have shown this to be largely ineffective (79). In this regard, we have unveiled a new axis involved in extranodal DLBCL pathogenesis amenable to therapeutic targeting. Despite advances in direct pharmacologic inhibition (80, 81) or proteolysis-targeting chimeras (82, 83) against transcription factors, blocking of signaling cascades upstream of T-BET, including the use of TLR7/9 inhibitors (84), appears as an alternative that could be more readily implemented. In addition to exploring these aspects, future studies should determine the exact mechanisms of actions of T-BET and other AiBC features in the context of extranodal lymphomagenesis and explore their potential value as predictive biomarkers for dissemination.

METHODS

Mouse Models

Animal care was in strict compliance with institutional guidelines established by Weill Cornell Medicine (WCM), the Guide for the Care and Use of Laboratory Animals (National Academy of Sciences, 1996), and the Association for Assessment and Accreditation of Laboratory Animal Care International. The Research Animal Resource Center of WCM (protocol #2011-0031) and the Landesamt für Natur, Umwelt und Verbraucherschutz NRW (LANUV; (AZ: 84-02.04.2014.A146, 84-02.04.2017.A131, 81-02.04.2019.A009) approved all mouse procedures. The following strains were obtained from The Jackson Laboratory: C57Bl/6J (CD45.2, stock 000664; RRID:IMSR_JAX:000664), C57BL/6-Myd88tm1.1Rein/J (*Myd88*-L252P, stock 029349; RRID:IMSR_JAX:029349), Cγ1-Cre (stock 010611; RRID:MMRRC_010611-UCD), CD19-Cre (stock 006785; RRID:IMSR_JAX:006785), B6.SJL-PtprcaPepcb/Boy (CD45.1, stock 002014; RRID:IMSR_JAX:002014), Rosa26-lox-stop-lox-YFP (*Rosa26YFP*; stock 006148; RRID:MMRRC_006148-UCD), and B1-8hi (stock 007594; RRID:IMSR_JAX:007594). The generation of the conditional *Tbl1xr1*-D370Y mouse model has been described (22). Animals were housed in specific pathogen–free facilities. Experiments were conducted using aged and sex-matched littermates wherever possible. Experiments were designed to include male and female specimens in all groups, and no sex-based influence/bias was detected in the observations made in this work. Unless stated otherwise in the text, animals were 8 to 12 weeks of age at the time of experimentation. BM transplantations to generate chimeric animals, immunization strategies, and use of CD40L-blocking antibodies were all conducted as described (22).

Cell Lines

The DLBCL cell lines OCI-Ly1 (CVCL_1879; male origin; RRID:CVCL_1879), OCI-Ly3 (CVCL_8800; male origin; RRID:CVCL_8800), OCI-Ly8 (CVCL_8803; male origin; CVCL_8803), and OCI-Ly10 (CVCL_8795; female origin; RRID:CVCL_8795) were grown in Iscove's Modified Dulbecco's Media (12440061; ThermoFisher Scientific) supplemented with 10% FBS and penicillin G/streptomycin; U2932 (CVCL_1896; female origin; CVCL_1896), HBL1 (CVCL_4213; male origin; RRID:CVCL_4213), TMD8 (CVCL_A442, male origin), MD901 (CVCL_D709; male origin; RRID:CVCL_A442), RIVA (CVCL_1885; female origin; RRID:CVCL_1885), RC-K8 (CVCL_1883; male origin; RRID:CVCL_1883), and HLY-1 (CVCL_H207; RRID:CVCL_H207) were grown in RPMI medium (10-040-CV; Corning) supplemented with 10% FBS, penicillin G/streptomycin, L-glutamine, and HEPES. All cells were grown in incubators at 37°C in a 5% CO_2 atmosphere. Cells were maintained in culture for up to 4 to 6 weeks between the time of thawing and experimentation. HBL-1, HLY-1, and U2932 were obtained from Jose Martinez-Climent (Universidad de Navarra, Pamplona, Spain); OCI-Ly3 were obtained from Anas Younes (Memorial Sloan Kettering Cancer Center, New York, NY; OCI-Ly1, OCI-Ly7, OCI-Ly8, and OCI-Ly10 were obtained from the Ontario Cancer Institute; TMD8 was obtained from Louis M. Staudt (NCI); and RC-K8 and RIVA were obtained from the German Collection of Microorganisms and Cell Cultures GmbH (DSMZ). Cell line authentication was performed at IDEXX BioResearch, using methods recommended by the American National Standards Institute (ASN-0002-2011). Cell lines were confirmed to be of human origin and tested for evidence of cross-species contamination (mouse, rat, Chinese hamster, and African green monkey). All cell lines were routinely tested for *Mycoplasma* contamination using a MycoAlert PLUS Detection Kit (LT07-705).

FC Analysis and Cell Sorting

Single-cell suspensions from mouse spleens, lymph nodes, BM, or tumors were stained using the following fluorescent-labeled anti-mouse antibodies: from eBioscience ThermoFisher Scientific: PE-Cy5.5 anti-CD11c (35-0114-80, dilution 1:200; RRID:AB_11219866), PE-Cy7 anti-CD11b (25-0112-82, dilution 1:400; RRID:AB_469588), APC anti-CD38 (17-0381, dilution 1:500; RRID:AB_469381), PE anti-CXCR4 (12-9991, dilution 1:400; RRID:AB_891391), PerCP-Cy5.5 anti-CD45.1 (45-0453, dilution 1:500; RRID:AB_1107003), FITC anti–PD-1 (11–9985, dilution 1:150; RRID:AB_465472); from BD Biosciences: AF647 anti–active caspase-3 (560626, dilution 1:100; RRID:AB_1727414), BUV615 anti-CD45 (752418, dilution 1:500; RRID:AB_2917432), BV421 and BV711 anti–Ki-67 (562899 and 563755, dilution 1:500; RRID:AB_2686897 and RRID:AB_2738406), FITC, PE-Cy7, and BV786 anti-B220 (553087, 552772 and 563894, dilution 1:500; RRID:AB_394617, RRID:AB_394458, and RRID:AB_2738472), BV421, BUV805, and PE-Cy7 anti-FAS (562633, 741968, and 557653, dilution 1:500; RRID:AB_2737690, RRID:AB_2871273, and RRID:AB_396768), BUV563 and BUV395 anti-CD38 (741271 and 740245, dilution 1:500; RRID:AB_2870812 and RRID:AB_2739992), PE-Cy7 anti-CXCR5 (560617, dilution 1:100; RRID:AB_1727521), PE-Cy7 anti-CD86 (560582 and 564198, dilution 1:300; RRID:AB_1727518 and RRID:AB_2738663), BV510 anti-IgD (563110, dilution 1:500; RRID:AB_2737003), APC and BUV737A anti-CD138 (558626 and 564430, dilution 1:500; RRID:AB_1645216 and RRID:AB_2738805), FITC anti-CD19 (553785, dilution 1:500; RRID:AB_395049), FITC and AF647 anti-GL7 (553666 and 561529, dilution 1:500; RRID:AB_394981 and RRID:AB_10716056); from BioLegend: APC anti-CD11b (101212, dilution 1:400; RRID:AB_312795), BV785 and APC-Cy7 anti-CD11c (117336 and 117324, dilution 1:200; RRID:AB_2565268 and RRID:AB_830649) BV711 and APC anti–T-BET (644820 and 644814, dilution 1:100; RRID:AB_2715766 and RRID:AB_10901173), PercP-Cy5.5 anti-CD138 (142510, dilution 1:500; RRID:AB_2561601) Spark NIR 685 anti-CD19 (115567, dilution 1:500; RRID:AB_2819828), AF488 anti-IgD (405717, dilution 1:500; RRID:AB_10730618), APC-Cy7 anti-CD4 (100414, dilution 1:500; RRID:AB_312699), APC-Cy7 anti-CD45.1 (110716, dilution 1:500; RRID:AB_313505), PerCP-Cy5.5 anti-CD45.2 (109828, dilution 1:500; RRID:AB_893350), APC anti-CD3 (100235, dilution 1:500; RRID:AB_2561455), APC-Cy7 and PE anti-B220 (103224 and 103208, dilution 1:500; RRID:AB_313007 and RRID:AB_312993), PerCP-Cy5.5 anti-GL7 (144610, dilution 1:500; RRID:AB_2562979), PerCP-Cy5.5 anti-FAS (152610, dilution 1:500; RRID:AB_2632905), BV605 anti-CD86 (105037, dilution 1:300; RRID:AB_11204429), PE

anti-TLR7 (160004, dilution 1:100; RRID:AB_2876562); and from Biosearch Technologies: PE NP (N-5070-1, dilution 1:100). NIP-haptenated FITC was obtained from M.J. Shlomchik (University of Pittsburgh, Pittsburgh, PA). A Zombie NIR Fixable Viability Kit (423105, BioLegend), a LIVE/DEAD Fixable Violet Dead Cell Stain Kit (L34963; ThermoFisher Scientific), or DAPI (D1306; ThermoFisher Scientific) was used for exclusion of dead cells. Intracellular stains, AnnexinV/DAPI stains, and detection of EdU incorporation were performed as described (22). Proliferation was assessed using a CellTrace CFSE Cell Proliferation Kit (C34554; ThermoFisher Scientific) according to the vendor's protocol. Data were acquired on a BD Fortessa or BD Symphony instrument (BD Biosciences) or a Cytek Aurora spectral FC analyzer (Cytek) and analyzed using a FlowJo software package (BD Biosciences; RRID:SCR_008520).

When B-cell populations were sorted, single-cell suspensions were preenriched in B cells using positive selection with anti-B220 magnetic microbeads (130-049-501; Miltenyi Biotec) or negative selection with the EasySep Mouse B-Cell Isolation Kit (19854; STEMCELL Technologies). The stated populations were then isolated using a BD FACSAria II or a BD Influx cell sorter (BD Biosciences).

Primary B-cell Cultures

Total splenocytes were harvested from 8- to 16-week-old naïve mice, and NBs were isolated using negative selection with CD43 magnetic beads (130-049-801; Miltenyi Biotec) in accordance with the manufacturer's protocol. In some experiments, cells were stained with a CellTrace proliferation dye as noted above. Cells were seeded at 1×10^6 cells/mL in RPMI media with 10% FBS, penicillin G/streptomycin, MEM nonessential AA (11140050, Thermo Fisher Scientific), 50 μmol/L 2-Mercaptoethanol (21985023, Thermo Fisher Scientific), containing the indicated concentrations of murine recombinant IL4 (0–25 ng/mL; 404-ML; R&D Systems) and a functional grade anti-CD40 monoclonal antibody (0–1 μg/mL; 16-0402-82, Thermo Fisher Scientific; RRID:AB_468945). Cells were incubated at 37°C with 5% CO_2, and the culture medium was renewed every 2 to 3 days.

CRISPR Editing of DLBCL Cell Lines and Primary B Cells

Human cell lines were electroporated using an Amaxa Nucleofector and the SF Cell Line 4D-Nucleofector X Kit (PBC2-22500; Lonza) to incorporate a recombinant Cas9 nuclease (Alt-R S.p. Cas9 Nuclease V3, #1081058), control (#1072544 or #1072545), or *TBX21*-targeting gRNAs (*Hs.Cas9.TBX21.1.AB "#1"*: 5′-GCGGUACCAGAGCGGCAAGU-3′; *Hs.Cas9.TBX21.1.AC "#2"*: 5′-GAUUAAACUUGGACCACAAC-3′), electroporation enhancer (#1075915), and a tracrRNA-ATTO550 (#1075927; all from Integrated DNA Technologies) following the vendor's recommendations. For primary murine B cells, the P4 Primary Cell 4D-Nucleofector X Kit L (V4XP4012; Lonza) was used, along with control or *Tbx21*-targeting (*Mm.Cas9.TBX21.1.AA*: 5′-UCCAAGGAAGCGACCCGGCG-3′; *Mm.Cas9.TBX21.1.AC:* 5′-GGUUGAACUUGGACCACAAC-3′; Integrated DNA Technologies) gRNAs.

B-cell Adoptive Transfer

For B-cell adoptive transfers, total splenocytes were harvested from 8- to 12-week-old donor mice (*Cd45.1/1* or *Cd45.1/2*), and B cells were isolated using negative selection as described above. To increase the number of productive (NP-binding) B cells in the mix, cells were further subjected to Igκ light chain–based depletion. To this end, an anti-Igκ antibody (409502, BioLegend; RRID:AB_2563297) biotinylated in-house (ab201796; Abcam) was added during magnetic B-cell isolation. Cells were grown overnight in complete media containing 25 ng/mL murine recombinant IL4 and 1 μg/mL of an anti-CD40 antibody. Cells were nucleofected with ATTO-labeled CAS9 ribonucleoprotein complexes as stated above and were allowed to recover overnight in complete media supplemented with IL4 and the CD40 agonist. The percentage of $ATTO^+$ and NP-binding cells in each population was determined by FC to allow for normalization across conditions. Cells were allowed to rest in complete media without IL4/anti-CD40 for >2 hours prior to transfer. A number of mature B cells corresponding to 1×10^5 $ATTO^+NP^+$ B cells were injected i.v. into C57Bl/6J recipient mice (*Cd45.2/2*). Recipient animals were immunized with an NP conjugate 16 hours after cell transfer and euthanized for analysis at the stated time points.

Quantitative Real-Time PCR

Total RNA extracts and cDNA synthesis were conducted as described (22). Expression of genes of interest was detected using a Fast SYBR Green Master Mix (4385614; Thermo Fisher Scientific) on a QuantStudio6 Flex Real-Time PCR System (Thermo Fisher Scientific). Gene expression was normalized to Actin or GAPDH levels using the ΔΔC(t) method. Primer sequences were as follows (5′→3′): hTBX21.F: GGTTGCGGAGACATGCTGA; hTBX21.R: GTAGGCGTAGGCTCCAAGG; mTbx21.F: AGCAAGGACGGCGAATGTT; mTbx21.R: GGGTGGACATATAAGCGGTTC; mItgax.F: CTGGATAGCCTTTCTTCTGCTG; mItgax.R: GCACACTGTGTCCGAACTCA; and mItgam.F: ATGGACGCTGATGGCAATACC; mItgam.R: TCCCCATTCACGTCTCCCA.

Targeted Genomic Sequencing

Genomic DNA from primary B cells or human DLBCL cell lines was extracted as described (22). DNA concentration was determined using Qubit Fluorometric Quantification, and the amount of template DNA across samples was normalized for amplification. The CRISPR-targeted *Tbx21* or *TBX21* loci were PCR-amplified using the following primers (5′→3′): hTBX21.AB.F: AGGATGTTTG TGGACGTGGT; hTBX21.AB.R: CAGGAAGCCAGAAACAGGAG; hTBX21.AC.F: AGGTGTCGGGGAAACTGAG; hTBX21.AC.R: CCT GTCTCCCTACGCTGAAG; and mTbx21AA.F: CTC AGCTTCCCAGACACCTC; mTbx21AA.R: GACCAACAGCATCGTTTCTTC. PCR products were resolved by agarose gel electrophoresis, bands of interest were excised, and DNA was retrieved using the QIAquick Gel Extraction Kit (28706 × 4; Qiagen). Library preparation, amplicon sequencing, and variant calling were performed by GENEWIZ or the Massachusetts General Hospital Center for Computational and Integrative Biology DNA Core.

BCR sequencing from primary murine cells was conducted by Adaptive Biotechnologies using an ImmunoSEQ Assay (85) as described (86). BCR repertoire analysis, including clonality and mutation burden calculations, was performed using the immunoSEQ Analyzer 3.0 (Adaptive Biotechnologies).

RNA-seq

Library preparation, sequencing, and post-processing of the raw data were performed at the Genomics Core at WCM, as described (22). Paired-end sequencing (PE75 × 2) was performed on an Illumina NextSeq 500 instrument (Illumina). Hierarchical clustering was performed using Euclidean distance of log transcripts per million (TPM) + 0.1 values of genes within the top 5th percentile of SD across replicates and Ward's minimum variance. Gene set enrichment analysis (GSEA) was performed using the GSEA algorithm as described in (87). Pathway analysis was performed using the PAGE algorithm (88).

Histology and IHC

Murine tissue preparation and staining were conducted by the Laboratory of Comparative Pathology at Memorial Sloan Kettering Cancer Center as described (22, 89). The following primary

antibodies were used for IHC: biotin-conjugated anti-B220 (550286; BD Biosciences; RRID:AB_393581) and anti-PNA (B1075; Vector Laboratories; RRID:AB_2313597). IHC on human specimens was performed at the BCCA as described previously (49, 52), using an anti–T-BET (4B10) antibody (561262; BD Biosciences; dilution 1:50; RRID:AB_10565981). T-BET staining was semiquantitatively assessed on tumor cells using HistoScore (HS = $I \times P$): intensity (I = [1–3]) and percentage of positive cells (P = [0–100]). Specimens with HS > 10 were defined as T-BET–positive.

Cell Lysis and Immunoblotting

Whole-cell protein lysate preparation and SDS-PAGE analysis were performed as described (22), using the following primary antibodies: β-ACTIN (C-4; sc-47778; Santa Cruz Biotechnology; RRID:AB_626632), T-BET (D6N8B; #13232; RRID:AB_2616022), IκBα (44D4; #4812; RRID:AB_10694416), and Phospho-IκBα (Ser32; 14D4; #2859S; RRID:AB_561111; Cell Signaling Technology).

Data Availability

RNA-seq data from this article have been deposited in the Gene Expression Omnibus database (RRID:SCR_005012) under accession number GSE201058. Gene expression data from individuals with *de novo* DLBCL from the NCI (47), BCCA (49), and Sun Yat-sen University Cancer Center (50) cohorts had been previously published. The code used for analysis is available upon request.

Statistical Analysis

Statistical parameters, including the exact value and definition of n, precision measures (mean ± SEM or SD), and statistical significance are reported in figures and figure legends. No statistical methods were used to predetermine animal sample sizes, but these were decided based on reports using similar models and approaches (13, 14, 22, 89). Statistical analysis was conducted using GraphPad Prism 8 (GraphPad Software; RRID:SCR_002798) or the R statistical language scripts and packages specified. Data were judged to be statistically significant when $P < 0.05$. Asterisks in figures denote statistical significance (*, $P < 0.05$; **, $P < 0.01$; ***, $P < 0.001$).

Authors' Disclosures

M.A. Rivas reports grants from the American Society of Hematology during the conduct of the study. M. Xia reports grants from Janssen outside the submitted work. C. Meydan reports personal fees from Thorne HealthTech outside the submitted work. C.E. Mason reports personal fees from Tempus Labs and is cofounder of Onegevity and Biotia outside the submitted work. C. Steidl reports personal fees from Bayer, and grants from Epizyme and Trillium Therapeutics outside the submitted work. D.W. Scott reports personal fees from AbbVie, AstraZeneca, and Incyte, grants and personal fees from Janssen, and grants from Roche outside the submitted work, as well as a patent describing the use of gene expression to subtype aggressive B-cell lymphomas pending, issued, and licensed to NanoString Technologies. H.C. Reinhardt reports grants from Deutsche Forschungsgemeinschaft, Deutsche Jose Carreras Leukâmie Stiftung, Else Kröner-Fresenius Stiftung, and Deutsche Krebshilfe during the conduct of the study; grants, personal fees, and other support from AstraZeneca and Gilead, personal fees and other support from AbbVie, Bristol Myers Squibb, Novartis, and Roche, personal fees from Merck and Vertex, and nonfinancial support and other support from SinABiomedics outside the submitted work; and is a cofounder of CDL Therapeutics GmbH. A.B. Pernis reports personal fees from Ono Pharmaceutical outside the submitted work, as well as a patent for US 11,147,829 B2 issued. A.M. Melnick reports grants from Janssen, grants and personal fees from Epizyme and Daiichi Sankyo, and personal fees from Treeline outside the submitted work. No disclosures were reported by the other authors.

Authors' Contributions

L. Venturutti: Conceptualization, resources, data curation, formal analysis, supervision, funding acquisition, investigation, visualization, methodology, writing–original draft, project administration, writing–review and editing. **M.A. Rivas:** Formal analysis, validation, investigation, project administration. **B.W. Pelzer:** Formal analysis, investigation, methodology, project administration. **R. Flümann:** Resources, investigation. **J. Hansen:** Resources, investigation. **I. Karagiannidis:** Investigation. **M. Xia:** Investigation, visualization, methodology. **D.R. McNally:** Data curation, formal analysis, investigation, visualization, methodology. **Y. Isshiki:** Investigation, methodology. **A. Lytle:** Formal analysis, investigation, methodology. **M. Teater:** Data curation, formal analysis, investigation, visualization, methodology. **C.R. Chin:** Data curation, formal analysis. **C. Meydan:** Data curation, formal analysis. **G. Knittel:** Resources, investigation, methodology. **E. Ricker:** Resources, methodology. **C.E. Mason:** Data curation, formal analysis. **X. Ye:** Resources. **Q. Pan-Hammarström:** Resources. **C. Steidl:** Resources. **D.W. Scott:** Resources. **H.C. Reinhardt:** Resources, formal analysis, supervision, funding acquisition, writing–review and editing. **A.B. Pernis:** Resources, formal analysis, methodology, writing–review and editing. **W. Béguelin:** Supervision, investigation, methodology, project administration, writing–review and editing. **A.M. Melnick:** Conceptualization, resources, formal analysis, supervision, funding acquisition, methodology, writing–original draft, project administration, writing–review and editing.

Acknowledgments

We thank all members of the Melnick lab for thoughtful discussions and suggestions, Mohamed Moustafa for his help with FC optimization, Hao Shen for his outstanding support with mouse colonies, the Genomics Core and Flow Cytometry Core (WCM), Molecular Cytology Core Facility (MSKCC), and Center of Comparative Medicine and Pathology (WCM/MSKCC). L. Venturutti is a Michael Smith Health Research BC Scholar and is funded by the BC Cancer Foundation, the Canadian Institutes of Health Research (Project Grant #180613), and The Leukemia & Lymphoma Society (LLS)-TRP 6663-23. M.A. Rivas was funded by an ASH Junior Faculty Scholar Award. B.W. Pelzer was funded by Deutsche Krebshilfe (Mildred Scheel Nachwuchszentrum Grant #70113307). C.E. Mason was funded by Scientific Computing Unit, XSEDE Supercomputing Resources, the Starr Cancer Consortium (I7-A765, I9-A9-071, I13-0052), the Vallee Foundation, the WorldQuant Foundation, the Pershing Square Sohn Cancer Research Alliance, the NIH (R01MH117406, R01CA249054, R01AI151059, P01CA214274), and the LLS (9238-16, LLS-MCL-982). Q. Pan-Hammarström was funded by the Swedish Research Council, the Swedish Cancer Society, CIMED, Radiumhemmets research fund, and the Knut and Alice Wallenberg Foundation. A.B. Pernis was funded by the NIH (AR064883 and AR070146). E. Ricker was funded by a T32 Rheumatology Research Training Grant. H.C Reinhardt was funded by Deutsche Forschungsgemeinschaft (RE2246/13-1, SFB-1430-A09, SFB-1530-A01), Deutsche Jose Carreras Leukämie Stiftung (R12/08), Else Kröner-Fresenius Stiftung (EKFS-2014-A06, 2016_Kolleg.19), and Deutsche Krebshilfe (1117240 and 70113041). A.M. Melnick was funded by NCI-R35 CA220499 and LLS-SCOR 7012-16.

The publication costs of this article were defrayed in part by the payment of publication fees. Therefore, and solely to indicate this fact, this article is hereby marked "advertisement" in accordance with 18 USC section 1734.

Note

Supplementary data for this article are available at Cancer Discovery Online (http://cancerdiscovery.aacrjournals.org/).

Received May 13, 2022; revised September 26, 2022; accepted October 17, 2022; published first October 20, 2022.

REFERENCES

1. Sehn LH, Salles G. Diffuse large B-cell lymphoma. N Engl J Med 2021;384:842–58.
2. Brink R, Phan TG. Self-reactive B cells in the germinal center reaction. Annu Rev Immunol 2018;36:339–57.
3. Victora GD, Nussenzweig MC. Germinal centers. Annu Rev Immunol 2022;40:413–42.
4. Venturutti L, Melnick AM. The role of epigenetic mechanisms in B cell lymphoma pathogenesis. Annu Rev Cancer Biology 2021;5: 311–30.
5. Bobillo S, Joffe E, Lavery JA, Sermer D, Ghione P, Noy A, et al. Clinical characteristics and outcomes of extranodal stage I diffuse large B-cell lymphoma in the rituximab era. Blood 2021;137:39–48.
6. Castillo JJ, Winer ES, Olszewski AJ. Sites of extranodal involvement are prognostic in patients with diffuse large B-cell lymphoma in the rituximab era: an analysis of the surveillance, epidemiology and end results database. Am J Hematol 2014;89:310–4.
7. Lu CS, Chen JH, Huang TC, Wu YY, Chang PY, Dai MS, et al. Diffuse large B-cell lymphoma: sites of extranodal involvement are a stronger prognostic indicator than number of extranodal sites in the rituximab era. Leuk Lymphoma 2015;56:2047–55.
8. Chapuy B, Stewart C, Dunford AJ, Kim J, Kamburov A, Redd RA, et al. Molecular subtypes of diffuse large B cell lymphoma are associated with distinct pathogenic mechanisms and outcomes. Nat Med 2018;24:679–90.
9. Wright GW, Huang DW, Phelan JD, Coulibaly ZA, Roulland S, Young RM, et al. A probabilistic classification tool for genetic subtypes of diffuse large B cell lymphoma with therapeutic implications. Cancer Cell 2020;37:551–68.
10. Ngo VN, Young RM, Schmitz R, Jhavar S, Xiao W, Lim KH, et al. Oncogenically active MYD88 mutations in human lymphoma. Nature 2011;470:115–9.
11. Shuai W, Lin P, Strati P, Patel KP, Routbort MJ, Hu S, et al. Clinicopathological characterization of chronic lymphocytic leukemia with MYD88 mutations: L265P and non-L265P mutations are associated with different features. Blood Cancer J 2020;10:86.
12. Treon SP, Xu L, Liu X, Hunter ZR, Yang G, Castillo JJ. Genomic landscape of waldenstrom macroglobulinemia. Hematol Oncol Clin North Am 2018;32:745–52.
13. Knittel G, Liedgens P, Korovkina D, Seeger JM, Al-Baldawi Y, Al-Maarri M, et al. B-cell-specific conditional expression of Myd88p. L252P leads to the development of diffuse large B-cell lymphoma in mice. Blood 2016;127:2732–41.
14. Flumann R, Rehkamper T, Nieper P, Pfeiffer P, Holzem A, Klein S, et al. An autochthonous mouse model of Myd88- and BCL2-driven diffuse large B-cell lymphoma reveals actionable molecular vulnerabilities. Blood Cancer Discov 2021;2:70–91.
15. Roco JA, Mesin L, Binder SC, Nefzger C, Gonzalez-Figueroa P, Canete PF, et al. Class-switch recombination occurs infrequently in germinal centers. Immunity 2019;51:337–50.
16. Cattoretti G, Buttner M, Shaknovich R, Kremmer E, Alobeid B, Niedobitek G. Nuclear and cytoplasmic AID in extrafollicular and germinal center B cells. Blood 2006;107:3967–75.
17. Venturutti L, Melnick AM. The dangers of deja vu: memory B cells as the cells of origin of ABC-DLBCLs. Blood 2020;136:2263–74.
18. Casola S, Cattoretti G, Uyttersprot N, Koralov SB, Seagal J, Hao Z, et al. Tracking germinal center B cells expressing germ-line immunoglobulin gamma1 transcripts by conditional gene targeting. Proc Natl Acad Sci U S A 2006;103:7396–401.
19. Merkenschlager J, Finkin S, Ramos V, Kraft J, Cipolla M, Nowosad CR, et al. Dynamic regulation of TFH selection during the germinal centre reaction. Nature 2021;591:458–63.
20. Rivas MA, Meydan C, Chin CR, Challman MF, Kim D, Bhinder B, et al. Smc3 dosage regulates B cell transit through germinal centers and restricts their malignant transformation. Nat Immunol 2021;22: 240–53.
21. Robinson MD, McCarthy DJ, Smyth GK. edgeR: a Bioconductor package for differential expression analysis of digital gene expression data. Bioinformatics 2010;26:139–40.
22. Venturutti L, Teater M, Zhai A, Chadburn A, Babiker L, Kim D, et al. TBL1XR1 mutations drive extranodal lymphoma by inducing a protumorigenic memory fate. Cell 2020;182:297–316.
23. Young RM, Wu T, Schmitz R, Dawood M, Xiao W, Phelan JD, et al. Survival of human lymphoma cells requires B-cell receptor engagement by self-antigens. Proc Natl Acad Sci U S A 2015;112:13447–54.
24. Soni C, Wong EB, Domeier PP, Khan TN, Satoh T, Akira S, et al. B cell-intrinsic TLR7 signaling is essential for the development of spontaneous germinal centers. J Immunol 2014;193:4400–14.
25. Bhattacharya D, Cheah MT, Franco CB, Hosen N, Pin CL, Sha WC, et al. Transcriptional profiling of antigen-dependent murine B cell differentiation and memory formation. J Immunol 2007;179:6808–19.
26. Suan D, Krautler NJ, Maag JLV, Butt D, Bourne K, Hermes JR, et al. CCR6 defines memory B cell precursors in mouse and human germinal centers, revealing light-zone location and predominant low antigen affinity. Immunity 2017;47:1142–53.
27. Takatsuka S, Yamada H, Haniuda K, Saruwatari H, Ichihashi M, Renauld JC, et al. IL-9 receptor signaling in memory B cells regulates humoral recall responses. Nat Immunol 2018;19:1025–34.
28. Srinivas S, Watanabe T, Lin CS, William CM, Tanabe Y, Jessell TM, et al. Cre reporter strains produced by targeted insertion of EYFP and ECFP into the ROSA26 locus. BMC Dev Biol 2001;1:4.
29. Burnett DL, Reed JH, Christ D, Goodnow CC. Clonal redemption and clonal anergy as mechanisms to balance B cell tolerance and immunity. Immunol Rev 2019;292:61–75.
30. Davis RE, Brown KD, Siebenlist U, Staudt LM. Constitutive nuclear factor kappaB activity is required for survival of activated B cell-like diffuse large B cell lymphoma cells. J Exp Med 2001;194:1861–74.
31. Shi GX, Harrison K, Wilson GL, Moratz C, Kehrl JH. RGS13 regulates germinal center B lymphocytes responsiveness to CXC chemokine ligand (CXCL)12 and CXCL13. J Immunol 2002;169:2507–15.
32. Umeshita-Suyama R, Sugimoto R, Akaiwa M, Arima K, Yu B, Wada M, et al. Characterization of IL-4 and IL-13 signals dependent on the human IL-13 receptor alpha chain 1: redundancy of requirement of tyrosine residue for STAT3 activation. Int Immunol 2000;12:1499–509.
33. Jackson SW, Jacobs HM, Arkatkar T, Dam EM, Scharping NE, Kolhatkar NS, et al. B cell IFN-gamma receptor signaling promotes autoimmune germinal centers via cell-intrinsic induction of BCL-6. J Exp Med 2016;213:733–50.
34. Prabhu N, Ho AW, Wong KH, Hutchinson PE, Chua YL, Kandasamy M, et al. Gamma interferon regulates contraction of the influenza virus-specific CD8 T cell response and limits the size of the memory population. J Virol 2013;87:12510–22.
35. Cancro MP. Age-associated B cells. Annu Rev Immunol 2020;38: 315–40.
36. Rubtsova K, Rubtsov AV, Thurman JM, Mennona JM, Kappler JW, Marrack P. B cells expressing the transcription factor T-bet drive lupus-like autoimmunity. J Clin Invest 2017;127:1392–404.
37. Wei C, Anolik J, Cappione A, Zheng B, Pugh-Bernard A, Brooks J, et al. A new population of cells lacking expression of CD27 represents a notable component of the B cell memory compartment in systemic lupus erythematosus. J Immunol 2007;178:6624–33.
38. Phalke S, Marrack P. Age (autoimmunity) associated B cells (ABCs) and their relatives. Curr Opin Immunol 2018;55:75–80.
39. Barnett BE, Staupe RP, Odorizzi PM, Palko O, Tomov VT, Mahan AE, et al. Cutting edge: B cell-intrinsic T-bet expression is required to control chronic viral infection. J Immunol 2016;197:1017–22.
40. Rubtsov AV, Rubtsova K, Fischer A, Meehan RT, Gillis JZ, Kappler JW, et al. Toll-like receptor 7 (TLR7)-driven accumulation of a novel CD11c(+) B-cell population is important for the development of autoimmunity. Blood 2011;118:1305–15.
41. Ricker E, Manni M, Flores-Castro D, Jenkins D, Gupta S, Rivera-Correa J, et al. Altered function and differentiation of age-associated

B cells contribute to the female bias in lupus mice. Nat Commun 2021;12:4813.
42. Russell Knode LM, Naradikian MS, Myles A, Scholz JL, Hao Y, Liu D, et al. Age-associated B cells express a diverse repertoire of VH and vkappa genes with somatic hypermutation. J Immunol 2017;198:1921–7.
43. Song W, Antao OQ, Condiff E, Sanchez GM, Chernova I, Zembrzuski K, et al. Development of Tbet- and CD11c-expressing B cells in a viral infection requires T follicular helper cells outside of germinal centers. Immunity 2022;55:290–307.
44. Han JH, Akira S, Calame K, Beutler B, Selsing E, Imanishi-Kari T. Class switch recombination and somatic hypermutation in early mouse B cells are mediated by B cell and Toll-like receptors. Immunity 2007;27:64–75.
45. Shih TA, Roederer M, Nussenzweig MC. Role of antigen receptor affinity in T cell-independent antibody responses in vivo. Nat Immunol 2002;3:399–406.
46. Hartweger H, McGuire AT, Horning M, Taylor JJ, Dosenovic P, Yost D, et al. HIV-specific humoral immune responses by CRISPR/Cas9-edited B cells. J Exp Med 2019;216:1301–10.
47. Schmitz R, Wright GW, Huang DW, Johnson CA, Phelan JD, Wang JQ, et al. Genetics and pathogenesis of diffuse large B-cell lymphoma. N Engl J Med 2018;378:1396–407.
48. Arthur SE, Jiang A, Grande BM, Alcaide M, Cojocaru R, Rushton CK, et al. Genome-wide discovery of somatic regulatory variants in diffuse large B-cell lymphoma. Nat Commun 2018;9:4001.
49. Ennishi D, Healy S, Bashashati A, Saberi S, Hother C, Mottok A, et al. TMEM30A loss-of-function mutations drive lymphomagenesis and confer therapeutically exploitable vulnerability in B-cell lymphoma. Nat Med 2020;26:577–88.
50. Ye X, Wang L, Nie M, Wang Y, Dong S, Ren W, et al. A single-cell atlas of diffuse large B cell lymphoma. Cell Rep 2022;39:110713.
51. Sutton HJ, Aye R, Idris AH, Vistein R, Nduati E, Kai O, et al. Atypical B cells are part of an alternative lineage of B cells that participates in responses to vaccination and infection in humans. Cell Rep 2021;34:108684.
52. Scott DW, Mottok A, Ennishi D, Wright GW, Farinha P, Ben-Neriah S, et al. Prognostic significance of diffuse large B-cell lymphoma cell of origin determined by digital gene expression in formalin-fixed paraffin-embedded tissue biopsies. J Clin Oncol 2015;33:2848–56.
53. Chapuy B, Roemer MG, Stewart C, Tan Y, Abo RP, Zhang L, et al. Targetable genetic features of primary testicular and primary central nervous system lymphomas. Blood 2016;127:869–81.
54. Wein F, Kuppers R. The role of T cells in the microenvironment of Hodgkin lymphoma. J Leukoc Biol 2016;99:45–50.
55. Schmidt K, Sack U, Graf R, Winkler W, Popp O, Mertins P, et al. B-cell-specific Myd88 L252P expression causes a premalignant gammopathy resembling IgM MGUS. Front Immunol 2020;11:602868.
56. Wang JQ, Jeelall YS, Beutler B, Horikawa K, Goodnow CC. Consequences of the recurrent MYD88(L265P) somatic mutation for B cell tolerance. J Exp Med 2014;211:413–26.
57. Farrugia M, Baron B. The role of toll-like receptors in autoimmune diseases through failure of the self-recognition mechanism. Int J Inflam 2017;2017:8391230.
58. Montesinos-Rongen M, Terrao M, May C, Marcus K, Blumcke I, Hellmich M, et al. The process of somatic hypermutation increases polyreactivity for central nervous system antigens in primary central nervous system lymphoma. Haematologica 2021;106:708–17.
59. Pindzola GM, Razzaghi R, Tavory RN, Nguyen HT, Morris VM, Li M, et al. Aberrant expansion of spontaneous splenic germinal centers induced by hallmark genetic lesions of aggressive lymphoma. Blood 2022;140:1119–31.
60. Ouk C, Roland L, Gachard N, Poulain S, Oblet C, Rizzo D, et al. Continuous MYD88 activation is associated with expansion and then transformation of IgM differentiating plasma cells. Front Immunol 2021;12:641692.
61. Holmes AB, Corinaldesi C, Shen Q, Kumar R, Compagno N, Wang Z, et al. Single-cell analysis of germinal-center B cells informs on lymphoma cell of origin and outcome. J Exp Med 2020;217:e20200483.
62. Garcia-Sanz R, Jimenez C, Puig N, Paiva B, Gutierrez NC, Rodriguez-Otero P, et al. Origin of Waldenstrom's macroglobulinaemia. Best Pract Res Clin Haematol 2016;29:136–47.
63. Glass DR, Tsai AG, Oliveria JP, Hartmann FJ, Kimmey SC, Calderon AA, et al. An integrated multi-omic single-cell atlas of human B cell identity. Immunity 2020;53:217–32.
64. Singh M, Jackson KJL, Wang JJ, Schofield P, Field MA, Koppstein D, et al. Lymphoma driver mutations in the pathogenic evolution of an iconic human autoantibody. Cell 2020;180:878–94.
65. Cuttner J, Spiera H, Troy K, Wallenstein S. Autoimmune disease is a risk factor for the development of non-Hodgkin's lymphoma. J Rheumatol 2005;32:1884–7.
66. Tessier-Cloutier B, Twa DD, Baecklund E, Gascoyne R, Johnson NA, Backlin C, et al. Cell of origin in diffuse large B-cell lymphoma in systemic lupus erythematosus: molecular and clinical factors associated with survival. Lupus Sci Med 2019;6:e000324.
67. Rong X, Wang H, Ma J, Pan S, Wang H, Jing S, et al. Chronic hepatitis B virus infection is associated with a poorer prognosis in diffuse large B-cell lymphoma: a meta-analysis and systemic review. J Cancer 2019;10:3450–8.
68. Visco C, Finotto S. Hepatitis C virus and diffuse large B-cell lymphoma: Pathogenesis, behavior and treatment. World J Gastroenterol 2014;20:11054–61.
69. Ren W, Ye X, Su H, Li W, Liu D, Pirmoradian M, et al. Genetic landscape of hepatitis B virus-associated diffuse large B-cell lymphoma. Blood 2018;131:2670–81.
70. Arcaini L, Rossi D, Lucioni M, Nicola M, Bruscaggin A, Fiaccadori V, et al. The NOTCH pathway is recurrently mutated in diffuse large B-cell lymphoma associated with hepatitis C virus infection. Haematologica 2015;100:246–52.
71. Mareschal S, Lanic H, Ruminy P, Bastard C, Tilly H, Jardin F. The proportion of activated B-cell like subtype among de novo diffuse large B-cell lymphoma increases with age. Haematologica 2011;96:1888–90.
72. Gibson KL, Wu YC, Barnett Y, Duggan O, Vaughan R, Kondeatis E, et al. B-cell diversity decreases in old age and is correlated with poor health status. Aging Cell 2009;8:18–25.
73. Wang X, Stollar BD. Immunoglobulin VH gene expression in human aging. Clin Immunol 1999;93:132–42.
74. Lee JH, Jeong H, Choi JW, Oh H, Kim YS. Clinicopathologic significance of MYD88 L265P mutation in diffuse large B-cell lymphoma: a meta-analysis. Sci Rep 2017;7:1785.
75. Niroula A, Sekar A, Murakami MA, Trinder M, Agrawal M, Wong WJ, et al. Distinction of lymphoid and myeloid clonal hematopoiesis. Nat Med 2021;27:1921–7.
76. Rodriguez S, Celay J, Goicoechea I, Jimenez C, Botta C, Garcia-Barchino MJ, et al. Preneoplastic somatic mutations including MYD88(L265P) in lymphoplasmacytic lymphoma. Sci Adv 2022;8:eabl4644.
77. Johnson JL, Rosenthal RL, Knox JJ, Myles A, Naradikian MS, Madej J, et al. The transcription factor T-bet resolves memory B cell subsets with distinct tissue distributions and antibody specificities in mice and humans. Immunity 2020;52:842–55.
78. Varettoni M, Zibellini S, Arcaini L, Boveri E, Rattotti S, Pascutto C, et al. MYD88 (L265P) mutation is an independent risk factor for progression in patients with IgM monoclonal gammopathy of undetermined significance. Blood 2013;122:2284–5.
79. Jeong H, Cho H, Kim H, Chae H, Lee JB, Lee K, et al. Efficacy and safety of prophylactic high-dose MTX in high-risk DLBCL: a treatment intent-based analysis. Blood Adv 2021;5:2142–52.
80. Cardenas MG, Yu W, Beguelin W, Teater MR, Geng H, Goldstein RL, et al. Rationally designed BCL6 inhibitors target activated B cell diffuse large B cell lymphoma. J Clin Invest 2016;126:3351–62.
81. Gilan O, Rioja I, Knezevic K, Bell MJ, Yeung MM, Harker NR, et al. Selective targeting of BD1 and BD2 of the BET proteins in cancer and immunoinflammation. Science 2020;368:387–94.
82. Jain N, Hartert K, Tadros S, Fiskus W, Havranek O, Ma MCJ, et al. Targetable genetic alterations of TCF4 (E2–2) drive immunoglobulin expression in diffuse large B cell lymphoma. Sci Transl Med 2019;11:eaav5599.

83. McCoull W, Cheung T, Anderson E, Barton P, Burgess J, Byth K, et al. Development of a novel B-cell lymphoma 6 (BCL6) PROTAC to provide insight into small molecule targeting of BCL6. ACS Chem Biol 2018;13:3131–41.
84. An B, Zhu S, Li T, Wu J, Zang G, Lv X, et al. A dual TLR7/TLR9 inhibitor HJ901 inhibits ABC-DLBCL expressing the MyD88 L265P mutation. Front Cell Dev Biol 2020;8:262.
85. Carlson CS, Emerson RO, Sherwood AM, Desmarais C, Chung MW, Parsons JM, et al. Using synthetic templates to design an unbiased multiplex PCR assay. Nat Commun 2013;4:2680.
86. Leung W, Teater M, Durmaz C, Meydan C, Chivu AG, Chadburn A, et al. SETD2 haploinsufficiency enhances germinal center-associated AICDA somatic hypermutation to drive B-cell lymphomagenesis. Cancer Discov 2022;12:1782–803.
87. Subramanian A, Tamayo P, Mootha VK, Mukherjee S, Ebert BL, Gillette MA, et al. Gene set enrichment analysis: a knowledge-based approach for interpreting genome-wide expression profiles. Proc Natl Acad Sci U S A 2005;102:15545–50.
88. Goodarzi H, Elemento O, Tavazoie S. Revealing global regulatory perturbations across human cancers. Mol Cell 2009;36:900–11.
89. Beguelin W, Teater M, Meydan C, Hoehn KB, Phillip JM, Soshnev AA, et al. Mutant EZH2 induces a pre-malignant lymphoma niche by reprogramming the immune response. Cancer Cell 2020;37:655–73.

SUPPLEMENTARY FIGURE S1

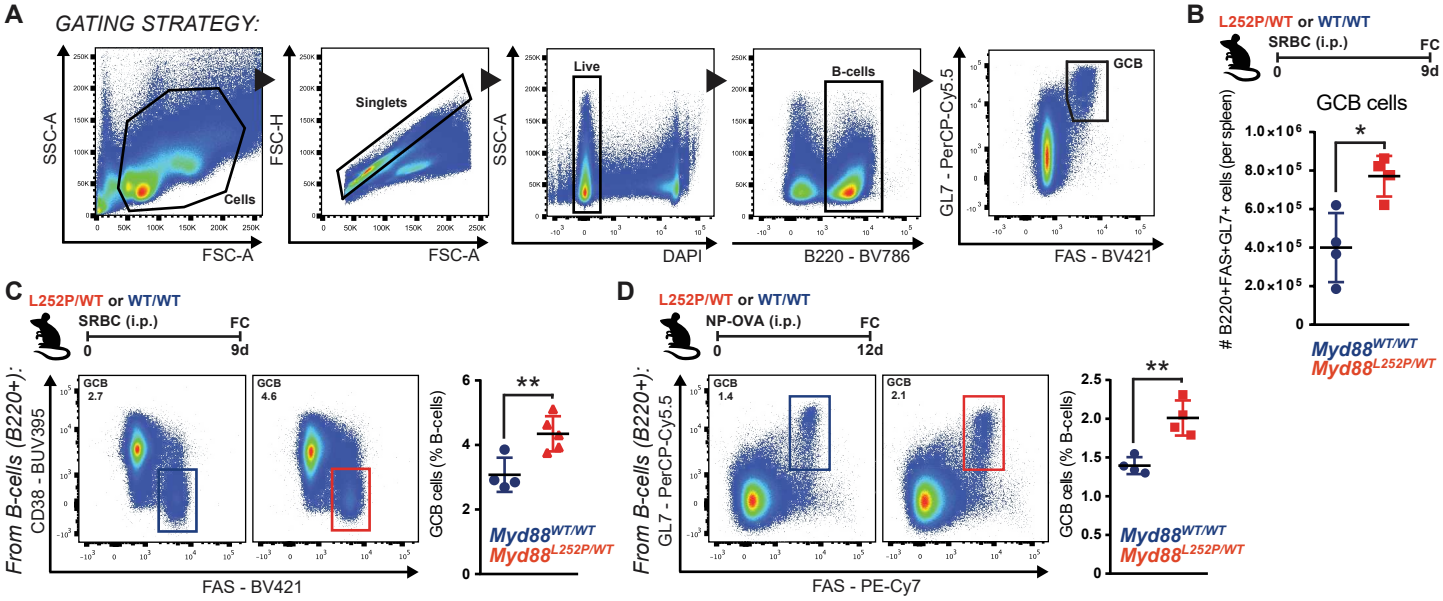

Supplementary Figure S1. *Related to Figure 1.*

A, Complete FC gating strategy for **Fig. 1A** and **1B**.

B, Absolute FC-based quantification total GCB from *Myd88*$^{L252P/WT}$ or *Myd88*$^{WT/WT}$ mice, 9 days after SRBC immunization.

C, FC analysis of splenic GCB, using an alternative gating strategy to that presented in **Fig. 1B**.

D, FC analysis of splenic GCB following immunization with an NP-OVA conjugate.

Values represent mean ± SEM. Data reproducible with two repeats. NS, not significant; *P < 0.05; **P < 0.01; ***P < 0.001, using unpaired two-tailed Student's t-test.

SUPPLEMENTARY FIGURE S2

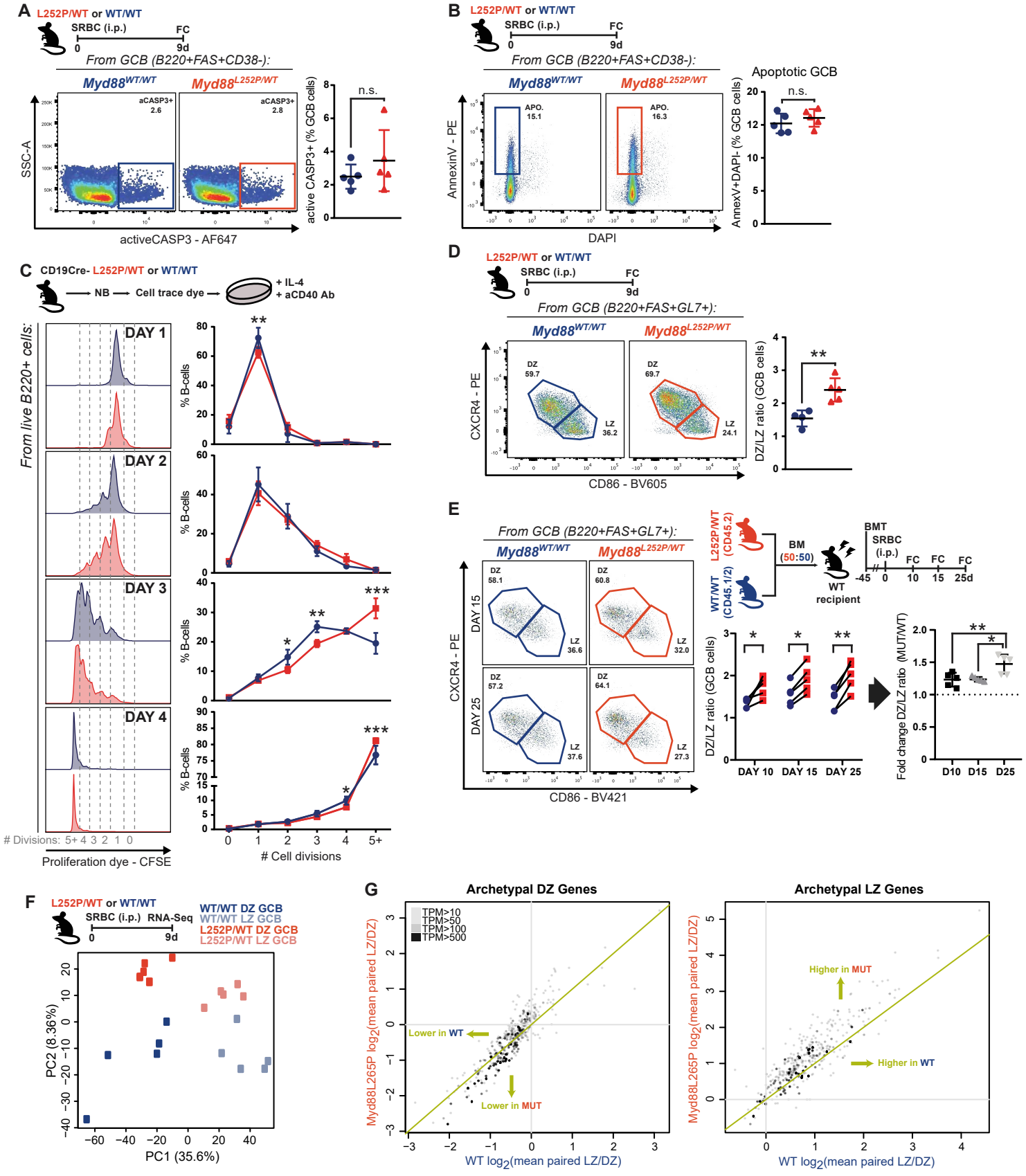

Supplementary Figure S2. *Related to Figure 2.*

A, FC analysis of active Caspase 3+ splenic GCB.

B, FC analysis of AnnexinV/DAPI staining of splenic GCB.

C, FC analysis of cell proliferation by CellTrace Dye dilution in B-cells stimulated *ex vivo*. Results for 3 animals per genotype.

D, FC analysis of DZ and LZ splenic GCB.

E, FC analysis of *Myd88*$^{L252P/WT}$ and *Myd88*$^{WT/WT}$ relative contribution to DZ GCB and LZ GCB, based on CD45 allele frequencies.

F, PCA plot for the RNA-Seq experiment in **Fig. 2G**.

G, Plot showing relative expression of archetypal DZ (left) or LZ (right) genes (GSE38696), in the RNA-Seq experiment from **Fig. 2G**.

Values represent mean ± SEM. Data reproducible with two repeats. NS, not significant; *P < 0.05; **P < 0.01; ***P < 0.001, using unpaired (**A**,**B**,**D**) or paired (**E**) two-tailed Student's t-test with the two-stage step-up method of Benjamini, Krieger and Yekutieli where applicable; or two-way ANOVA with Tukey's post-test (**C**).

SUPPLEMENTARY FIGURE S3

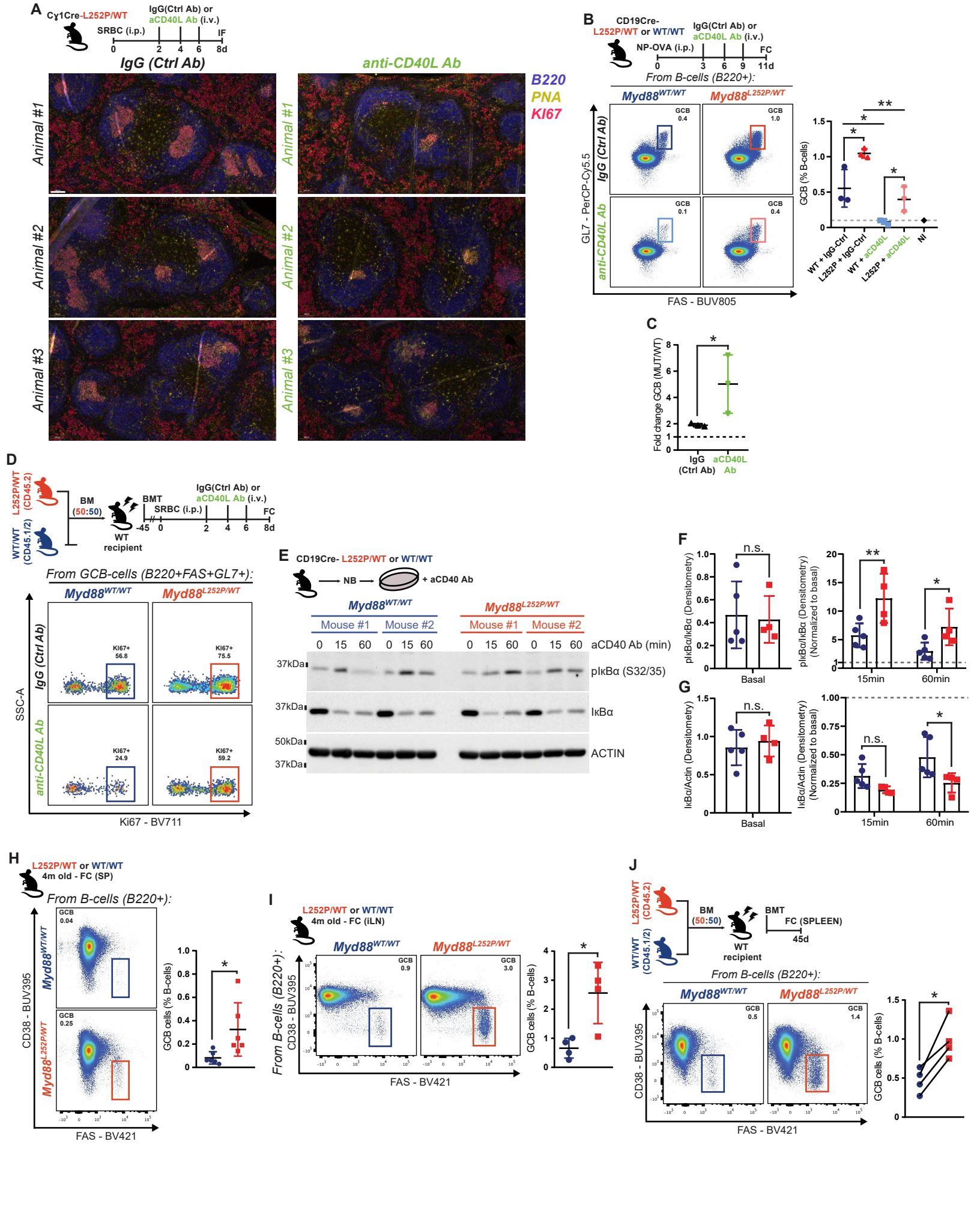

Supplementary Figure S3. *Related to Figure 3.*

A, Multicolor immunofluorescence staining for B220 (purple), PNA (yellow) and KI67 (red) in representative splenic sections. Scale = 100µm.

B-**C**, FC analysis of splenic GCB expressed as (**B**) percentage of B-cells or (**C**) relative fold change between conditions.

D, Representative FC plots for Ki67+ splenic GCB from **Fig. 3G**.

E, WB-based assessment of (p)IκBα expression in naive B-cells stimulated with an agonistic anti-CD40 antibody. Representative blots are shown for 2 animals per genotype.

F-**G**, Densitometry analysis for immunoblot assays in (**E**), under basal (left) or stimulated (right) conditions. Dots represent individual animals. Results pooled from 2 independent experiments.

H, FC analysis of splenic GCB, using an alternative gating strategy to that presented in **Fig. 3K**.

I, FC analysis of GCB in the inguinal lymph nodes of naive mice at 3-4m of age.

J, FC analysis of splenic GCB, using an alternative gating strategy to that presented in **Fig. 3O**.

Values represent mean ± SEM. P-values calculated using unpaired (**B**,**C**,**F**-**I**) or paired (**J**) two-tailed Student's t-test.

SUPPLEMENTARY FIGURE S4

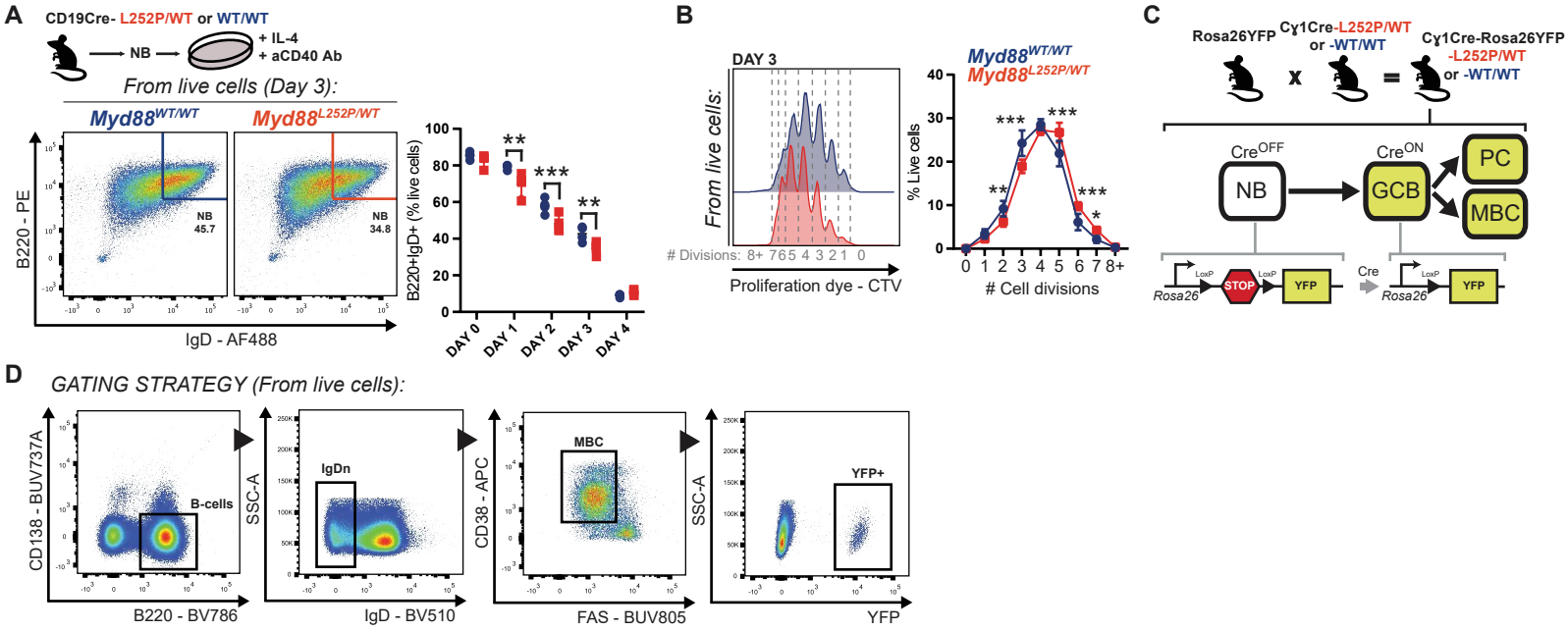

Supplementary Figure S4. *Related to Figure 4.*

A, FC analysis of NB cell abundance among B-cells stimulated *ex vivo* from **Fig. 4C**.

B, FC analysis of cell proliferation by CellTrace Dye dilution in B-cells stimulated *ex vivo* from **Fig. 4C**. Results for 3 animals per genotype.

C, Schematic use of the *Rosa26YFP* reporter.

D, Complete FC gating strategy for **Fig. 4H**.

Values represent mean ± SEM. P-values calculated using a two-way ANOVA with Tukey's post-test.

SUPPLEMENTARY FIGURE S5

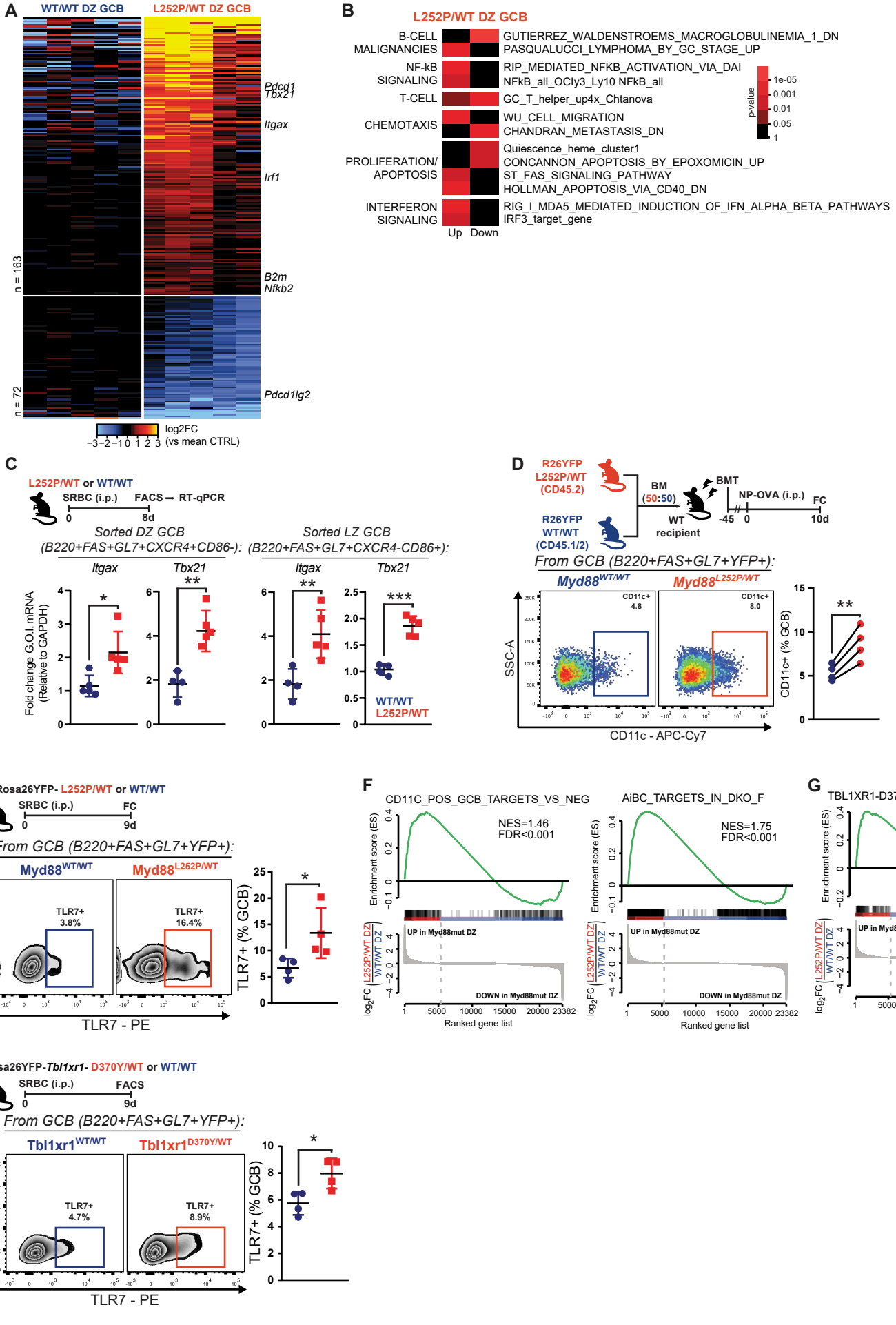

Supplementary Figure S5. *Related to Figure 5.*

A, Differentially expressed genes in splenic *Myd88*$^{L252P/WT}$ DZ GCB from experiment in **Fig. 2G**.

B, Pathway enrichment analysis for genes in (**A**).

C, Real Time-qPCR (RT-qPCR) validation of selected genes from (**A**) and **Fig. 5A**, performed on independent animals. Results expressed as fold change of gene-of-interest (G.O.I.), normalized to GAPDH expression levels.

D, FC analysis of CD11c+ splenic GCB following immunization with an NP-OVA conjugate.

E, FC analysis of TLR7+ splenic GCB in *Myd88*$^{L252P/WT}$ mice.

F, GSEA of canonical murine AiBC signatures (GSE175365), against *Myd88*$^{L252P/WT}$ DZ GCB.

G, GSEA of *Tbl1xr1* mutant GCB (GSE139059), against *Myd88*$^{L252P/WT}$ DZ GCB.

H, FC analysis of TLR7+ splenic GCB in *Tbl1xr1*$^{D370Y/WT}$mice.

Values represent mean ± SEM. P-values calculated using unpaired (**C**,**E**,**H**) or paired (**D**) two-tailed Student's t-test.

SUPPLEMENTARY FIGURE S6

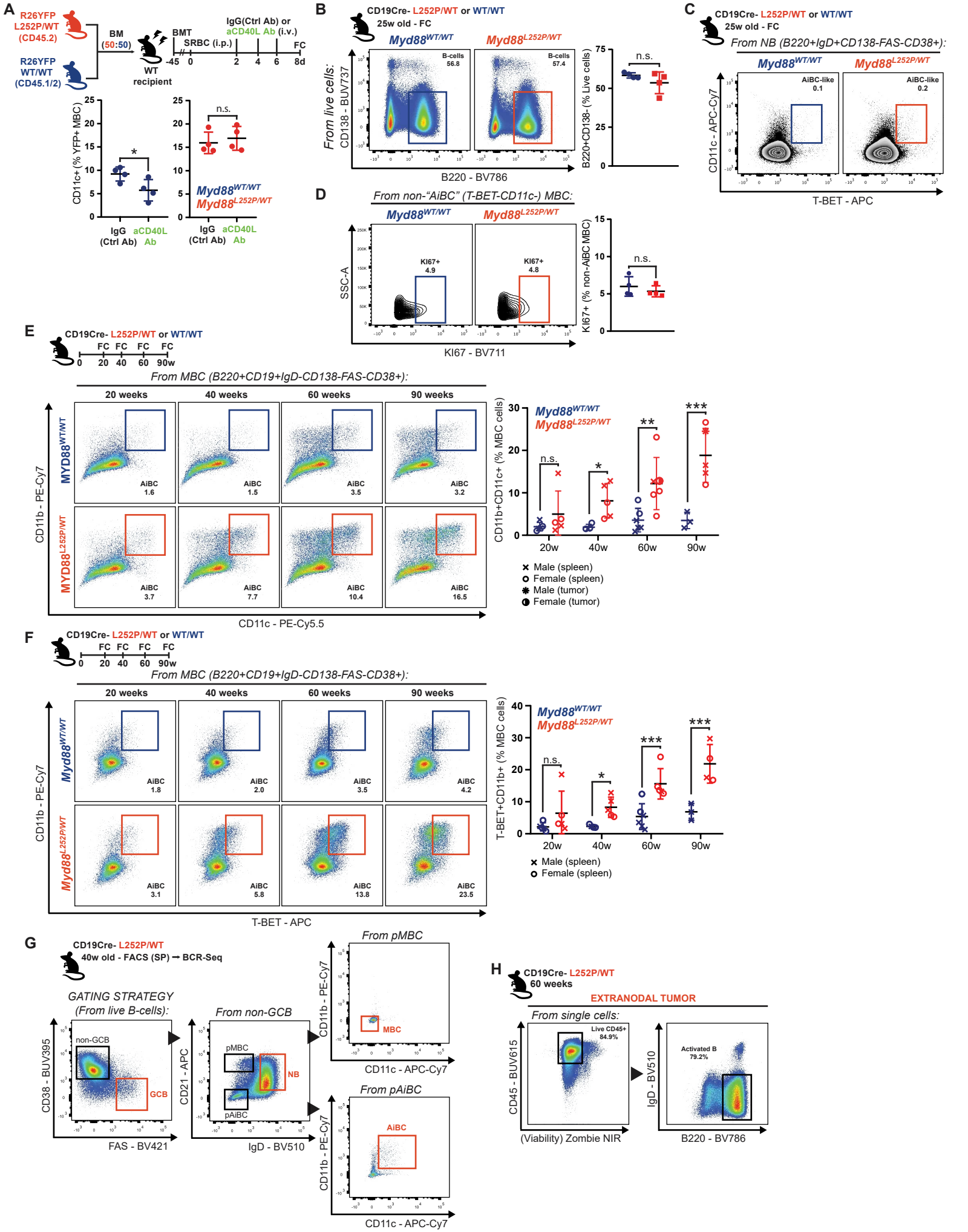

Supplementary Figure S6. *Related to Figure 6.*

A, FC analysis of CD11c+ splenic YFP+ MBC in IgG(Ctrl Ab) or anti-CD40L treated mice (**Fig. 6E**), segregated by genotype.
B, FC analysis of total splenic B-cells in animals from **Fig. 6F**.
C, FC analysis of AiBC markers among splenic naive B-cells, from animals in **Fig. 6F**. Representative plots shown for 1 animal per genotype.
D, FC analysis of KI67+ non-AiBC-like MBC in mice from **Fig. 6F**.
E-**F**, FC analysis of splenic AiBC-like MBC in non-immunized animals at different ages, using alternative gating strategies to that in **Fig. 6H**. Tumor samples are plotted in (**E**), but were not considered for statistical analysis.
G, Gating strategy employed for sorting B-cell populations from non-immunized aged animals from **Fig. 6J** for BCR sequencing.
H, FC analysis of tumor cell composition from an aged *Myd88*$^{L252P/WT}$ mouse (**Fig. 6L**).
Values represent mean ± SEM. P-values calculated using unpaired two-tailed Student's t-test with the two-stage step-up method of Benjamini, Krieger and Yekutieli.

SUPPLEMENTARY FIGURE S7

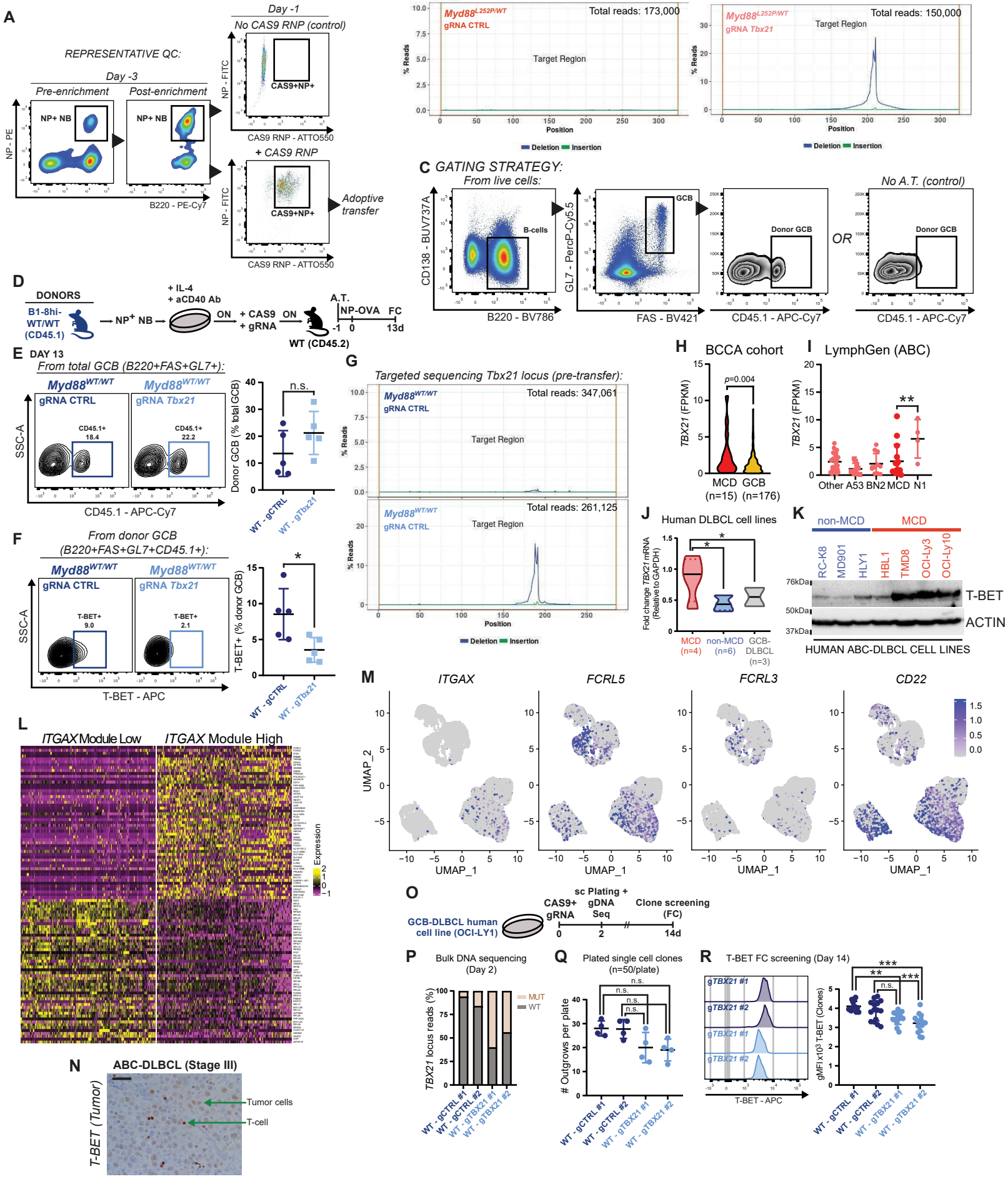

Supplementary Figure S7. *Related to Figure 7.*

A, Representative FC plots of donor B-cells at different stages during pre-transfer preparation, from experiment in **Fig. 7A**.

B, Disruptive mutations at the targeted *Tbx21* genomic locus, based on bulk targeted DNA sequencing, on the day of transfer, from experiment in **Fig. 7A**. Results shown for 1 representative donor per group.

C, Complete gating strategy for total and donor GCB from experiment in **Fig. 7B**.

D, Experimental scheme and timeline for experiments in **E**-**G**.

E, Representative FC plots (left) and quantification (right) of GCB derived from adoptively transferred B-cells, in the spleen of recipient animals at endpoint.

F, Representative FC plots (left) and quantification (right) of T-BET expression in GCB derived from adoptively transferred B-cells, at endpoint.

G, Disruptive mutations at the targeted *Tbx21* genomic locus, based on bulk targeted DNA sequencing, on the day of transfer (Day -1). Sequencing results shown for one representative donor per group.

H, RNA-Seq-based expression levels of *TBX21* in MCD DLBCL specimens, compared to GCB-DLBCL cases, from the BCCA cohort.

I, RNA-Seq-based expression levels of *TBX21* based on the LymphGen subclassification of ABC-DLBCL tumors, from the BCCA cohort.

J, RT-qPCR assessment of *TBX21* mRNA basal expression in a panel of human DLBCL cell lines grown in their corresponding complete media.

K, WB-based assessment of T-BET basal expression in a panel of human DLBCL cell lines grown in their corresponding complete media.

L, Heatmap depiction of genes included in the *ITGAX* module. The module was derived using the top 200 genes with the highest correlated expression to ITGAX in the full DLBCL cohort (n=17) from Ye *et al.*.

M, Relative expression of representative genes in the *ITGAX* module, known to be expressed by canonical AiBCs.

N, Representative image illustrating the differential intensity of T-BET IHC staining in ABC-DLBCL tumor cells and infiltrating T-cells. Scale = 20µm.

O, Experimental scheme and timeline for experiments in **P**-**R**

P, Quantification of disruptive mutations at the targeted *TBX21* genomic loci, based on bulk targeted DNA sequencing.

Q, Quantification of the number of clonal outgrows from single cells for the different gRNAs, at endpoint.

R, Representative histograms (left) and quantification (right) for T-BET expression in clonal outgrows (n=15 per gRNA), at endpoint.

Values represent mean ± SEM. P-values calculated using unpaired two-tailed Student's t-test (**E**,**F**,**H**), or one-way ANOVA with Tukey's post-test (**I**,**J**,**Q**,**R**).